1994-12

Correlation of inclusion size and chemistry with weld metal composition and microstructure in arc weldments of high strength steels

Eakes, Mark W.

Monterey, California. Naval Postgraduate School

NAVAL POSTGRADUATE SCHOOL
MONTEREY, CALIFORNIA

THESIS

CORRELATION OF INCLUSION SIZE AND CHEMISTRY WITH WELD METAL COMPOSITION AND MICROSTRUCTURE IN ARC WELDMENTS OF HIGH STRENGTH STEELS

by

Mark W. Eakes

December, 1994

Thesis Advisor: Alan G. Fox

Approved for public release; distribution is unlimited.

REPORT DOCUMENTATION PAGE

Form Approved OMB No. 0704-0188

1. AGENCY USE ONLY *(Leave blank)*	2. REPORT DATE	3. REPORT TYPE AND DATES COVERED
	December 1994	Master's Thesis

4. TITLE AND SUBTITLE CORRELATION OF INCLUSION SIZE AND CHEMISTRY WITH WELD METAL COMPOSITION AND MICROSTRUCTURE IN ARC WELDMENTS OF HIGH STRENGTH STEELS

5. FUNDING NUMBERS

6. AUTHOR(S) Eakes, Mark W.

7. PERFORMING ORGANIZATION NAME(S) AND ADDRESS(ES)
Naval Postgraduate School
Monterey CA 93943-5000

8. PERFORMING ORGANIZATION REPORT NUMBER

9. SPONSORING/MONITORING AGENCY NAME(S) AND ADDRESS(ES)
Naval Surface Warfare Center, Annapolis, MD 21402

10. SPONSORING/ MONITORING AGENCY REPORT NUMBER

11. SUPPLEMENTARY NOTES The views expressed in this thesis are those of the author and do not reflect the official policy or position of the Department of Defense or the U.S. Government.

12a. DISTRIBUTION/AVAILABILITY STATEMENT
Approved for public release; distribution is unlimited.

12b. DISTRIBUTION CODE

13. ABSTRACT Non-metallic inclusions are crucial to the development of acicular ferrite, the desired microstructure for optimal strength and toughness in weld metal. This study focused on obtaining correlation between the size and chemistry of inclusions and weld metal properties, especially the amount of acicular ferrite, in Gas Metal Arc (GMA) and Submerged Arc (SA) weldments in HY-100 and HSLA-100 steel. A strong correlation was found between the amount of acicular ferrite, flux basicity and inclusion composition and volume fraction in SAW weld metal samples. An index developed to consider the effect of chemistry and volume fraction of inclusions on acicular ferrite showed good correlation. The GMA weld samples were found to contain less acicular ferrite than the SAW samples, principally because of their lower oxygen content. However, it was again found possible to correlate inclusion chemistry and volume fraction with acicular ferrite formation. Unfortunately, the large amount of data scatter precluded the development of an index in this case.

14. SUBJECT TERMS Non-metallic inclusions, acicular ferrite, HY-100 steel, HSLA-100 steel, gas metal arc welding, submerged arc welding

15. NUMBER OF PAGES 144

16. PRICE CODE

17. SECURITY CLASSIFICATION OF REPORT	18. SECURITY CLASSIFICATION OF THIS PAGE	19. SECURITY CLASSIFICATION OF ABSTRACT	20. LIMITATION OF ABSTRACT
Unclassified	Unclassified	Unclassified	UL

NSN 7540-01-280-5500

Standard Form 298 (Rev. 2-89)
Prescribed by ANSI Std. 239-18 298-102

Approved for public release; distribution is unlimited.

CORRELATION OF INCLUSION SIZE AND CHEMISTRY WITH WELD METAL COMPOSITION AND MICROSTRUCTURE IN ARC WELDMENTS OF HIGH STRENGTH STEELS

by

Mark W. Eakes
Lieutenant, United States Navy
B.S., United States Naval Academy, 1986

Submitted in partial fulfillment
of the requirements for the degree of

MASTER OF SCIENCE IN MECHANICAL ENGINEERING

from the

NAVAL POSTGRADUATE SCHOOL
December 1994

Author: [redacted]
Mark W. Eakes

Approved by: [redacted]
Alan G. Fox, Thesis Advisor

[redacted]
Matthew D. Kelleher, Chairman
Department of Mechanical Engineering

Accesion For	
NTIS CRA&I	☑
DTIC TAB	☐
Unannounced	☐
Justification	
By	
Distribution /	
Availability Codes	
Dist	Avail and / or Special
A-1	

ABSTRACT

Non-metallic inclusions are crucial to the development of acicular ferrite, the desired microstructure for optimal strength and toughness in weld metal. This study focused on obtaining correlation between the size and chemistry of inclusions and weld metal properties, especially the amount of acicular ferrite, in Gas Metal Arc (GMA) and Submerged Arc (SA) weldments in HY-100 and HSLA-100 steel. A strong correlation was found between the amount of acicular ferrite, flux basicity and inclusion composition and volume fraction in SAW weld metal samples. An index developed to consider the effect of chemistry and volume fraction of inclusions on acicular ferrite showed good correlation. The GMA weld samples were found to contain less acicular ferrite than the SAW samples, principally because of their lower oxygen content. However, it was again found possible to correlate inclusion chemistry and volume fraction with acicular ferrite formation. Unfortunately, the large amount of data scatter precluded the development of an index in this case.

TABLE OF CONTENTS

ACKNOWLEDGEMENT

My heartfelt thanks goes to Dr. Alan G. Fox for all of his assistance, advice and guidance in this effort. My research was made easier through the assistance of Rich Hashimoto and Doug Shelton. Special credit goes to my wife, Debbie, and my children for their support and patience during the long hours spent on this project.

I. INTRODUCTION

Steel plays an invaluable role in society. In the Navy, the development of higher strength steels has allowed weight savings or increases in the allowed loading for a given weight. Submarines are limited in their maximum depth by the strength of their steel hulls, for example, so it is obvious why there is a strong motivation for developing stronger steels. Advances in technology and in the understanding of metallurgy has produced new methods for making stronger steels with other important properties such as high toughness.

While carefully controlled alloy additions and thermomechanical processing have given society these very strong and tough steels, the fact that the principle means of joining steel structures is by arc welding means that this fairly "crude" process becomes the "weak link," so to speak, in the effective utilization of these steels. Welding, while seemingly simple, is a very complex process which can actually degrade the material properties of the metals it joins. A thorough understanding of welding and its effect on steel properties is thus vital.

It is an accepted axiom in metallurgy that properties follow microstructure, and thus to control the properties the microstructure must be thoroughly understood. Welding is no exception and a great deal of effort has gone into trying to understand how weld metal microstructure develops. One of the key areas in furthering understanding of microstructural development is the study of those features which are principally responsible for the nucleation and growth of the desirable microstructures. Non-metallic inclusions are one of those features.

Non-metallic inclusions, a product of chemical reactions, are an inevitable fact of life in steels. Even in the cleanest methods of producing steels, there will still be a

very large number of them present, of the order of 10^9-10^{12} inclusions per ton with only 1 ppm each of oxygen and sulphur (Kiessling, 1989). It is traditionally understood that large inclusions are detrimental to mechanical properties, specifically in regards to fracture toughness as crack initiation sites and as potential sites for void nucleation in the ductile failure regime. Therefore, efforts have been ongoing to reduce the size and number of inclusions.

Welding of steels, however, results in the formation of many additional inclusions in the form of oxides, nitrides, sulfides and carbides through the mutual contact of the weld pool, surrounding atmosphere and welding consumables. Weld metal inclusions are smaller and have a critical size for crack initiation of the order of 20-30 times smaller than in wrought steels (Kiessling, 1989). It is now understood, though, that inclusions play an important role in the development of beneficial weld metal microstructures through their effect on grain boundary size and as nucleating sites for certain types of ferrite.

A greater understanding of the role that inclusions play in the development of weld metal microstructures, and thus on properties, will lead to the ability to more accurately design welding consumables and obtain desired weld metal properties. It is with this goal in mind that this study is undertaken.

II. BACKGROUND

A. HIGH STRENGTH STEELS

High strength steels are those categorized by higher yield strengths, of the order of 40 to over 100 ksi. The driving force for the development of these steels was to obtain greater strength-to-weight ratios (Metals Handbook, 1983). In general, increasing the carbon content of steel will result in an increase in strength, but with a corresponding decrease in toughness. To achieve both strength and toughness improvements, alloying, heat treatments and mechanical processing are applied which allow precipitation hardening, quenching and tempering and grain size control to develop these desired mechanical properties.

1. High Yield (HY-100) Steels

High Yield (HY) steels are quenched and tempered low-alloy steel grades which offer high strength and good toughness. Table 2.1 shows the compositions and military specifications. These properties are developed by heating to at least 900 degrees C (1650 degrees F), quenching in water or oil, and tempering at not less than 600 degrees C (1100 degrees F) to provide microstructures of tempered martensite plus bainite. The major drawback with this steel grade, however, is that it is more difficult to weld due to required pre- and post-heat treatments to obtain the required postweld material characteristics and avoid hydrogen induced cracking.

2. High Strength Low Alloy (HSLA-100) Steels

High Strength Low Alloy (HSLA) steels rely on additions of copper for precipitation strengthening and the addition of other alloys, such as manganese, nickel, molybdenum, and in particular niobium for grain size control, to achieve an increase in hardenability without increasing the carbon content. The nominal values and military specifications for

HSLA-100 steel are shown in Table 2.1. Often called microalloyed steels, the principle benefit of this grade of steel is its improved weldability without the costly weld heat treatments. Figure 2.1 shows the weldability of HY-100 and HSLA-100 as a function of carbon content and an index called the Carbon Equivalent, CE, which is a measure of the influence that the alloying constituents have on hardenability.

3. Alloying Elements

Alloying elements are added to the steels to achieve optimal properties. In order to limit the oxygen content and prevent porosity, certain elements present in the weld metal, or added through the flux or weld wire, are particularly important for the deoxidation process. Aluminum, titanium, manganese and silicon are the principle deoxidants.

The most effective deoxidizing element is aluminum. In addition to its affinity for oxygen, aluminum also forms AlN, which serves to refine the grain structure by pinning grain boundaries and inhibiting grain growth (Porter, 1982). The second most effective deoxidizer added is titanium, which can exist as one of several forms of oxide, such as TiO, Ti_2O_3 or TiO_2. In high concentrations, however, titanium can form TiN, leading to deterioration in fracture toughness (Brothers, 1994).

Manganese and silicon also participate in the deoxidation process. Manganese is added primarily as an austenite stabilizer which serves to increase the strength and hardenability of the steel. Although a weak deoxidizer, its relatively high concentration in the weld metal allows it to participate to a high degree. Silicon, a much stronger deoxidizer than manganese, is a primary deoxidant in molten steel. Silicon decreases the solubility of carbon in iron, allowing less carbon for similar strength (Ellis, 1990).

B. WELDING PROCESS

The arc welding process relies on an electric arc between the workpiece and the electrode for the heat source. Two methods used extensively in industry are the Gas Metal Arc (GMA) and the Submerged Arc (SA) welding processes. While each process has its own distinct characteristics, the reactions which occur in the weld pool and the type of microstructure which develops are in general common and are functions of the weld pool thermal cycle, which differs quite a bit from the "typical" equilibrium reactions often studied and applied to the steel making process.

1. Gas Metal Arc Welding (GMAW)

The Gas Metal Arc Welding (GMAW) process consists of a continuously fed consumable electrode, which acts as a filler metal, shielded by a cover gas. Figure 2.2 shows a diagram of this process. This process is frequently referred to as MIG, for Metal Inert Gas, when an inert gas such as He or Ar is used. The cover gas is important to minimize contamination of the weld metal with the atmosphere. Frequently, however, reactive gases, such as oxygen and carbon dioxide, are added to the cover gas to improve arc stability.(Grong, 1986) The addition of these reactive gases results in addition of oxygen to the weld metal which directly affects inclusion formation, as will be discussed in more detail later.

Metal transfer in GMA welding can occur in one of three ways: short-circuiting, globular, and spray transfers. Short-circuiting occurs when the electrode touches the workpiece surface. Globular and spray transfer occurs under the influence of gravity or electromagnetic forces, respectively. Direct-current reverse polarity (electrode-positive) is usually used to obtain a smooth metal transfer, a stable arc with low spatter loss, and good weld penetration.(Kou, 1987)

2. Submerged Arc Welding (SAW)

In Submerged Arc Welding (SAW), the arc occurs between a bare consumable electrode and the workpiece, with the arc being shielded by a layer of granular flux deposited ahead of the electrode, as shown in Figure 2.3. The flux is a mixture of various oxides and/or halides which serve to protect the weld metal from atmospheric contamination, insulate the weld pool allowing lower heat loss to surroundings, and, along with the choice of the weld wire, help control the weld metal composition. Because the weld pool is covered by the flux and molten slag, high welding currents can be used without causing violent arcs, allowing a greater deposition rate, which along with the protecting and refining action of the slag, are principle advantages of SAW.(Kou, 1987)

When welding steels, oxide fluxes are normally used and are usually categorized as either basic or acidic. The Basicity Index (BI), in general, is the ratio of basic oxides to non-basic oxides (Kou, 1987). This provides a convenient means of quantifying a given flux and allows correlation of flux to various microstructures and properties. For example, it has been found that the higher the BI, the cleaner the weld is in regards to non-metallic inclusions (Jang, 1987).

3. Weld Thermal Cycle

One of the factors which makes studying the welding process so difficult is the thermal cycle which occurs during welding. The very nature of arc welding results in extremely high heat input over a very small area and short time interval which in turn results in a process very removed from equilibrium. Peak weld metal temperatures can reach over 2000 degrees C with temperature gradients on the order of 1000 K mm^{-1} and cooling rates up to 1000 K sec^{-1}. In Figure 2.4, a schematic diagram of the main welding process stages in GMA welding is shown. It is apparent that there is a very complex interaction between the different elements of the welding process.(Grong, 1986)

A useful way of describing this process is by using the concept of pseudo-steady-state, where the temperature does not appear to vary with time as seen from the tip of the heat source. Figure 2.5 shows such a diagram which illustrates the weld centerline peak temperature at different distances from the root of the arc. Another interpretation of this diagram is a temperature-time graph if the welding occurs at constant speed. This figure demonstrates the different temperature ranges where the various chemical and physical reactions occur. The thermal cycle not only affects solidification, but also the time available for the austenite to ferrite transformation in the so called critical temperature range, of 800 to 500 degrees C, in addition to influencing the weld metal chemical composition, inclusion chemistry and size distribution, and the solidification microstructure.(Grong, 1986)

a. Weld Pool Reactions

During this short, intense heating cycle, some very complex chemical reactions take place. One of the principle reactions is the oxidation/deoxidation of the weld pool. Since oxygen is introduced in the cover gas in GMAW or the reduction of such oxides as MnO, TiO_2, and SiO_2 in the flux of SAW, deoxidation becomes important to prevent porosity and maintain a low solidified weld metal oxygen content. Deoxidation is accomplished by the addition of strong deoxidizers such as Ti, Al, Si, and Mn in the welding consumables. Because the solubility of oxygen in solid steel is very low, the weld metal oxygen is present primarily in the form of oxide inclusions.(Widgery, 1975)

The exact mechanism of how oxygen enters the weld metal is unknown. One classic view is that because of the larger surface area-to-volume ratio of the metal droplets as they fall from the electrode to the surface, most of the gas/metal reaction occurs on the falling drops. The rapid

solidification implied that there would be insufficient time for such reactions to take place in the weld pool. Francis, Jones and Olson, however, concluded that there was adequate time before solidification for the dissolved gases to reach near-equilibrium and that gas/metal reactions in the weld pool did indeed represent a "significant contribution to the total gas/metal reaction."(Francis, 1990)

One model proposed to describe the oxidation/deoxidation reaction is shown schematically in Figure 2.6. The model divides the weld pool into two zones, a hot zone and a cold zone. In the hot zone, oxidation takes place simultaneously with deoxidation and phase separation, which refers to the removal of the inclusions formed in the deoxidation process to the surface as a component called microslag. This region is characterized by high temperatures (above about 1900 degrees C) and very turbulent conditions. In the cold zone, deoxidation also occurs, but with incomplete phase separation, resulting in trapped oxide inclusions. Phase separation results in the removal of the inclusions and thus helps control the final oxygen content in the weld metal. Grong, et al, concluded that phase separation is controlled solely by the fluid flow fields generated by the turbulent flow conditions which exist just beneath the root of the arc. Thus, any change in welding parameters, flux or cover gas composition which alters the fluid flow patterns will affect the oxygen content in the weld metal.(Grong, 1986)

b. Weld Metal Microstructure Development

Weld pool solidification occurs spontaneously, unlike solidification of castings or ingots, by epitaxial growth of the new grains on the partially melted grains along the fusion boundary (David, 1992). The growth of the new grains, whose width is controlled by the Heat Affected Zone (HAZ) grain morphology, follows the maximum thermal gradient and results in long columnar grains. In low carbon steels,

the weld metal solidifies as delta-ferrite. The growth process follows a cellular-dendritic pattern as a result of the high cooling rate and extensive segregation of alloying and impurity elements along the interdendritic spaces ensues.(Grong, 1986)

As the weld metal continues to cool after solidification, solid state transformations occur. Because the heat flow characteristics in welding are dynamic, the temperature gradient is different during this phase and the new austenite grain boundaries do not coincide with the prior delta-ferrite grain boundaries. This results in the inclusions which had segregated along the initial solidification boundaries now becoming intragranular, as shown in Figure 2.7 (Sugden, 1987). This becomes important when considering the effect of intragranular nucleation of the particularly favorable microstructure called acicular ferrite, which will be discussed in more detail in a later section.

Further cooling results in the transformation of austenite into various forms of ferrite. There has been much confusion over the terminology describing the different microstructures. Two classification and terminology schemes have been developed in an attempt at standardization. Table 2.2 shows a comparison of the Japan Welding Society (JWS) and the International Institute of Welding (IIW) systems.

The first microstructure to form is primary ferrite, occurring both as grain boundary ferrite and intragranular ferrite. Grain boundary ferrite will form at relatively high temperatures (above 700 degrees C). It nucleates and grows along prior austenite grain boundaries, which serve as nucleation sites due to the relatively higher energy associated them. At lower temperatures (750-650 degrees C), needle like laths, called Widmanstätten or side plate ferrite, grow from the grain boundary ferrite into the adjacent austenite grains. As temperature drops below 600 degrees C,

intragranular acicular ferrite may form, nucleated on inclusions. This microstructure and its formation will be discussed in more depth later. At even lower temperatures and as a result of enrichment of carbon, acicular ferrite formation can be suppressed and another phase called bainite, or ferrite with aligned second phase, will form. Martensite can also form if cooling rates are high enough and carbon content has been enriched enough in certain areas.(Liu, 1992)

While there are many variables which affect the final weld metal microstructure, cooling rate is one of the most important. In general, a slow cooling rate will result in coarser microstructure due to the increased time at higher temperature for grain growth. Typically, blocky or grain boundary ferrite is associated with slower cooling rates. At higher cooling rates, if the optimum conditions exist, acicular ferrite will form (Francis, 1990). At even higher cooling rates, bainite becomes energetically favored. A schematic Continuous Cooling Transformation (CCT) diagram is shown in Figure 2.8.

Also shown in Figure 2.8 are the effects of other variables on final microstructure in addition to cooling rate. For example, hardenability agents such as manganese shift the curves to the right (longer delay times), which serves to refine the microstructure. Inclusion formers, on the other hand, promote the formation of higher temperature microstructures, shifting the curves to the left.(Liu, 1992)

The role of oxygen in microstructural development warrants special treatment. As discussed earlier, increasing the cover gas oxygen activity in GMA welds results in an increase in weld metal oxygen, while a similar effect occurs in SA weldments due to the reduction of flux oxides. Increasing the oxygen content provides more reactants for heterogeneous nucleation of oxide inclusions. In SA welds with oxygen contents greater than 600 ppm, a high inclusion

content exists which acts to pin grain boundaries (Figure 2.9) and leave a fine-grained structure. This increase in grain boundary surface area provides more grain boundary nucleating potential and grain boundary ferrite predominates. At oxygen levels of about 300 ppm, the austenite grain size is somewhat larger and there exists sufficient intragranular inclusions which, provided other conditions are optimum, produce a microstructure of mostly acicular ferrite. At low oxygen content, there are insufficient inclusions to nucleate much acicular ferrite and a bainitic microstructure predominates.(Abson, 1986)

C. EFFECT OF MICROSTRUCTURE ON WELD METAL PROPERTIES

The reason for studying and quantifying microstructure is because weld metal mechanical properties are a direct function of it. The principle properties of concern are strength and toughness. It is generally understood that increasing the carbon content will produce steel with increased strength, but with the drawback of reduced toughness. The higher strength in this case comes from the larger amount of martensite formed, which unfortunately also embrittles the steel. In the case of micro-alloyed steels, such as HSLA, grain refining is used to produce both increased strength and toughness. The fine grains provide more barriers to crack propagation. The reason that acicular ferrite is such a desired microstructure is because of its fine, characteristic basket weave morphology. This microstructure offers an even more convoluted path for crack propagation, as shown in Figure 2.10. Figure 2.11 shows how weld metal mechanical properties improve with increasing acicular ferrite. The other principle types of ferrite do not have this favorable characteristic. Side plate and grain boundary ferrite are, in fact, detrimental to toughness. (Edmonds, 1990)

D. ACICULAR FERRITE

1. Nature of Acicular Ferrite

Acicular means shaped and pointed like a needle. In two dimensions, acicular ferrite appears as small randomly oriented laths separated by high angle grain boundaries with an aspect ratio between 3:1 and 10:1 (Liu, 1992). In three dimensions, it is believed to exist as thin, lenticular plates (Bhadeshia, 1990). Known to nucleate primarily on intragranular inclusions, with sufficient undercooling acicular ferrite can also nucleate on laths of growing acicular ferrite, a process called sympathetic nucleation. Acicular ferrite exists when there is a sufficient density of optimally sized inclusions, such that the growing laths impinge on one another and produce the characteristic basket weave pattern which is resistant to crack propagation.

Strangwood and Bhadeshia have concluded that acicular ferrite is actually bainite which nucleates intragranularly and subsequently grows by a diffusionless mechanism (as opposed to diffusion controlled) where carbon redistribution between austenite and ferrite takes place after the transformation (Strangwood, 1989). Bhadeshia noted that conventional bainite or acicular ferrite can be obtained under the same isothermal transformation conditions, the primary difference between the two being the size of the austenite grains. With small grains, grain surface area dominates and the growth of bainite fills the interior of the austenite grains. With larger grains, the intragranularly nucleated acicular ferrite dominates. This is shown schematically in Figure 2.12 (Bhadeshia, 1990).

2. Formation Theories

The transformation of austenite to ferrite can be viewed as a competition between grain boundary and intragranular nucleation. Increasing the amount of grain boundary nucleated

products implies less intragranularly nucleated acicular ferrite. Inclusions directly influence the formation of acicular ferrite, but since they are always less effective sites for nucleation than grain boundaries (Edwards, 1990), the indirect role that grain boundary effects play must be considered. The different factors which affect acicular ferrite formation, direct and indirect, are considered next.

Although the exact mechanism of how inclusions nucleate acicular ferrite remains unknown, several influencing factors can be considered qualitatively. The chemical composition of the inclusions, to be discussed in more detail later, may play a role. Since non-metallic inclusions form principally as a result of deoxidation reactions in the weld pool, an understanding of the composition of the inclusions is important in order to understand what role, if any, chemistry plays. Extensive research has shown that the most common oxide inclusions formed contain MnO, SiO_2, Al_2O_3 and TiO_2 (Edwards, 1992). Although other oxides can form, quantitative analysis have shown that these predominate, and are thus the focus of most chemical correlation studies. Cumulative studies to date suggest that minute quantities of specific elements in the inclusions are more influential in phase transformations than the bulk composition (Edwards, 1990).

Crystallographic disregistry may also influence acicular ferrite formation. TiN, TiO, and $MnO.Al_2O_3$ (Galaxite) are known to have low planar disregistry with ferrite (values of 3.8, 3.0, and 1.8 percent, respectively). One proposal is that TiO exists on the surface of inclusions which are associated with large volume fractions of acicular ferrite. However, insufficient experimental evidence exists to support this claim. Another consideration is that some of the other constituents in these inclusions have rather high disregistry values, 16 percent for Al_2O_3, for example.(Edwards, 1990)

Thermal mismatch induced strain has also been considered as a possible influence on nucleating acicular ferrite. The thermal expansion coefficient for low carbon iron is much greater than for the inclusion constituents, of the order two to three times larger, and the resulting strain field present during the cooling cycle could have sufficient energy to favor nucleation. However, studies of this phenomenon suggest that the thermal strain effect is not a major factor in generating steel weld metal microstructures. (Edwards, 1990)

The size distribution of inclusions also may contribute to acicular ferrite nucleation. This role is not only associated with sufficient inclusions for acicular ferrite formation, but also in terms of grain size control, an indirect effect. Large numbers of small inclusions can effectively pin grain boundaries, resulting in a greater propensity for grain boundary ferrite to form.

Certain elements are known to effectively reduce the formation of grain boundary ferrite. Micro quantities of boron, for example, are known to be effective in this regard. The exact mechanism is unknown, but is thought to be related to the reduction in grain boundary energy as the tiny boron atoms rapidly migrate to austenite grain boundaries. Reduction in the number of ferrite nucleation sites, reduction in iron diffusivity or even retardation of ferrite nucleation by fine borocarbides are also possibilities. Regardless of the mechanism, the reduction in grain boundary ferrite nucleation allows for increased amounts of acicular ferrite. (Edwards, 1990)

E. NON-METALLIC INCLUSIONS

1. Origin

Inclusions can be classified into one of three groups: primary inclusions, secondary inclusions, and exogenous inclusions. Primary inclusions are formed before

solidification, secondary inclusions are formed in the supersaturated melt between dendritic arms growing during solidification, and exogenous inclusions come from sources outside the melt (Dowling, 1985). Nitrides, carbides and sulfides form from precipitation reactions as the solubility of the given species changes during solidification. The majority of inclusions formed in weld metal, however, are the result of oxidation reactions occurring between oxygen and the deoxidizers present in the weld metal or added through consumables during the welding process. Although nitrides of Al, Nb, V and Ti can have an influence in weld metal properties, oxides and, to some extent, sulfides are of primary interest (Kiessling, 1989). The intrinsic relationship between inclusions and weld metal microstructure, and thus properties, motivates the effort to better understand the nature of inclusions.

2. Chemical Composition

Oxide inclusions can be broadly classified into the general ternary system, AO-SiO_2-B_2O_3, where the A stands for one of the binary metals Mn, Fe^{2+}, Mg and Ca, and the B stands for one or several of the ternary metals Al, Cr or Fe^{3+}. The majority of inclusions in arc weldments fall into the MnO-SiO_2-Al_2O_3 system shown in Figure 2.13. It must be understood, however, that other elements, such as Ti and Zr, also form oxides such that the true representation of the inclusion may require a quaternary or higher diagram. Figure 2.14 shows the standard free energies of formation for various oxides, from where the relative order of formation can be approximated, keeping in mind the very non-equilibrium nature of the weld cycle. (Kiessling, 1978)

Inclusions in steel making, whose sizes can be of the order of tens of microns, have been extensively studied. Using microanalysis techniques, relatively detailed mapping of inclusion composition has been performed. Figure 2.15 shows

the summary of one such study of inclusions in different varieties of steel (Kiessling, 1978). This diagram shows the composition range of the inclusions studied.

In trying to transfer knowledge gained through this type of study to weld metal inclusions, however, two important factors must be kept in mind. First, detailed analysis of weld inclusions are extremely difficult due to their very small size, of the order of a fraction of a micron, which is often smaller than the limit of spatial resolution of the Energy Dispersive X-ray (EDX) microanalysis mode in the scanning electron microscope. Detailed composition determination, therefore, is often impossible. Compounding this problem is the difficulty of obtaining accurate inclusion oxygen content because of the limit of detection capability of low atomic number elements using EDX.

The second factor which makes comparison difficult is that the conditions which exist for inclusion formation are very different. Extrapolation of data from inclusions formed in near equilibrium conditions, such as found in steelmaking, to weld metal inclusions, where severe spatial and thermal gradients make equilibrium assumptions generally invalid, is risky at best.(Kiessling, 1978)

3. Role of Inclusions

While the exact chemical composition of the different inclusion phases may not be able to be determined, it is still possible to draw conclusions based on the elements present. Aluminum, for example, was found to have a negative impact on weld mechanical properties when in both low and high concentrations. The aluminum content was correlated with oxygen into an empirical deoxidation parameter, $m=[\%Al]/[\%O]^2$, and plotted versus the ductile to brittle transition temperature as shown in Figure 2.16. The optimum transition behavior occurred when m was approximately 28, which was also associated with a peak in the total number of aluminum-

containing inclusions. At levels below this, there was not enough weld metal aluminum to produce sufficient inclusions containing aluminum. At higher levels, clustering of aluminum oxides resulted in large inclusion diameters but lead to a drop in the total number of aluminum-containing inclusions. There appears, then, to be an optimal oxygen content for a given amount of aluminum to achieve a sufficient number of aluminum bearing inclusions to nucleate extensive amounts of acicular ferrite.(Grong, 1986)

Perhaps the most promising element to study is titanium. There has been considerable circumstantial evidence that titanium oxides (TiO, Ti_2O_3, and TiO_2) are very potent in nucleating acicular ferrite, while Al_2O_3 is not (Bhadeshia, 1990). Titanium nitride may also be an effective nucleant, but is less stable at high temperatures than titanium oxide. Titanium and aluminum are frequently studied together due to the synergistic roles they seem to play. Aluminum is a stronger deoxidant than titanium and reacts first in the melt followed by titanium, which then often grows as a thin coat on the aluminum oxide particles (Bhadeshia, 1990). Complicating this study is the fact that it is nearly impossible to exactly determine which titanium oxide is present in the multi-phase inclusions.

At low weld metal aluminum content, titanium seems to play a prominent role in the nucleation of acicular ferrite. Figure 2.17 demonstrates how the addition of titanium in quantities greater than 0.0045% resulted in a marked increase in acicular ferrite formation with increasing carbon equivalence. Figure 2.18 shows the relationship between acicular ferrite content and the $[\%Al]/[\%O]^2$ ratio with and without added titanium. Titanium in high concentrations, though, can lead to a deterioration in toughness thought to be associated with the precipitation of fine coherent TiN particles.(Grong, 1986)

Other researchers have found interesting results related to titanium. Evans, in his study of titanium in submerged metal arc C-Mn steel weld deposits, found that the addition of approximately 20 ppm Ti caused the modification of the microstructure from 80% ferrite sideplates to almost 70% acicular ferrite (Evans, 1991). Fox and Brothers were able to isolate a titanium rich phase called Pyrophanite, $MnO-TiO_2$, which they postulated leads to a decrease in the hardenability of the surrounding matrix and because they solidify after the weld metal the large interface strains complements the reduced hardenability in nucleating acicular ferrite (Fox, 1994).

F. SCOPE OF PRESENT WORK

The focus of this work is to attempt to obtain correlation between average inclusion composition and weld metal properties, especially acicular ferrite content, in gas metal arc and submerged arc weldments of HY-100 and HSLA-100 steel. This has been done for varying oxygen contents by varying the basicity index in SAW and the gas composition in GMAW. The ultimate goal is to gain a better understanding of the role that non-metallic inclusions play in high strength steel weld metal microstructure development and properties, and thus be able to more accurately design welding consumables to achieve desired weld metal properties.

	HY-100 NOMINAL	HY-100 MIL-S1621K	HSLA-100 NOMINAL	HSLA-100 MIL-S24645A
C	.17	0.14-0.20	0.04	0.06
Mn	.25	0.10-0.40	0.90	0.75-1.05
P	.01	0.015	0.01	0.015
S	.01	0.008	0.005	0.006
Si	.25	0.15-0.38	0.25	0.40
Cr	1.40	1.40-1.80	0.60	0.45-0.75
Ni	2.90	2.75-3.50	3.50	3.35-3.65
Mo	.40	0.35-0.60	0.60	0.55-0.65
Cu	.05	0.25	1.60	1.45-1.75
Cb	--	nil	0.03	0.02-0.06
V	.01	nil	--	--
C.E.	0.81		0.81	

C.E.=(Carbon Equivalent)

$$C.E. = C + (Mn+Si)/6 + (Ni+Cu)/15+(Cr+Mo+V)/5$$

Table 2.1. Nominal compositions of HY-100 and HSLA-100 steels in weight percent. (Czyryca, 1990)

JWS System	IIW System
Ferrite - Grain boundary ferrite - Intragranular polygonal ferrite - Ferrite side plate	Primary Ferrite - Grain boundary ferrite - Intragranular polygonal ferrite
Pearlite - Pearlite	Ferrite Carbide Aggregate - Pearlite
Acicular Ferrite - Acicular ferrite	Acicular Ferrite - Acicular ferrite
Bainite - Upper bainite - Lower bainite	Ferrite with Second Phase - Ferrite with aligned second phase - Ferrite with non-aligned second phase
Martensite - Lath martensite - M-A constituent	Martensite - Lath martensite - Twin martensite

Table 2.2. Comparison between the International Institute of Welding system and Japan Welding Society system in classification and terminology of microstructure. (Liu, 1992)

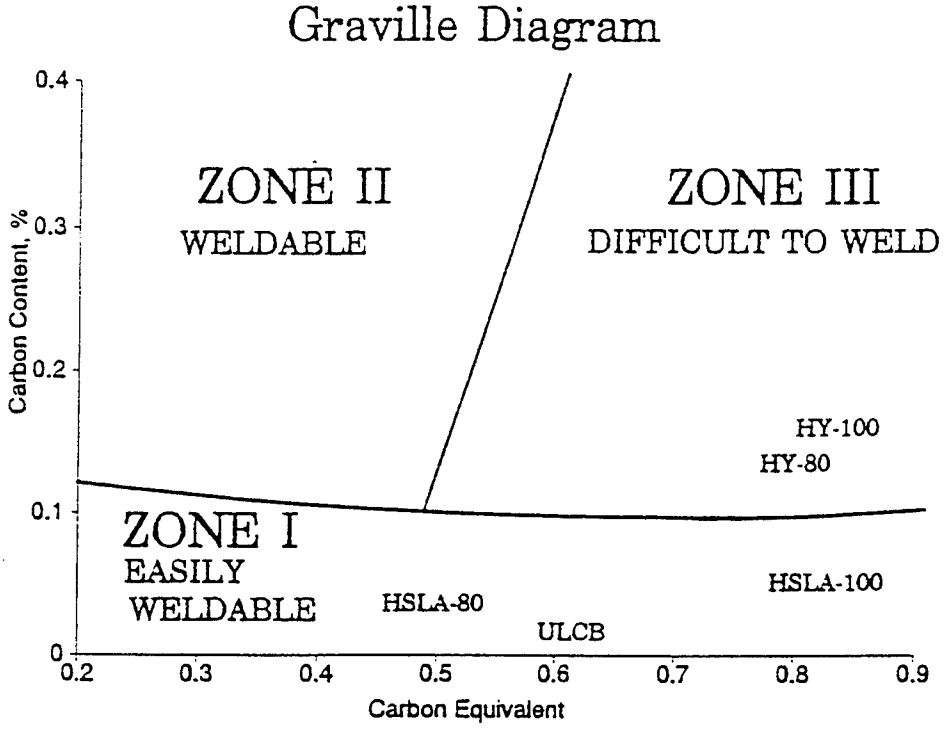

$$CE = C + \frac{Mn+Si}{6} + \frac{Ni+Cu}{15} + \frac{Cr+Mo+V}{5}$$

Figure 2.1. Graville Diagram. (Graville, 1978)

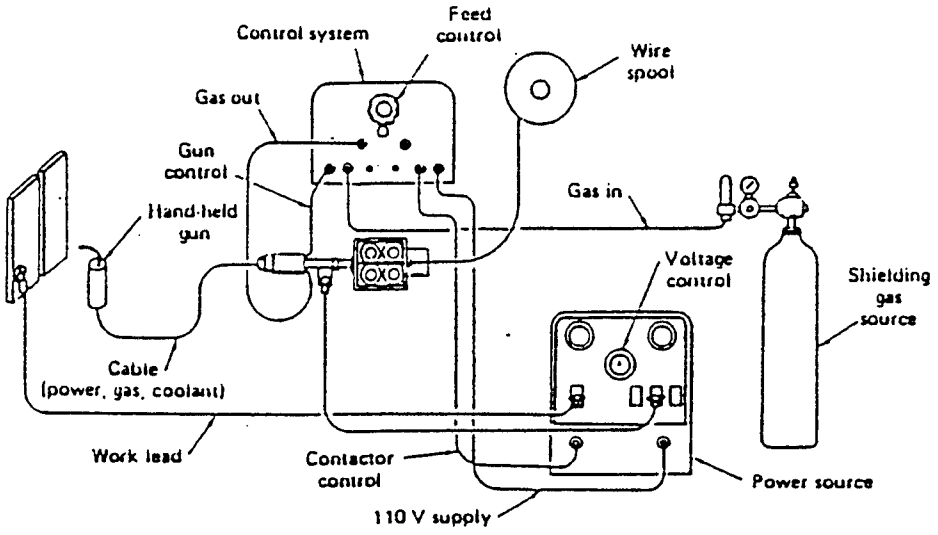

Figure 2.2. GMAW Process. (Metals Handbook, 1983)

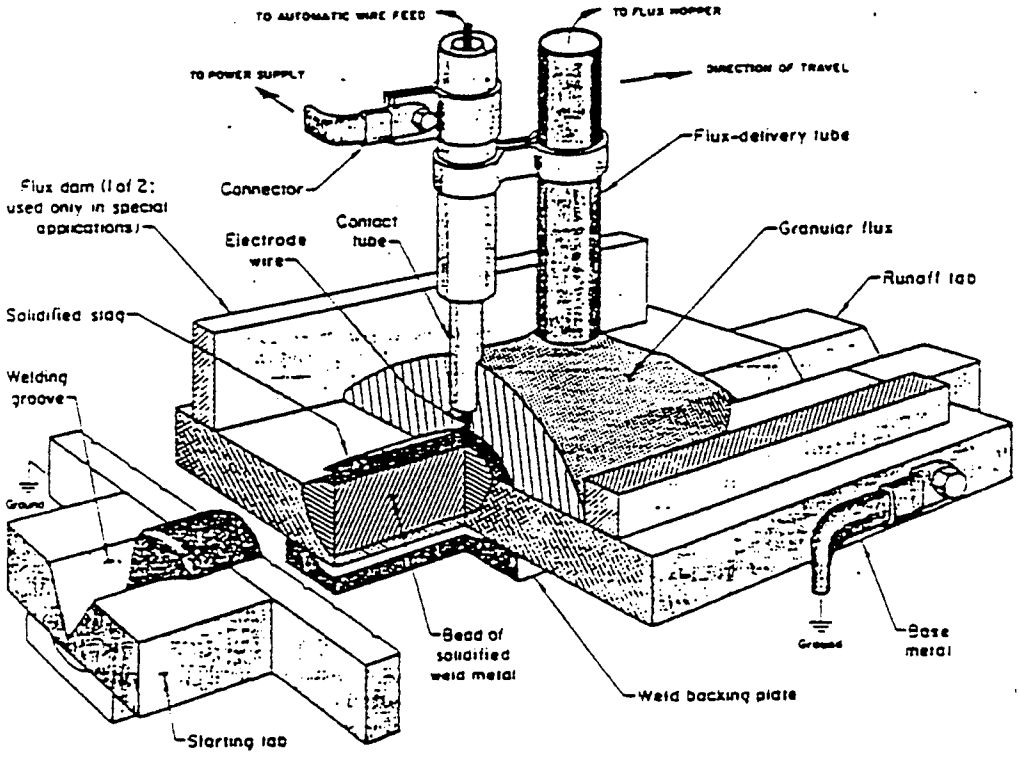

Figure 2.3. SAW Process. (Metals Handbook, 1983)

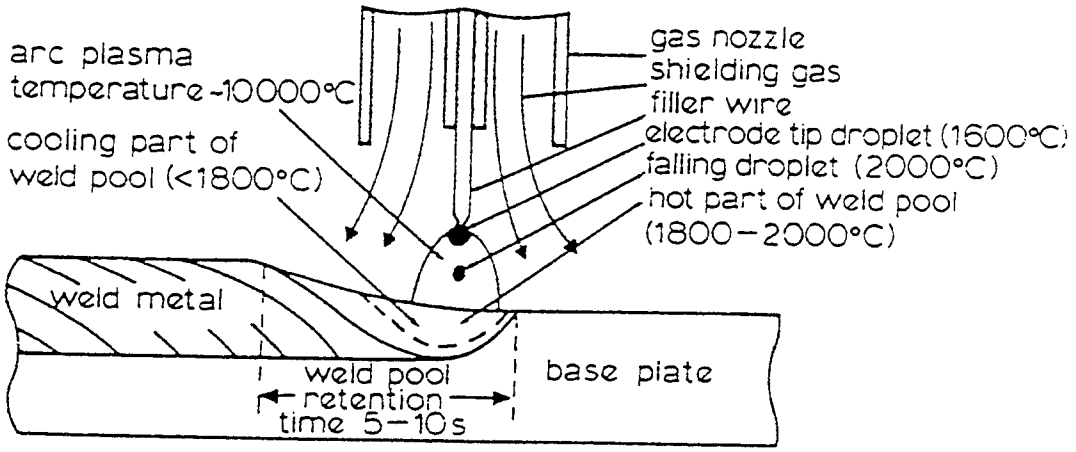

Figure 2.4. Schematic digram of main process stages in GMA welding. (Grong, 1986)

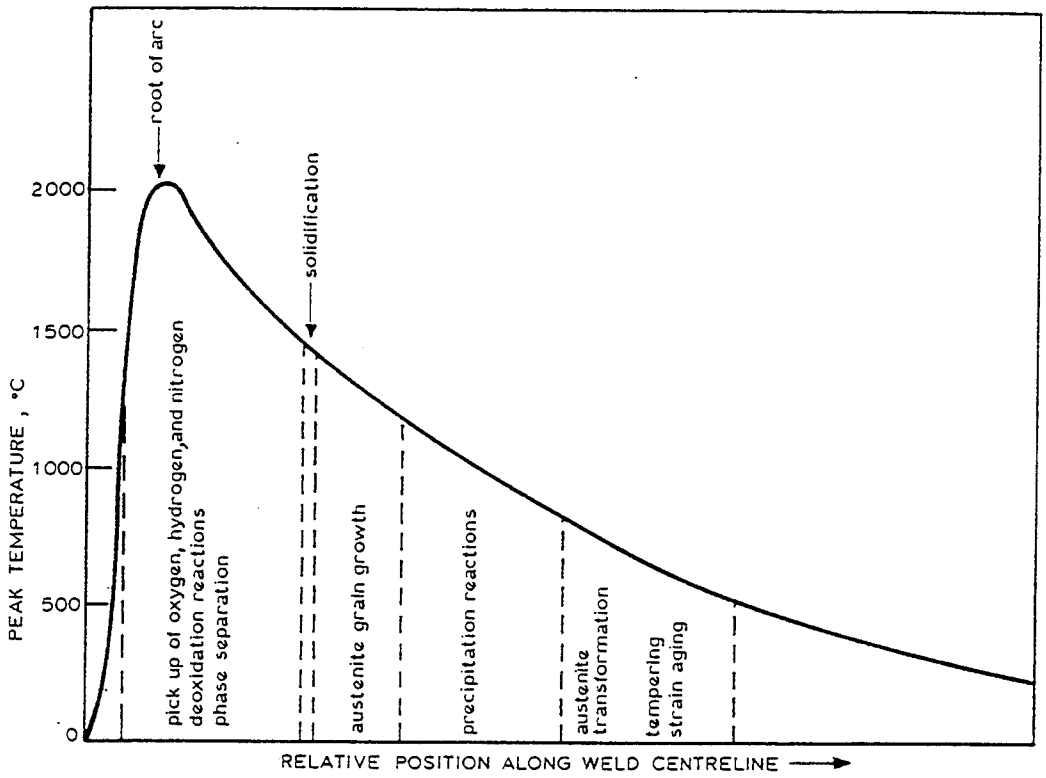

Figure 2.5. Schematic diagram illustrating weld centerline peak temperature at different distances from root of arc. (Grong, 1986)

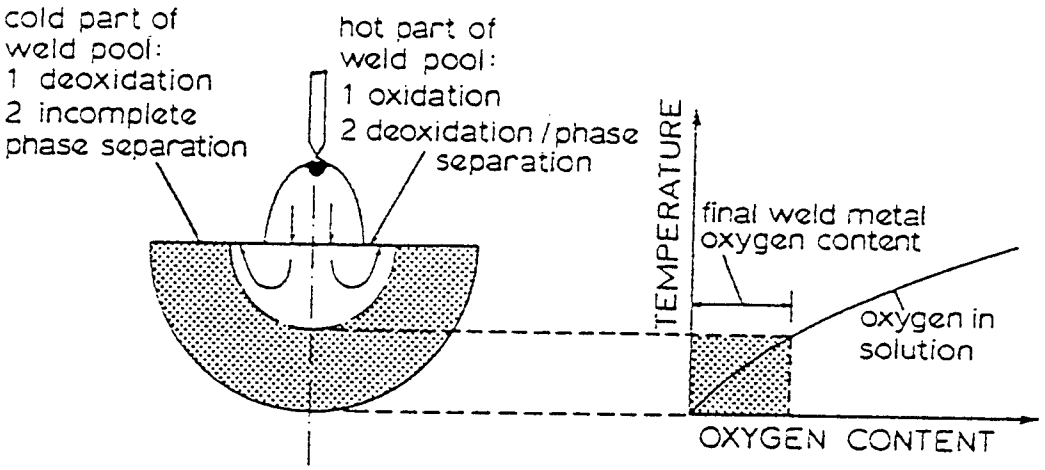

Figure 2.6. Schematic representation of sequences of deoxidation reactions occurring during cooling in weld pool. (Grong, 1986)

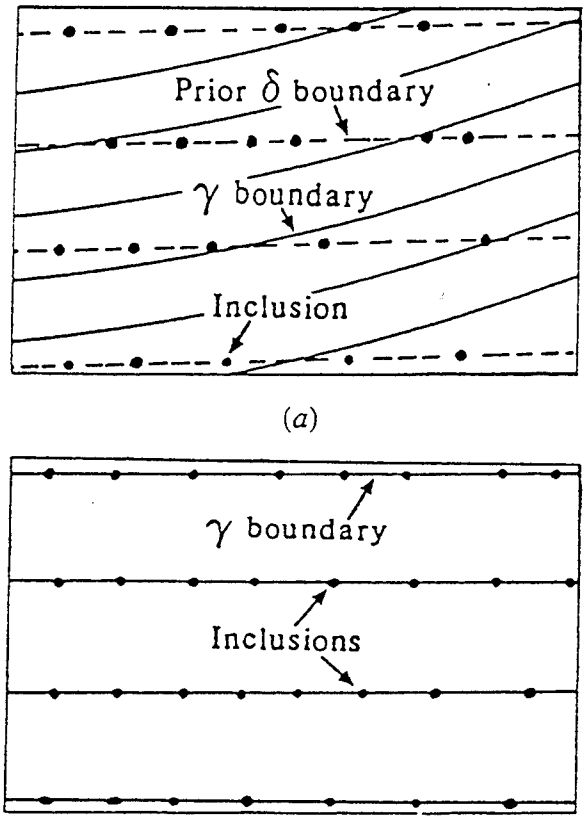

Figure 2.7. Diagram showing the location of inclusions in the microstructure of a weld for solidification as(a) δ-ferrite and (b) austenite. (Sugden, 1987)

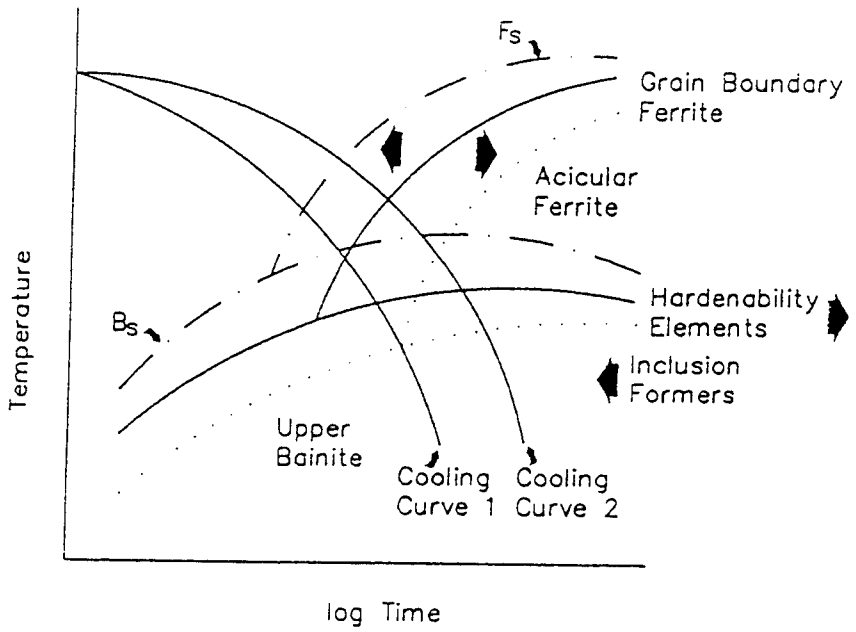

Figure 2.8. Continuous cooling transformation (CCT) diagram of an HSLA steel weld metal showing the effect of alloying elements, inclusion formers, and cooling rate. (Liu, 1992)

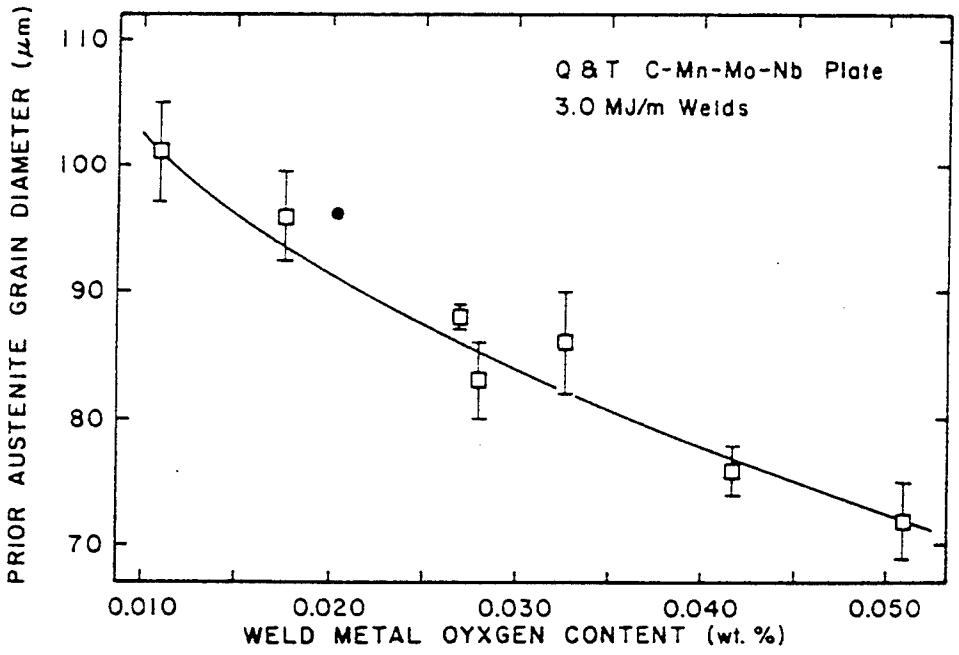

Figure 2.9. Prior austenite grain diameter as a function of weld metal oxygen content in submerged arc welds. (Kou, 1987)

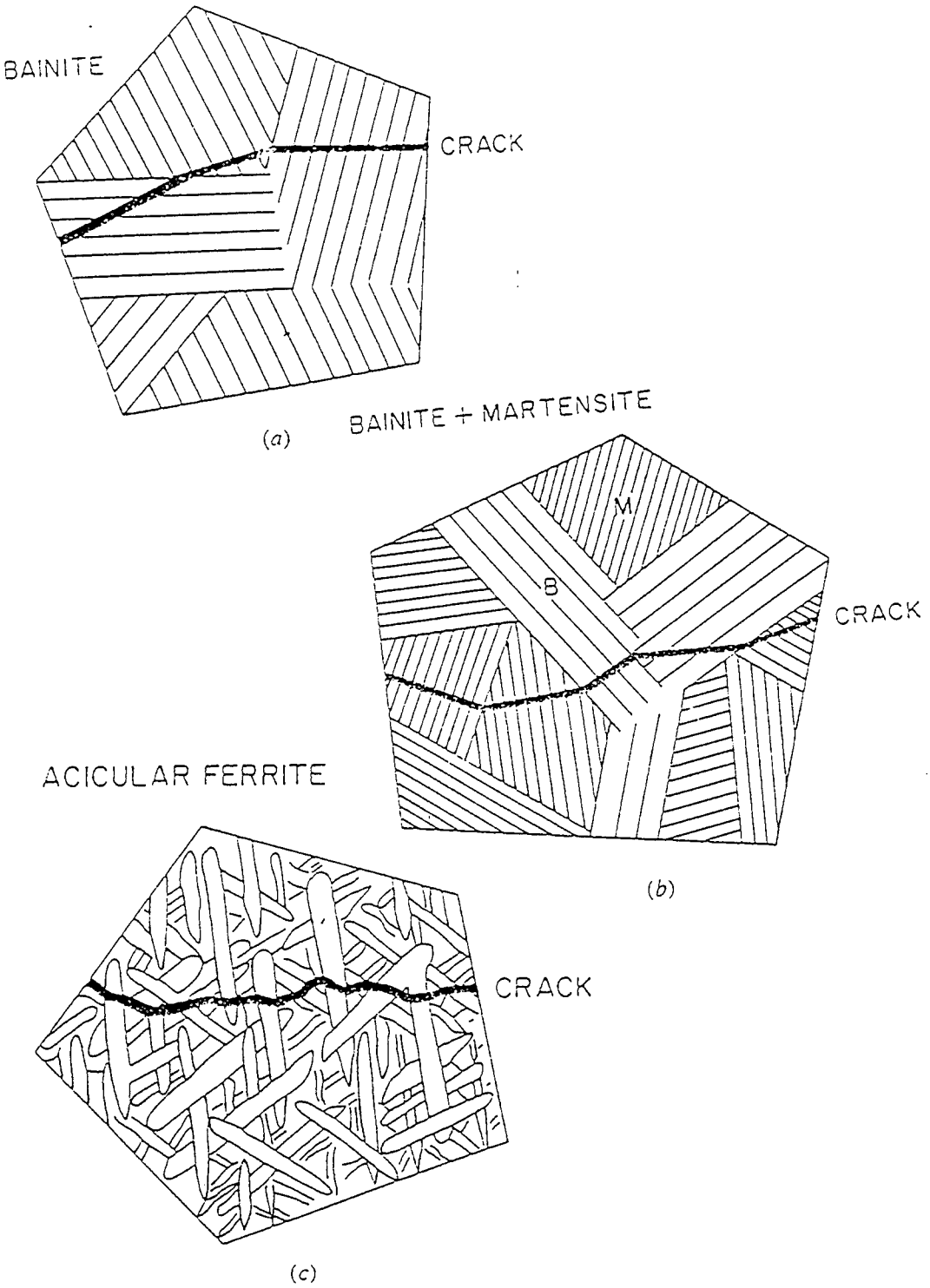

Figure 2.10. Schematic diagram showing crack propagation through (a) Bainite, (b) Bainite + Martensite and (c) Acicular Ferrite. (Edmonds, 1990)

(a)

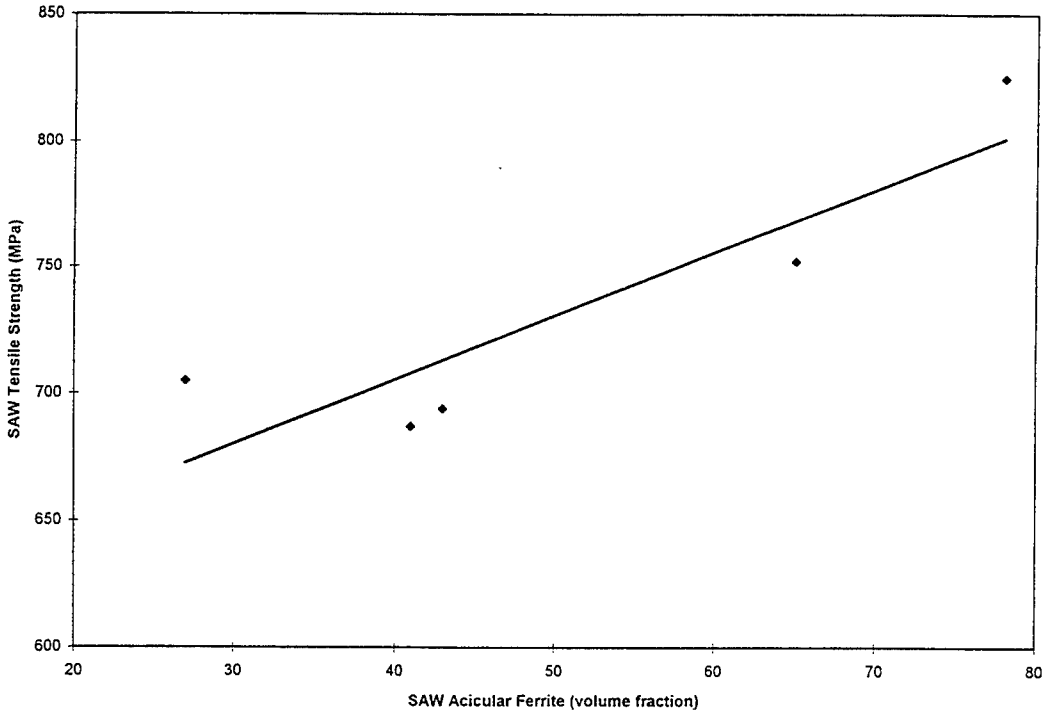

(b)

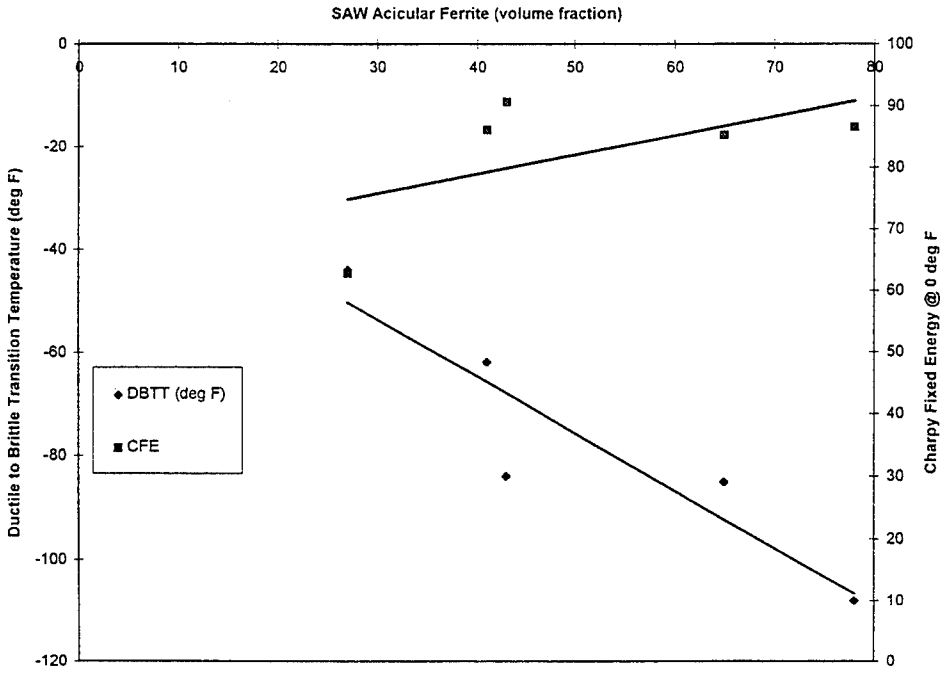

Figure 2.11. SAW (a)Tensile strength vs acicular ferrite, (b)Ductile to Brittle Transition Temperature(DBTT) and Charpy Fixed Energy(CFE @ 0 deg F) vs acicular ferrite. (Brothers, 1994)

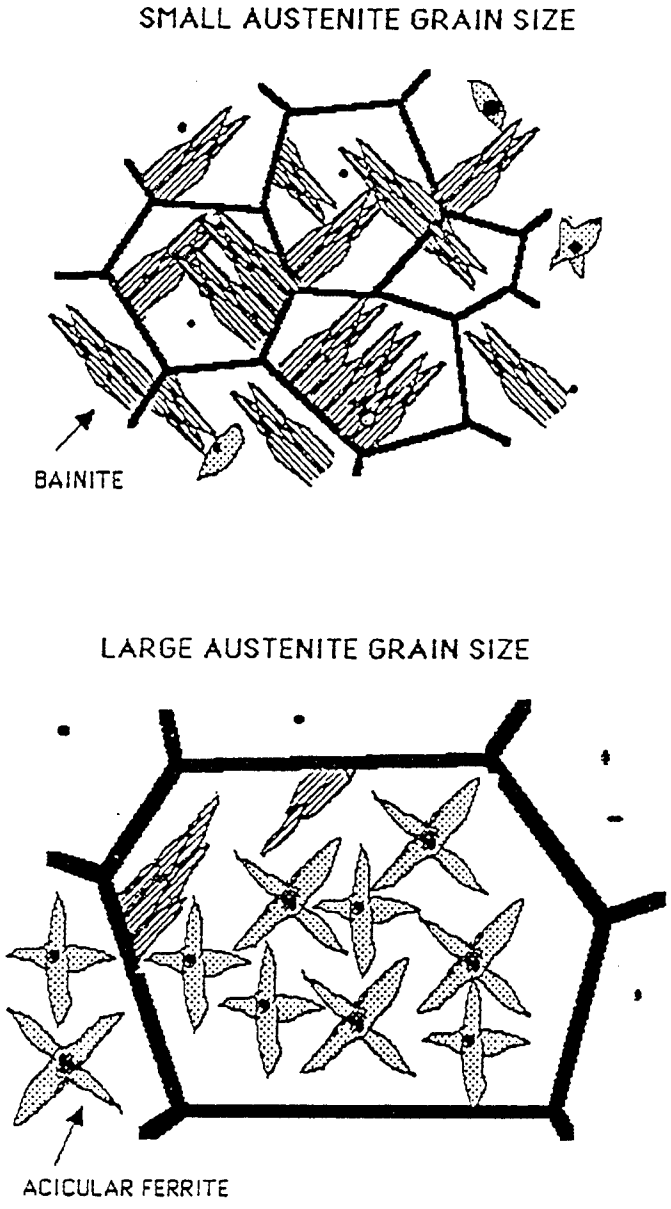

Figure 2.12. Schematic showing the effect of austenite grain size in determining whether the microstructure is predominantly acicular ferrite or bainite. (Bhadeshia, 1990)

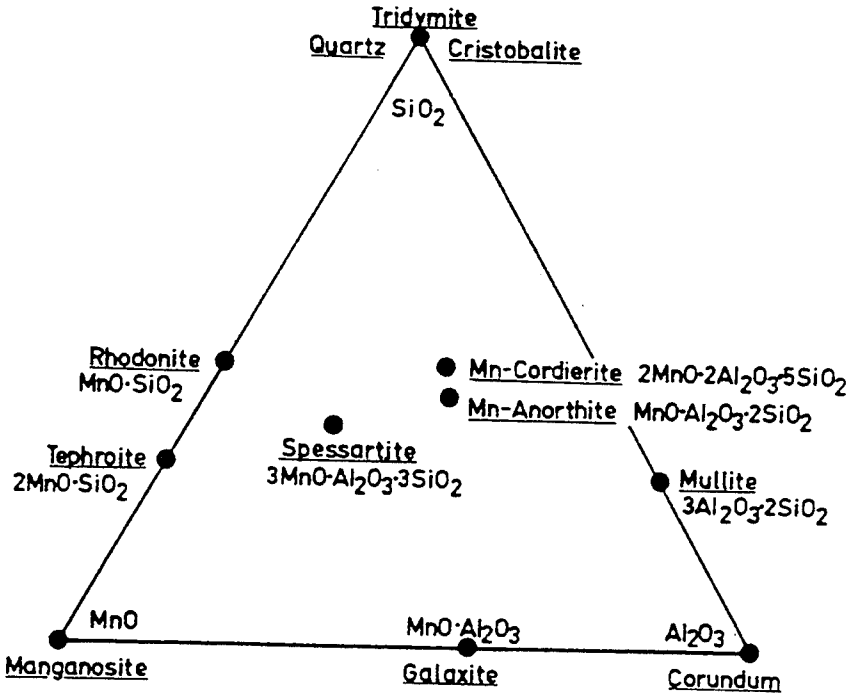

Figure 2.13. Schematic diagram of the pseudoternary system $MnO-SiO_2-Al_2O_3$. (Kiessling, 1978)

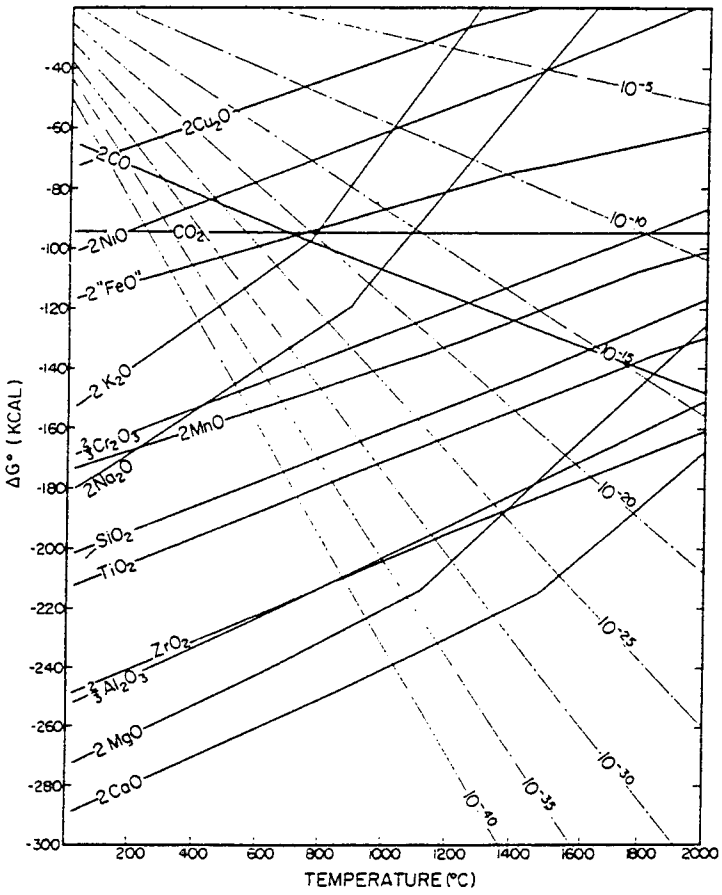

Figure 2.14. Standard free energies of formation ΔG (kcal) for various oxides of the elements as a function of temperature. (Kiessling, 1978)

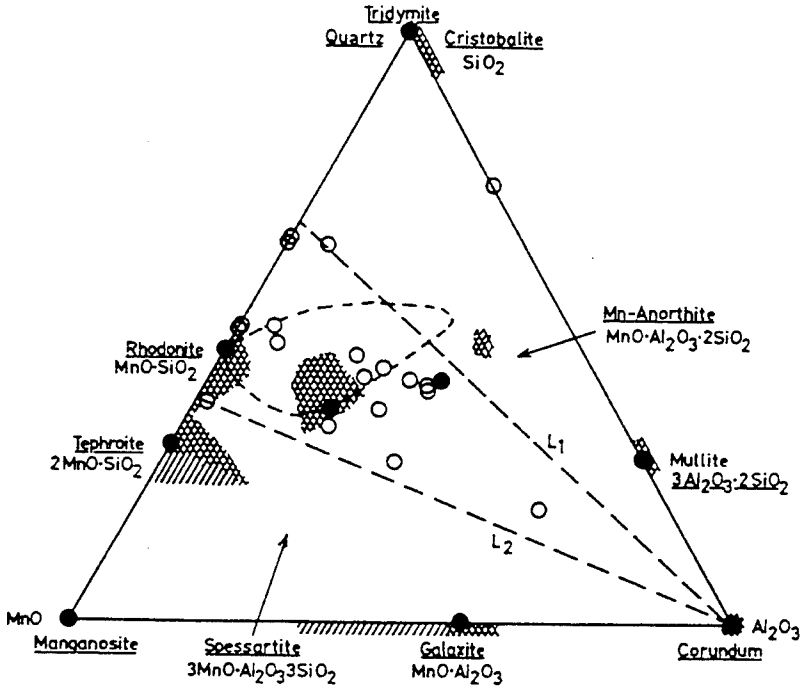

Figure 2.15. Summary of the analytical results regarding occurrence and homogeneity ranges for the different phases in the $MnO-SiO_2-Al_2O_3$ system. (Kiessling, 1978)

(a)

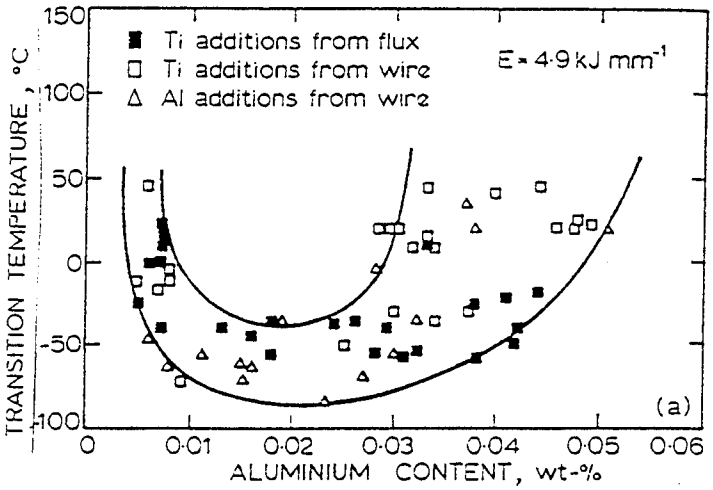

(b)

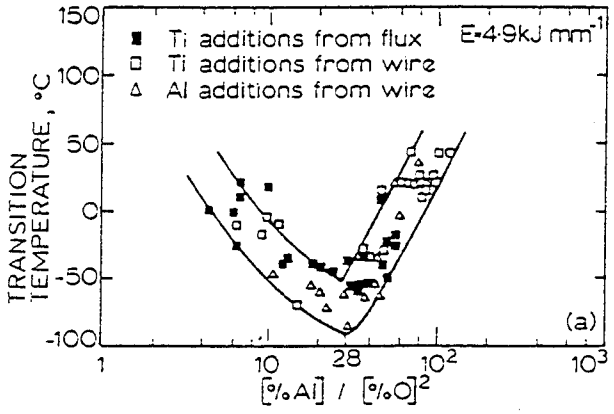

(c)

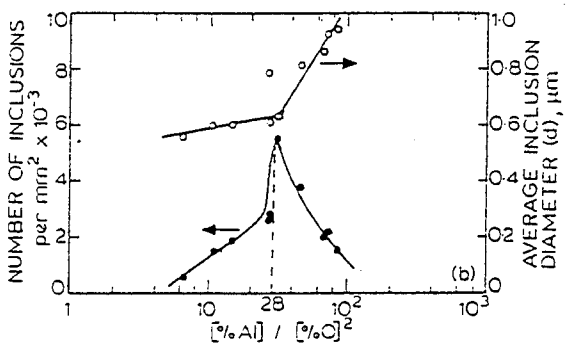

Figure 2.16. Transition temperature behavior as a function of (a) aluminum content and (b) empirical deoxidation parameter, m=[%Al]/[%O]^2. (c) Number of inclusions and inclusion size as a function of m. (Grong, 1986)

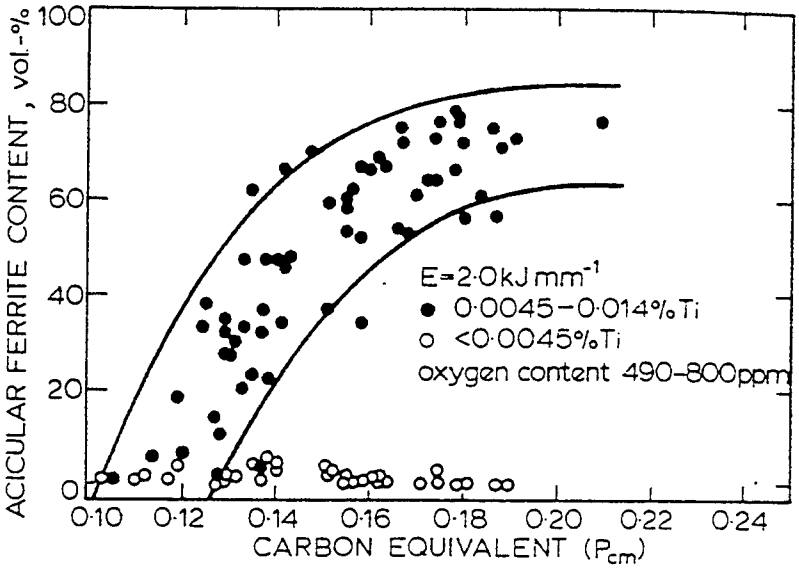

Figure 2.17. Role of Ti in the formation of acicular ferrite at low Al levels. (Grong, 1986)

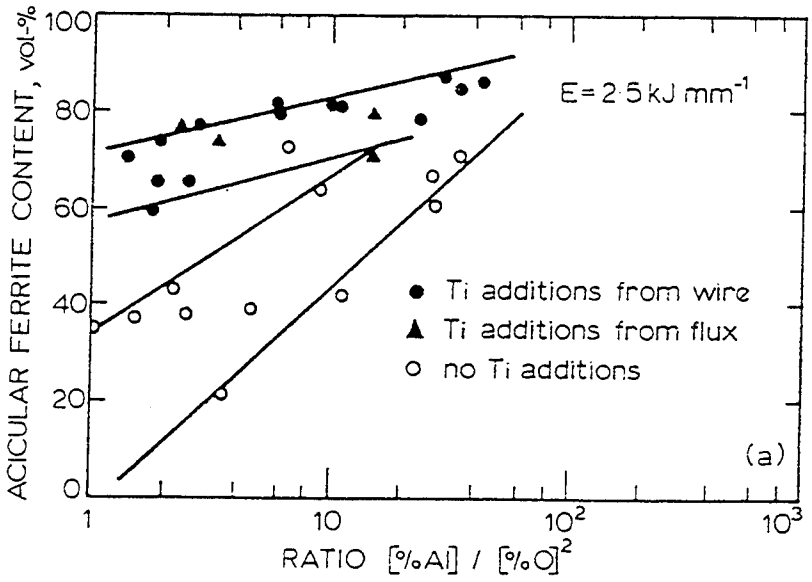

Figure 2.18. Acicular ferrite content versus $[\%Al]/[\%O]^2$ with and without Ti additions. (Grong, 1986)

III. EXPERIMENTAL PROCEDURE

A. WELD SAMPLES

The weld samples studied consisted of five SAW HY-100 weldments, seven GMAW single pass HSLA-100 weldments, and seven GMAW multi pass HSLA-100 weldments, welded by the Annapolis Detachment of the Carderock Division of Naval Surface Warfare Center (NSWC). Conditions were very carefully controlled with only the flux in the SAW and cover gas composition in the GMAW being varied. The welding control parameters are listed in Table 3.1. The basicity index for each of the SAW fluxes is listed in Table 3.2. Additional flux information is available in the Master's Thesis of K.W. Kettel from the Naval Postgraduate School (Kettel, 1993). Chemical analysis of the weldments was performed by Luvak Incorporated laboratories. Chemical analysis methods and confidence levels are listed in Table 3.3. The chemical analysis results for the SAW weldments, filler wire and base plate are shown in Table 3.4. Chemical analysis results for the GMAW base and filler wire are listed in Table 3.5, while the results for the GMAW single and multi pass weldments are shown in Table 3.6 and Table 3.7, respectively.

The cover gas for the GMAW welds was varied by the amount of oxygen (O_2) or carbon dioxide (CO_2) added to pure argon (Ar). Seven cover gas combinations were used and are shown schematically in Figure 3.1, referred to as a simplex design. The cover gas combinations uses are as follows:

- 100% Ar (Ar)
- 5% CO_2 / 95% Ar (C-5)
- 10% CO_2 / 90% Ar (C-10)
- 2% O_2 / 98% Ar (M-2)
- 4% O_2 / 96% Ar (M-4)
- 50% C-10 / 50% M-4 (C-10/M-4)
- 33.3% Ar / 33.3% C-10 / 33.3% M-4 (MIDPT).

B. SAMPLE PREPARATION

The cut and sectioned samples were ground using various grit grinding cloth and polished to one micron using diamond paste. For Scanning Electron Microscope (SEM) work, the samples were used as polished. For optical microscopy, the polished samples were etched for twelve seconds in 5% nital.

Carbon extraction replicas were made for Transmission Electron Microscope (TEM) Energy Dispersive X-ray (EDX) analysis. The samples were polished and then etched in 5% nital for 25 seconds. They were then carbon coated using a EFFA Mk II carbon coater using two carbon strands at a distance of 1.25 inches from the strand to the sample surface. The samples were then scribed in approximately three millimeter squares in the region of interest, in this case the center part of the fusion zone, and placed in a container of 5% nital with the carbon side up. After about five minutes, the carbon squares would loosen and one was then placed in a container of 20% by volume acetone in water solution where the surface tension of the solution would cause the carbon sample to straighten. The sample was finally transferred to a 400 mesh copper grid for TEM analysis.

C. SCANNING ELECTRON MICROSCOPY

A Cambridge Stereo Scan S200 scanning electron microscope with a LaB_6 filament energized to 20,000 volts was used for determining size distribution and concentration of non-metallic inclusions. Used in the backscatter mode to enhance the resolution and contrast of the inclusions, 100 fields were randomly selected from the central portion of the fusion zone and inclusion size and number were recorded. The SAW samples were analyzed at 7040 times magnification at a working distance of nine millimeters resulting in a field of view of 180 square millimeters. The GMAW samples were analyzed at

4000 times magnification at a working distances of eight millimeters for a 500 square millimeter field of view. The data collected was then analyzed to provide average inclusion size and volume fraction. Inclusion size distribution information for the SAW and GMAW single pass samples were determined in previous research, while the same information for the GMAW multi pass samples was determined in this work.

D. TRANSMISSION ELECTRON MICROSCOPY

A JEM-100 CX II transmission electron microscope with a LaB_6 filament energized to 120,000 volts was used to perform EDX analysis on inclusions in the carbon extraction replicas. Twenty inclusions chosen randomly from each sample were analyzed. Only twenty inclusions were chosen because the composition of the inclusions varied very little. The advantage of using the carbon extraction replicas in the TEM is that the carbon film will pull inclusions out of the matrix when it is lifted off the surface of the weldment. This allows for analysis of the inclusions without the interference of the surrounding steel matrix as is the case when SEM EDX is performed. The reason for this is because the "bulb of interaction" in the SEM, the volume which the electron beam interacts with and thus extracts information from, is around two microns, which is much larger than the average inclusion size of around 0.5 microns. A fair amount of collected x-ray information is thus actually from the matrix and is not necessarily representative of the inclusions.

E. OPTICAL MICROSCOPY

A Jenaphot 2000 optical photomicroscope was used to obtain optical micrographs of the microstructure of the samples. Quantitative analysis of microstructure using optical micrographs had been performed earlier and was not

repeated in this research. Micrographs taken in this study were utilized for demonstration and qualitative study.

	SAW	GMAW
Base Plate Type	HY-100	HSLA-100
Plate Thickness	1 inch	1 inch
Number of Passes	21 or 24	1 [4]
Wire Type	L-TEC 120 (HT 120022)	Airco 140-S (HT 14005)
Wire Diameter	3/32 inch	1/16 inch
Current	500 amps, DCRP	260 amps
Voltage	35 volts	28 volts (29 Volts for argon)
Weld Speed	19 in/min	9 in/min
Heat Input	55.3 KJ/in	43.6 KJ/in
Preheat/Interpass Temperature	250-275 deg F	Room Temp [150 deg C]
Cooling rate	18-23 deg F/sec at 1000 deg F	-
Shield Gas Flow Rate	None	50 ft^3/hr

Values in [] are for GMAW multi-pass welds.

Table 3.1. Welding control parameters.
(Kettel 1993, Seraiva 1993)

	BI (without CaF_2)	BI (with CaF_2)
F289	1.74	2.65
F292	1.87	2.83
F293	2.14	2.75
F295	1.93	2.63
F296	2.04	2.97

$$BI = \frac{CaO+CaF_2+MgO+Na_2O+K_2O+Li_2O+0.5(MnO+FeO)}{SiO_2+0.5(Al_2O_3+TiO_2+ZrO_2)}$$

BI based on Easterling and Eagar relationships (Kou, 1987).

Table 3.2. Basicity index for SAW fluxes. (Kettel, 1993)

ELEMENT	METHOD OF ANALYSIS	CONFIDENCE LIMIT +/- wt%
Carbon	Combustion Infrared	0.001
Manganese	Plasma Emission	0.02
Silicon	Plasma Emission	0.01
Phosphorus	Plasma Emission	0.002
Sulfur	Combustion Automatic Titration	0.001
Nickel	Plasma Emission	0.05
Molybdenum	Plasma Emission	0.01
Chromium	Plasma Emission	0.02
Vanadium	Plasma Emission	0.001
Aluminum	Plasma Emission	0.002
Titanium	Plasma Emission	0.001
Zirconium	Plasma Emission	0.001
Copper	Plasma Emission	0.001
Oxygen	Inert Gas Fusion, TC136	0.001
Nitrogen	Inert Gas Fusion, TC136	0.001
Boron	Plasma Emission	0.001
Hydrogen	Vacuum Hot Extraction	0.00001
Niobium	Plasma Emission	0.001

Information provided by Luvak, Inc.

Table 3.3. Chemical analysis methods. (Gibson, 1992)

	FILLER	BASE	F289	F292	F293	F295	F296
C	.081	.157	.062	.062	.056	.064	.064
Mn	1.57	.33	1.45	1.49	1.28	1.51	1.54
Si	.40	.30	.38	.46	.42	.28	.34
P	.004	.003	.007	.005	.004	.015	.008
S	.006	.005	.010	.006	.006	.011	.007
Ni	2.25	2.79	2.33	2.56	2.51	2.34	2.34
Mo	.42	.36	.46	.52	.47	.47	.49
Cr	.28	1.46	.25	.43	.40	.47	.50
V	.001	.006	.003	.003	.002	.004	.003
Al	.012	.018	.013	.020	.011	.011	.014
Ti	.014	.004	.006	.008	.004	.005	.006
Zr	.012	0.0	.003	.003	.003	.002	.004
Cu	.011	.097	.020	.023	.017	.021	.026
O	.003	.0054	.030	.027	.034	.035	.032
N	.004	.016	.007	.006	.006	.009	.006
B	.004	.001	.004	.003	.004	.004	.001
H*	2.8	1.1	0.2	0.4	0.4	0.3	0.8

* All values given in weight percent (wt%) except H in ppm. Note that 0.03 wt% equals 300 ppm.

Table 3.4. SAW samples base plate, filler wire, and weld metal chemical composition. (Kettel, 1993)

	FILLER WIRE	BASE
C	.079	.075
Mn	1.518	.793
Si	.428	.365
P	.005	.010
S	.002	<.001
Ni	2.518	3.307
Mo	.852	.587
Cr	.746	.543
Nb	<.001	.024
V	.003	.003
Al	.007	.020
Ti	.016	.004
Zr	.005	<.001
Cu	.034	1.633
O	.014	.002
N	.004	.011
B	.004	.003
H*	N/A	.3

* All values in weight percent (wt%) except H in ppm. Note that 0.014 wt% oxygen is 140 ppm.

Table 3.5. GMAW base metal and filler wire chemical composition. (Gibson, 1992)

	Ar	M2	MIDPT	C5	M4	C10	M4/C10
C	.068	.066	.070	.069	.064	0.70	.066
Mn	1.193	1.132	1.098	1.072	1.033	1.032	1.045
Si	.412	.383	.366	.353	.325	.332	.342
P	.008	.009	.009	.008	.008	.008	.006
S	.0002	.0005	.001	.0002	.0008	.001	<.001
Ni	2.873	2.787	2.895	2.882	2.812	2.915	2.858
Mo	.78	.765	.757	.765	.768	.760	.737
Cr	.698	.665	.682	.690	.653	.682	.670
Nb	.016	.015	.015	.016	.014	.015	.015
V	.003	.003	.003	.003	.003	.003	.003
Al	.015	.011	.010	.011	.008	.010	.010
Ti	.013	.008	.007	.007	.006	.006	.006
Zr	<.001	<.001	<.001	<.001	<.001	<.001	<.001
Cu	.74	.713	.72	.767	.688	.823	.800
O	.003	.019	.019	.026	.022	.026	.024
N	.006	.008	.008	.008	.008	.009	.008
B	.004	.004	.004	.004	.004	.004	.005
H*	.35	.45	.412	.40	.40	.417	.383

*All values in weight percent (wt%) except H in ppm.
Note that .014 wt% oxygen is 140 ppm.

Table 3.6. GMAW (SINGLE pass) weld metal chemical composition. (Gibson, 1992)

	Ar	M2	MIDPT	C5	M4	C10	M4/C10
C	.068	.063	.063	.075	.055	.069	.063
Mn	1.28	1.22	1.11	1.14	1.20	1.12	1.17
Si	.38	.32	.34	.34	.32	.32	.31
P	.005	.005	<.004	.008	<.004	.008	.004
S	.004	.002	.003	.003	.003	.002	.003
Ni	2.43	2.44	2.42	2.56	2.43	2.42	2.60
Mo	.69	.71	.70	.72	.79	.74	.73
Cr	.68	.68	.65	.66	.71	.65	.73
V	.003	.003	.003	.003	.003	.003	.003
Cb	.013	.014	.013	.014	.011	.012	.011
Cu	.38	.35	.44	.60	.22	.32	.30
Al	.006	.006	.007	.008	.005	.005	.004
Ti	.013	.009	.008	.009	.009	.010	.008
O	.0067	.028	.018	.019	.023	.027	.027
N	.0062	.0049	.0085	.0051	.0062	.0047	.0058
H*	0.4	0.5	0.6	0.7	0.9	0.3	0.7

*All values in weight percent (wt%) except H in ppm.
Note that .014 wt% oxygen is 140 ppm.

Table 3.7. GMAW (MULTI pass) weld metal chemical composition.

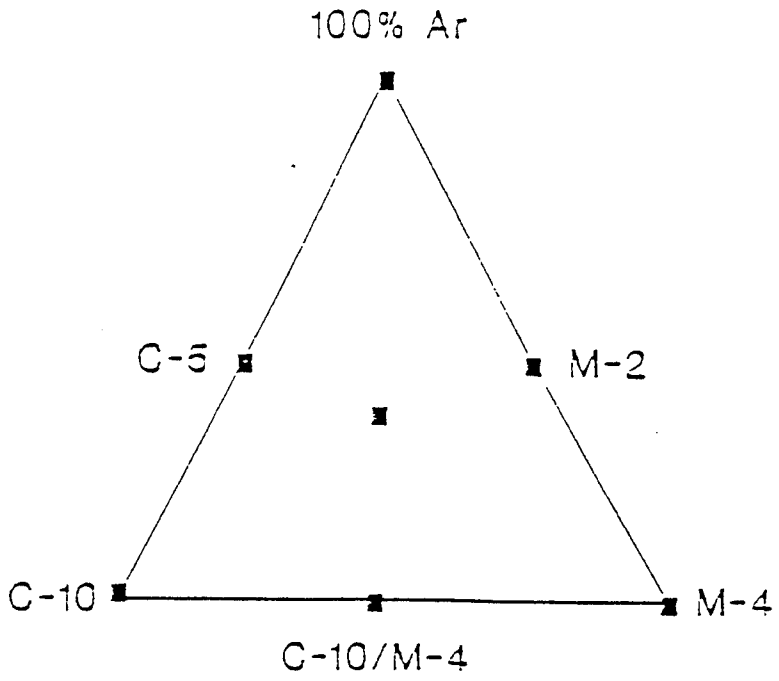

Figure 3.1. Diagram of shielding gas combinations.

IV. RESULTS AND DISCUSSION

A. WELD METAL CHEMISTRY

The chemistry of the weld metal, as presented in Tables 3.4 to 3.7, was analyzed in an attempt to find correlation between the welding consumables and the resulting chemistry. In the case of GMAW, the cover gas oxygen content was varied. In the case of SAW, different fluxes were used. Inclusion correlation and acicular ferrite analysis are discussed in later sections.

1. GMAW

The amount of oxygen in the cover gas was calculated assuming 100% activity for oxygen added and 75% of the oxygen from the complete dissociation of carbon dioxide added (Brothers, 1994). Figure 4.1 shows that the calculated oxygen activity is a fairly good indicator of weld metal oxygen content. This is an important result as it demonstrates that weld metal oxygen behavior can be reasonably assessed using known cover gas oxygen information.

Weld metal Al, Ti, Mn and Si plotted against both cover gas oxygen and weld metal oxygen are shown in Figures 4.2 and 4.3 for the single pass welds. Aluminum and titanium contents drop sharply with increasing oxygen, while manganese and silicon drop off more slowly. This is expected as the increasing oxygen reacts with the stronger deoxidizers, Al and Ti, first and then with the weaker deoxidizers, Mn and Si. Some of the deoxidation products then are carried to the surface as slag where they are removed. At low levels of oxygen, Al and Ti will dominate the deoxidation reactions and relatively more of these elements will be removed from the weld metal as compared to Mn and Si. At higher oxygen levels, Mn and Si participate to a greater relative degree and are removed in increasing amounts from the weld metal.

Figures 4.4 and 4.5 show the same plots as above for the multiple pass welds. There is more data scatter and the overall trend as described above is not as clear. This is most likely due to the complicated effects of multiple pass welding, where remelting of prior passes releases additional inclusions, floats out previously formed inclusions and reduces the amount of the different reactants in a less predictable fashion.

2. SAW

Due to the complex nature of the flux systems used, there is no easy way of quantifying the flux so as to readily infer what the resulting weld chemistry or other properties will be. As discussed earlier, the Basicity Index (BI) is the preferred measure of describing a particular flux. Of particular interest is just how the weld metal oxygen varies with the different fluxes used. Figure 4.6 shows that there is a slight correlation between oxygen in the weld metal and BI, where oxygen appears to decrease somewhat with increasing BI. This is in agreement with other studies, where there was noted a large reduction in oxygen content with increasing BI for acidic fluxes, but a fairly constant oxygen level with increasing BI in basic fluxes (Abson, 1986). Thus, BI does not appear to offer a good means to assess oxygen behavior in the weld metal in this study.

The complex chemical reactions occurring between the flux, weld wire and base plate result in the release of the oxygen in the flux where it either enters deoxidation reactions which form inclusions, which either float away or are trapped in the weld metal, or remains uncombined in the weld metal. The weld metal oxygen analyzed does not distinguish between oxygen in inclusions or in the weld metal. This is one of the principle difficulties in trying to understand the role that oxygen plays in microstructural development.

Oxygen correlates with Al, Ti, Mn and Si in almost the same fashion as it did in the GMAW samples. In Figure 4.7, Al, Ti and Si drop with increasing oxygen, but Mn stays pretty constant, except for the sample (F293) where the MnO was low in the flux (0.051 wt% compared to 0.8 to 2.5 wt% in the other fluxes, Kettel, 1993). When these elements are plotted against BI, as in Figure 4.8, there is a slight correlation and, as expected, Al, Ti and Si increase with the BI, but the correlation coefficient is poor. Mn stays fairly constant, with the exception of sample F293 for reasons discussed above.

B. INCLUSION COMPOSITION AND SIZE

Inclusion composition data for the GMAW and SAW samples are presented in Tables 4.1 to 4.19. Table 4.20 contains the inclusion count, size and volume fraction information for the samples, while the inclusion size distribution for GMAW single pass and multiple pass and SAW samples is presented in Tables 4.21,4.22 and 4.23, respectively.

1. GMAW

a. Inclusion Chemistry

Figures 4.9 and 4.10 show inclusion Al, Ti, Mn and Si plotted against cover gas oxygen and weld metal oxygen for the GMAW single pass samples. While there is large data scatter for the inclusion titanium, the inclusion aluminum values drop with increasing oxygen while the manganese and silicon values rise. This is expected and agrees with the earlier discussion of weld metal element behavior. With increasing oxygen levels, the more reactive elements, aluminum and titanium, will be consumed allowing the less reactive elements, manganese and silicon, to participate to a greater degree in the deoxidation reaction, increasing their relative percentage of inclusion composition. It must be pointed out that even though manganese is not very reactive with oxygen as compared with the other elements, it will dominate the inclusion

composition because it is more abundantly present in the base metal and filler wire.

The same parameters plotted for the GMAW multiple pass samples are shown in Figures 4.11 and 4.12. As in the weld metal chemistry results, there is considerable scatter, although the trends are similar to the single pass samples. When plotted against cover gas oxygen, the local behavior of the elements do correlate as discussed above, where increasing Al and Ti is associated with decreasing Mn and Si and vice-versa. This local trend is also apparent in the plots with weld metal oxygen.

The large amount of scatter in these multi run data is most likely due to the random nature of inclusion selection for sampling. As opposed to single pass welding, multiple pass weldments will contain different regions, varying from zones completely remelted to prior passes becoming heat affected zones of subsequent passes. This results in a range of conditions existing in a small region of the weld. Here, for example, a remelted region, where previously formed inclusions could float out, may lie adjacent to an HAZ, where previously formed inclusions are still trapped but can undergo further reactions at the elevated temperature. These varying conditions will have a pronounced effect on the inclusion composition, and the sampling procedure did not attempt to select inclusions from a particular weld zone in a given part of the weld pass.

b. Inclusion Size

Taking into account both the average diameter and number of inclusions, volume fraction provides a convenient way to quantify the effect of the "size" of inclusions on other parameters. Even though neither the spatial distribution nor inclusion size distribution, each important factors, are specifically delineated in the volume fraction, it still serves as an important measure. Volume fraction of

inclusions for both single pass and multiple pass weld samples plotted against cover gas oxygen and weld metal oxygen is shown in Figures 4.13 and 4.14. The volume fraction is smaller for multiple pass welds than for single pass welds. Table 4.20 shows that multiple pass inclusions have a smaller average diameter, yet a larger inclusion count for the same number of fields analyzed. Since volume fraction is determined from area fraction, assuming the area fraction can be linearly scaled to volume fraction, the squared term in area determination offsets the larger number of inclusions counted per field.

The reason that multiple pass welds have a smaller average inclusion size than single pass welds is most likely due to losses of larger inclusions on subsequent passes and formation of new smaller ones. Since larger inclusions will tend to rise to the surface of the weld more easily than smaller inclusions, reducing the quantity of these inclusions will result in a lower average size. Subsequent passes where oxygen is reintroduced into the remelted weld pool can result in the nucleation and growth of additional oxide inclusions. Thus, the removal of larger inclusions and the formation of additional inclusions on subsequent passes could give lower average inclusion sizes and larger numbers of inclusions in multiple pass welds.

Increases in oxygen should result in more and larger inclusions, which lead to a larger volume fraction. This effect is shown in Figures 4.13 and 4.14 to a limited degree. A general increase in volume fraction is seen for both single and multiple pass welds, showing a more pronounced relation in multiple pass welds, but there is significant data scatter. For multiple pass welds, as shown in Figure 4.15, mean inclusion size shows a stronger correlation with oxygen than does the number of inclusions. For single pass welds, Figure

4.16 shows that there is very little correlation if the argon (negligible oxygen) sample is ignored.

One point to keep in mind in this discussion is the fact that the inclusion size information was gathered from the central portion of the weld samples. The oxygen information, on the other hand, is more representative of the average weld conditions. If oxygen information could be directly gathered from the same region as inclusion size information, a stronger correlation might be obtained. It appears, then, that GMAW multiple pass welds show a stronger correlation with oxygen than GMAW single pass welds. This may be due to the remelting and thus homogenization.

2. SAW

a. Inclusion Chemistry

The inclusion elements behave the same with increasing oxygen in the SAW weld samples as was discussed for the GMAW samples. In Figure 4.17, aluminum and titanium drop while manganese and silicon rise as the oxygen content is raised. When plotted against BI, though, no clear correlation is apparent, as demonstrated in Figure 4.18. This is no doubt because of the large amount of scatter.

b. Inclusion Size

Figure 4.19 shows that there is no apparent correlation between volume fraction and either oxygen or BI. The volume fraction is fairly uniform, with the exception of that for sample F296. When inclusion size and count are plotted against oxygen and BI, as in Figure 4.20, there is still no definite trend, although inclusion size appears to increase slightly with increasing BI. This apparent trend and the behavior of sample F296 remain unexplained.

The lack of expected oxygen and inclusion size correlation might be related to the complex nature of flux decomposition. How the flux decomposes to release oxygen and

the extent that the resulting oxygen participates in deoxidation reactions is not well understood. Add to this the complexity of multiple pass welding and the uncertainty in the relative apportioning of the measured oxygen between the inclusions and that dissolved in the weld metal, as discussed earlier, it is understandably difficult, if not impossible, to achieve a straightforward correlation.

C. ACICULAR FERRITE

1. GMAW

Since the most desirable microstructure is acicular ferrite, particular attention was placed on seeking correlation with inclusion chemistry and size information. Acicular ferrite quantification of the GMAW and SAW samples was performed in a previous study and the data is presented in Table 4.24. Since there is essentially no acicular ferrite in the argon cover gas samples, they were ignored. Figure 4.21 shows acicular ferrite plotted against inclusion titanium and aluminum for the single pass samples. Acicular ferrite appears to decrease slightly with increasing inclusion Ti and Al. This is surprising because we usually associate increased Ti in inclusions with increasing acicular ferrite. However, in this case increasing the Ti decreases the oxygen away from values appropriate to the formation of acicular ferrite.

When plotted against weld metal oxygen and inclusion volume fraction (Figure 4.22), some correlation is found with oxygen and a stronger one for volume fraction. Figure 4.23 shows a plot of acicular ferrite versus weld metal oxygen multiplied by volume fraction. A stronger correlation is evident emphasizing the role that volume fraction and oxygen play in the growth of acicular ferrite. Repeating the above plots with the multiple pass samples (Figures 4.24, 4.25 and 4.26) revealed a similar relationship between acicular ferrite

and the other parameters; however, there is quite a bit of data scatter.

In general, an oxygen content of around 250-300 ppm with an average inclusion size of around 0.3 to 0.5 microns and a cooling time through the austenite to ferrite transformation region (called the $dt_{8/5}$ for the time to cool from 800 to 500 degrees C) of between 5 and 30 seconds is optimal for maximum acicular ferrite formation (Brothers, 1994). The GMAW samples had a lower oxygen content, a larger average inclusion size and a $dt_{8/5}$ of around 6 to 8 seconds. Despite the large amount of data scatter in the results, there is evidence of the expected effects of chemistry. However, the correlation is very weak. Inclusion chemistry may play an important role in the nucleation of acicular ferrite, but unless the inclusion density is great enough and spatial distribution within the weld metal is sufficiently uniform to allow the growth of these grains into an interlocking matrix, there will be minimal amounts of acicular ferrite. Such appears to be the case with the GMAW samples, with fewer and larger inclusions than desired. An additional point to keep in mind is the fact that variation of acicular ferrite between samples was not very large, making assessment as a function of chemistry difficult.

In summary, the relative insensitivity of acicular ferrite content in the GMAW samples to inclusion chemistry, yet notable sensitivity to inclusion volume fraction, lies more with the growth of acicular ferrite than with its formation. The $dt_{8/5}$ was also on the low end of the optimal cooling time range. Had the inclusion size distribution been optimal for growth of acicular ferrite, a stronger correlation would perhaps have been found with inclusion chemistry.

2. SAW

To test the above theory on acicular ferrite formation and growth, the SAW samples proved to be ideal candidates due to the larger volume fractions of acicular ferrite, the near optimal inclusion volume fractions and sizes and a $dt_{8/5}$ of about 16 seconds, right in the middle of the desired band. This would infer that inclusion chemistry would get to "play" in a clearer manner, since the conditions for growth of acicular ferrite were already established.

Comparing acicular ferrite content to inclusion volume fraction and weld metal oxygen (Figure 4.27) shows almost no correlation with volume fraction and a slight correlation with oxygen, where acicular ferrite seems to decrease with increasing oxygen, opposite to the trend in the GMAW samples. When compared to inclusion aluminum, titanium and manganese (Figures 4.28 and 4.29), acicular ferrite shows some degree of correlation, where it increases with titanium and aluminum and decreases with manganese content. Increasing inclusion aluminum and titanium with decreasing manganese content is associated with decreasing oxygen, as is demonstrated in Figure 4.17. When plotted against BI (Figure 4.30), an apparent correlation exists. Since no apparently simple correlation exists between BI and inclusion chemistry (see Figure 4.18) or inclusion size and count (see Figures 4.19 and 4.20), yet a relatively strong one exists with acicular ferrite, which requires inclusions for its existence, there has to be a connection of some sort.

This can be better understood by considering a schematic diagram of acicular ferrite versus weld metal oxygen (Figure 4.31). The optimal oxygen content for maximum acicular ferrite is approximately 270 ppm. At oxygen levels below this value, which characterize the GMAW samples, acicular ferrite increases with increasing oxygen and decreasing Ti and Al. The SAW samples, on the other hand, are on the "high" side of

the curve where acicular ferrite increases with decreasing oxygen and increasing Ti and Al.

Reviewing the SAW sample inclusion composition and size information (Tables 4.15 to 4.20) and assuming that a two-step process is involved in acicular ferrite formation (nucleation as a function of chemistry and growth as a function of inclusion volume fraction), an index was developed to connect these two processes into the final product: the measured volume fraction of acicular ferrite. Called the Acicular Ferrite Index (AFI), it is defined as:

AFI=(Al+Ti+Zr)/(Mn+Si)*Volume Fraction of Inclusions,

with the inclusion elements in weight percent. This index measures the chemistry portion of acicular ferrite nucleation as well as the acicular ferrite growth stage. Figure 4.32 shows acicular ferrite plotted against the AFI, where a very strong correlation exists. When BI is plotted against this same parameter, an almost equally strong relationship exists (Figure 4.33).

This index is important because it shows a relationship between inclusions and acicular ferrite and also ties in the seemingly unrelated BI. Notably, oxygen is not represented directly in this index. This is a key point in that the measured weld metal oxygen is an average value, while the inclusion composition, size information and acicular ferrite content are taken from a specific area (central portion) of the weld in these samples. While oxygen may not be directly accounted for, it is indirectly represented in the inclusion element weight percent ratio. This ratio of strong deoxidizers to weaker deoxidizers can be used without knowing the exact way or ways that titanium actually reacts with oxygen, which is the major unknown.

In order to correlate the acicular ferrite in GMAW welds with inclusion composition, one would have to use an index where the deoxidizer ratio is the reciprocal of that for the

SAW weldments. This was tried, but because of the small amounts of acicular ferrite in the GMAW samples, and the rather large amount of scatter, only a very weak correlation was found. This apparently limits the usefulness of the Acicular Ferrite Index to instances where the inclusion chemistry, volume fraction (assuming uniform distribution as well) and $dt_{8/5}$ favor the formation of acicular ferrite and the weld metal oxygen lies on the "high" side of the curve.

D. MICROSTRUCTURAL ANALYSIS

Presented in Figure 4.34 are micrographs of SAW sample F295 which had the lowest measured acicular ferrite volume fraction (27%). Figure 4.35 shows micrographs of the SAW sample with the highest acicular ferrite volume fraction, F296 (78%), for comparison. While all the SAW microstructures are very fine, there is notably more and larger grain boundary ferrite in F295 than in the other samples.

For GMAW single pass welds, Figure 4.36 demonstrates the effect of low oxygen. The samples welded in pure argon have very coarse micro- and macrostructure, predominantly Widmanstätten ferrite and bainite. On the other hand, sample M4 (Figure 4.37), having a higher oxygen content in the cover gas, clearly reveals a finer microstructure than the pure argon sample, demonstrating the shift of CCT curves to the left (see Figure 2.8) where higher temperature microstructures will form. Figure 4.37(b) shows the characteristic columnar grain structure found in weld metal.

Figure 4.38(a) demonstrates the multiple pass weld macrostructure found in the C10/M4 GMAW multiple pass sample. Acicular ferrite growing from an inclusion is shown in Figure 4.38(b). The GMAW multiple pass samples had the lowest acicular ferrite, but samples with higher oxygen contents still produced a fairly fine microstructure. Figure 4.39(a) shows the blocky microstructure in sample C5, having 190 ppm

oxygen. Sample C10, with an oxygen content of 270, is clearly finer (even taking into account the magnification difference) as shown in Figure 4.39(b).

It is the effect of microstructure on mechanical properties that is most important. As shown in Figure 2.11, tensile strength, ductile to brittle transition temperature and Charpy fixed energy clearly improve with increasing amounts of acicular ferrite in the SAW samples. Other factors also affect weld metal mechanical properties, including the amount of columnar grains, manganese content and microstructure fineness. For the SAW samples, there was a large amount of acicular ferrite present, so it played a major role in determining the final mechanical properties. In the case of the GMAW samples, though, there is quite a bit less acicular ferrite present. In this case, the other factors affecting mechanical properties play a much greater role as was shown by Brothers (Brothers, 1994) and, consequently, no simple correlation between the amount of acicular ferrite and strength and charpy v-notch toughness could be demonstrated.

ELEMENT ATOMIC PERCENT					OXIDE WEIGHT PERCENT		
Mn	Ti	Al	Si	Zr	MnO	Al_2O_3	SiO_2
0.24	1.26	31.48	2.76	64.26	0.40	93.79	5.82
0.14	2.26	26.90	3.09	67.61	0.27	92.24	7.49
0.99	6.34	14.73	0.32	77.62	3.55	94.99	1.46
0.00	0.16	30.51	69.24	0.09	0.00	38.39	61.61
0.28	2.98	25.77	0.28	70.69	0.60	98.65	0.76
1.84	3.09	43.11	1.21	50.75	2.28	95.82	1.90
0.34	3.25	20.63	0.69	75.09	0.89	96.82	2.29
2.45	13.52	43.78	1.66	38.29	2.94	94.53	2.53
2.02	0.77	25.16	1.45	70.60	4.12	92.13	3.75
2.22	13.01	34.90	4.02	45.86	3.17	89.54	7.29
0.90	18.42	50.54	0.64	29.50	0.97	98.15	0.88
0.15	89.57	2.48	1.02	6.78	2.54	75.50	21.96
0.57	23.83	38.57	1.76	35.27	0.79	94.11	3.10
0.51	0.00	1.25	3.54	94.70	7.03	30.96	62.01
0.82	10.94	29.64	0.63	57.97	1.49	97.05	1.46
3.15	1.43	12.71	0.00	82.71	12.13	87.87	0.00
7.95	16.98	34.59	1.05	39.44	11.12	87.01	1.86
0.82	42.01	16.91	1.05	39.22	2.52	93.38	4.10
0.62	47.04	12.88	1.00	38.46	2.48	92.45	5.08
3.60	5.87	77.29	1.25	11.99	2.50	96.40	1.10
AVERAGE							
1.48	**15.14**	**28.69**	**4.83**	**49.86**	**3.09**	**87.09**	**9.82**

Mn adjusted assuming MnS forms.

Table 4.1. GMAW (SINGLE) ARGON inclusion composition data.

ELEMENT ATOMIC PERCENT					OXIDE WEIGHT PERCENT		
Mn	Ti	Al	Si	Zr	MnO	Al_2O_3	SiO_2
45.58	10.15	18.48	22.94	2.85	42.23	30.76	27.01
39.92	12.88	22.37	22.07	2.76	36.91	37.16	25.93
40.38	16.46	18.63	19.66	4.87	40.86	33.86	25.28
34.85	16.16	25.28	18.81	4.90	33.45	43.60	22.94
31.89	19.03	20.91	21.52	6.65	32.94	38.81	28.25
38.66	16.26	20.94	22.71	1.44	36.77	35.78	27.45
36.74	11.70	28.78	21.87	0.91	31.61	44.48	23.91
46.10	14.19	18.64	20.13	0.95	43.83	31.84	24.33
35.24	16.30	25.49	20.41	2.56	32.95	42.81	24.24
34.91	12.27	28.86	21.27	2.69	30.68	45.57	23.75
39.10	10.27	27.47	22.35	0.80	33.46	42.23	24.31
38.67	7.35	22.26	29.16	2.55	33.42	34.56	32.02
38.47	8.89	23.60	27.81	1.23	33.11	36.48	30.41
41.24	9.57	20.79	26.83	1.56	36.60	33.15	30.25
35.74	15.47	26.25	21.53	1.02	32.42	42.77	24.81
39.19	9.80	22.77	26.47	1.77	34.46	35.97	29.58
34.33	12.15	27.66	22.29	3.57	30.56	44.23	25.21
32.60	20.89	21.47	25.04	0.00	31.65	37.45	30.90
34.84	12.18	29.14	20.55	3.29	30.75	46.20	23.05
37.51	7.17	27.12	26.32	1.88	31.34	40.72	27.94
AVERAGE							
37.80	**12.96**	**23.84**	**22.99**	**2.41**	**34.50**	**38.92**	**26.58**

Mn adjusted assuming MnS forms.

Table 4.2. GMAW (SINGLE) M2 inclusion composition data.

ELEMENT ATOMIC PERCENT					OXIDE WEIGHT PERCENT		
Mn	Ti	Al	Si	Zr	MnO	Al_2O_3	SiO_2
43.52	27.73	15.12	12.89	0.75	49.99	31.19	18.82
34.82	21.24	21.66	17.27	5.02	36.39	40.67	22.94
32.36	21.51	21.40	21.00	3.73	33.19	39.43	27.38
30.99	22.82	24.08	18.25	3.86	31.81	44.40	23.79
35.91	20.97	21.57	17.22	4.33	37.19	40.14	22.66
33.70	18.10	23.14	21.67	3.38	32.78	40.44	26.78
32.13	18.69	24.08	19.57	5.53	32.05	43.15	24.81
31.88	21.65	22.95	17.49	6.03	33.44	43.25	23.31
37.32	17.79	20.22	21.34	3.33	37.04	36.05	26.92
25.94	19.40	32.80	18.80	3.08	23.85	54.19	21.96
36.93	18.18	22.63	17.68	4.57	36.91	40.64	22.46
34.39	23.75	18.31	20.33	3.22	36.93	35.33	27.74
35.71	17.32	21.57	24.13	1.27	33.97	36.86	29.17
41.29	12.81	19.24	24.90	1.75	38.41	32.16	29.43
46.12	13.24	14.32	24.61	1.70	44.73	24.95	30.32
43.48	13.67	15.20	26.12	1.53	41.81	26.27	31.91
42.68	13.68	15.05	25.47	3.12	41.81	26.49	31.70
42.67	11.93	17.73	26.90	0.78	39.26	29.30	31.44
43.33	18.08	13.49	23.64	1.47	44.40	24.83	30.77
43.29	14.40	14.59	27.68	0.04	41.35	25.04	33.61
AVERAGE							
37.42	**18.35**	**19.96**	**21.35**	**2.93**	**37.37**	**35.74**	**26.90**

Mn adjusted assuming MnS forms.

Table 4.3. GMAW (SINGLE) MIDPT inclusion composition data.

ELEMENT ATOMIC PERCENT					OXIDE WEIGHT PERCENT		
Mn	Ti	Al	Si	Zr	MnO	Al_2O_3	SiO_2
49.58	14.53	11.42	24.48	0.00	48.99	20.28	30.73
45.50	12.29	15.14	27.07	0.00	42.49	25.40	32.11
55.24	12.40	9.87	22.50	0.00	54.39	17.46	28.15
50.96	13.42	11.71	23.84	0.07	49.87	20.57	29.62
46.28	14.86	13.74	25.11	0.01	44.99	24.00	31.01
54.85	17.08	8.53	19.54	0.00	57.73	16.13	26.14
47.50	13.86	12.93	25.71	0.00	45.94	22.47	31.59
48.86	11.92	12.19	27.02	0.00	46.49	20.84	32.67
53.08	11.62	10.45	24.85	0.00	51.32	18.15	30.53
45.02	13.17	15.18	26.64	0.00	42.42	25.69	31.89
47.50	13.85	12.97	25.68	0.01	45.93	22.52	31.55
51.64	12.20	9.84	25.89	0.44	50.52	17.30	32.18
51.96	10.34	10.02	27.68	0.00	49.43	17.12	33.45
50.10	11.63	13.05	25.22	0.00	47.45	22.20	30.35
48.46	10.21	13.98	27.35	0.00	44.74	23.19	32.08
44.37	24.47	7.05	24.11	0.00	50.61	14.44	34.94
46.41	7.56	16.08	29.94	0.00	40.94	25.49	33.56
44.41	10.91	13.20	30.65	0.84	41.48	22.15	36.37
50.39	10.89	9.66	28.72	0.34	48.34	16.65	35.01
47.01	14.20	12.16	26.43	0.21	45.89	21.33	32.78
AVERAGE							
48.96	**13.07**	**11.96**	**25.92**	**0.10**	**47.50**	**20.67**	**31.84**

Mn adjusted assuming MnS forms.

Table 4.4. GMAW (SINGLE) C5 inclusion composition data.

ELEMENT ATOMIC PERCENT					OXIDE WEIGHT PERCENT		
Mn	Ti	Al	Si	Zr	MnO	Al_2O_3	SiO_2
49.02	10.29	10.61	28.42	1.65	47.05	18.30	34.65
43.89	5.08	13.58	37.31	0.14	37.94	21.09	40.98
46.68	6.80	11.16	35.14	0.22	41.91	18.00	40.09
45.65	8.56	14.42	30.80	0.58	41.24	23.40	35.36
46.03	8.76	13.52	29.64	2.06	42.63	22.49	34.88
43.76	9.90	13.15	31.66	1.53	40.66	21.96	37.38
43.15	7.07	13.49	36.28	0.00	38.02	21.36	40.62
45.94	3.08	15.41	34.67	0.90	39.04	23.53	37.43
41.63	7.70	18.63	32.04	0.00	35.94	28.91	25.15
44.41	9.15	14.84	29.98	1.62	40.68	24.42	34.90
46.16	12.85	13.66	26.83	0.48	44.05	23.42	32.53
42.39	5.79	15.89	34.05	1.88	37.12	25.00	37.88
41.50	12.36	15.49	29.18	1.47	39.00	26.16	34.84
40.79	9.63	17.36	31.86	0.36	36.27	27.74	35.99
42.18	12.17	15.61	29.59	0.46	39.12	26.01	34.87
44.11	11.53	13.30	29.68	1.37	41.72	22.61	35.67
44.76	9.22	13.73	30.83	1.47	41.22	22.72	36.07
39.61	15.88	13.88	26.00	4.63	40.60	25.55	33.85
44.19	5.30	15.43	33.76	1.33	38.49	24.15	37.36
42.03	11.97	14.85	29.01	2.14	39.81	25.27	34.92
AVERAGE							
43.89	**9.15**	**14.40**	**31.34**	**1.21**	**40.13**	**23.60**	**36.27**

Mn adjusted assuming MnS forms.

Table 4.5. GMAW (SINGLE) M4 inclusion composition data.

ELEMENT ATOMIC PERCENT					OXIDE WEIGHT PERCENT		
Mn	Ti	Al	Si	Zr	MnO	Al_2O_3	SiO_2
44.99	15.58	11.02	28.41	0.00	44.59	19.63	35.78
49.00	13.42	11.42	26.11	0.04	47.71	19.98	32.30
42.26	6.03	16.18	35.53	0.00	36.28	24.96	38.76
52.29	12.14	9.61	25.90	0.07	51.03	18.85	32.12
58.37	14.49	6.73	20.40	0.00	60.56	12.54	28.90
51.75	16.55	7.98	23.72	0.00	53.78	14.91	31.32
47.98	12.90	12.37	26.72	0.03	46.07	21.33	32.60
43.22	15.09	15.77	25.91	0.00	41.37	27.12	31.51
49.97	13.72	10.44	25.84	0.03	49.21	18.47	32.33
44.46	18.78	12.33	24.35	0.08	45.58	22.71	31.71
47.54	7.16	13.61	31.69	0.00	42.35	21.78	35.87
47.94	18.38	10.78	22.89	0.01	49.73	20.10	30.17
48.23	8.84	12.72	30.20	0.00	44.06	20.88	35.06
48.05	11.53	12.28	28.14	0.00	45.38	20.84	33.77
47.56	8.68	13.13	30.63	0.00	43.21	21.43	35.36
47.17	9.29	12.88	30.65	0.01	43.17	21.18	35.64
45.96	12.09	13.84	28.10	0.01	43.15	23.33	33.52
46.72	8.94	12.99	31.34	0.00	42.52	21.23	36.24
46.00	7.02	14.32	32.66	0.00	40.63	22.72	36.65
51.78	10.05	11.62	26.54	0.01	48.67	19.63	31.70
AVERAGE							
48.06	**12.03**	**12.10**	**27.79**	**0.01**	**45.95**	**20.58**	**33.47**

Mn adjusted assuming MnS forms.

Table 4.6. GMAW (SINGLE) C10/M4 inclusion composition data.

ELEMENT ATOMIC PERCENT					OXIDE WEIGHT PERCENT		
Mn	Ti	Al	Si	Zr	MnO	Al_2O_3	SiO_2
49.11	14.96	12.13	23.80	0.00	46.22	22.70	31.08
47.01	15.26	12.85	24.88	0.00	46.69	22.12	31.19
48.28	13.50	12.73	25.39	0.10	44.49	22.69	32.82
45.04	15.91	12.79	26.15	0.11	42.36	25.28	32.37
42.79	17.27	14.21	25.73	0.00	43.66	22.66	33.68
45.16	14.38	13.04	27.42	0.00	48.10	20.19	31.71
48.73	14.60	11.38	25.29	0.01	50.06	21.42	28.52
48.27	18.44	11.49	21.64	0.16	46.02	22.59	31.39
46.55	15.74	12.72	24.99	0.00	46.77	22.75	30.47
44.81	20.08	12.13	22.97	0.00	48.62	22.20	29.19
47.78	17.50	12.14	22.58	0.00	43.46	23.91	32.63
45.61	13.45	13.97	26.95	0.02	35.78	24.44	39.77
42.62	3.85	16.21	37.29	0.03	45.26	21.12	33.62
47.78	11.87	12.41	27.94	0.00	50.35	19.69	29.97
49.77	16.08	10.83	23.32	0.00	41.50	24.56	33.94
44.75	11.71	14.74	28.80	0.00	41.11	26.63	32.27
44.07	12.82	15.89	27.22	0.00	50.17	20.59	29.24
49.99	15.66	11.42	22.93	0.00	47.70	20.23	32.07
48.99	13.52	11.56	25.93	0.00	45.62	24.77	29.61
AVERAGE							
46.71	**14.56**	**12.94**	**25.76**	**0.03**	**45.47**	**22.66**	**31.87**

Mn adjusted assuming MnS forms.

Table 4.7. GMAW (SINGLE) C10 inclusion composition data.

ELEMENT ATOMIC PERCENT					OXIDE WEIGHT PERCENT		
Mn	Ti	Al	Si	Zr	MnO	Al_2O_3	SiO_2
2.98	5.30	77.54	0.00	14.18	2.09	97.97	0.00
4.58	3.47	76.19	0.22	15.54	3.23	96.57	0.20
0.00	12.55	4.66	2.52	80.27	0.00	72.34	27.66
7.28	16.20	62.10	0.76	13.66	6.08	93.12	0.81
0.07	2.06	85.28	0.39	12.20	0.05	99.63	0.32
1.29	3.70	87.02	0.31	7.67	0.82	98.93	0.25
8.10	14.62	60.65	1.78	14.85	6.79	91.32	1.90
4.97	17.70	62.90	0.39	14.04	4.19	95.38	0.42
0.50	27.48	43.88	1.40	26.74	0.61	97.19	2.20
4.48	6.19	56.82	0.00	32.51	4.20	95.80	0.00
6.82	42.63	40.14	0.53	9.87	8.57	90.59	0.85
1.66	12.24	44.93	0.61	40.56	2.00	97.06	0.94
4.84	20.71	62.78	0.61	11.06	4.09	95.26	0.66
0.59	61.43	31.67	0.60	5.70	1.02	97.66	1.32
3.31	4.80	75.07	0.00	16.82	2.39	97.61	0.00
3.17	15.19	44.34	0.11	37.19	3.82	96.01	0.17
5.20	8.65	37.09	2.28	46.78	6.96	89.17	3.88
4.44	49.11	34.90	0.64	10.92	6.53	92.27	1.20
5.79	42.09	38.06	0.60	13.46	7.73	91.26	1.02
0.00	75.21	17.14	0.41	7.25	0.00	98.35	1.65
AVERAGE							
3.50	**22.07**	**52.16**	**0.71**	**21.56**	**3.56**	**94.17**	**2.27**

Mn adjusted assuming MnS forms.

Table 4.8. GMAW (MULTI) ARGON inclusion composition data.

ELEMENT ATOMIC PERCENT					OXIDE WEIGHT PERCENT		
Mn	Ti	Al	Si	Zr	MnO	Al_2O_3	SiO_2
54.00	17.63	2.90	24.83	0.65	59.50	5.74	34.76
57.50	13.30	3.42	24.53	1.25	60.65	6.47	32.88
51.32	13.99	4.16	29.24	1.28	53.48	7.80	38.72
50.23	17.59	3.74	27.03	1.42	55.02	7.36	37.62
52.51	9.30	4.45	32.84	0.90	51.37	7.82	40.81
50.75	12.95	4.43	30.85	1.02	51.84	8.12	40.04
51.31	12.77	3.51	30.14	2.27	53.50	6.57	39.93
47.10	19.06	6.12	25.72	2.00	51.88	12.12	36.00
54.35	12.51	4.18	24.80	4.17	58.21	8.04	33.75
56.10	9.46	3.73	28.60	2.10	56.59	6.76	36.65
50.72	14.41	4.40	30.17	0.30	52.31	8.16	39.54
54.73	13.73	3.82	26.78	0.94	57.24	7.17	35.59
48.94	27.33	3.52	19.57	0.63	61.08	7.89	31.03
49.99	6.80	5.54	37.50	0.17	46.46	9.25	44.28
54.28	11.79	3.86	29.72	0.35	54.84	7.01	38.15
51.84	14.38	4.48	28.73	0.57	53.78	8.35	37.87
52.06	6.72	5.01	34.63	1.58	49.55	8.57	41.88
52.10	15.75	5.09	25.55	1.50	55.60	9.77	34.64
51.99	6.65	6.46	33.15	1.76	49.18	10.98	39.84
49.67	16.74	5.04	28.36	0.19	52.41	9.56	38.03
AVERAGE							
52.07	**13.64**	**4.39**	**28.64**	**1.25**	**54.22**	**8.18**	**37.60**

Mn adjusted assuming MnS forms.

Table 4.9. GMAW (MULTI) M2 inclusion composition data.

ELEMENT ATOMIC PERCENT					OXIDE WEIGHT PERCENT		
Mn	Ti	Al	Si	Zr	MnO	Al_2O_3	SiO_2
53.23	11.54	4.64	29.81	0.78	53.53	8.39	38.08
49.15	5.60	7.62	35.85	1.78	45.35	12.63	42.03
49.48	14.94	5.30	30.24	0.03	50.79	9.77	39.44
50.49	13.89	4.80	29.97	0.85	51.95	8.87	39.18
47.13	18.88	6.12	26.30	1.57	51.49	12.01	36.50
47.61	14.57	7.74	30.08	0.00	47.74	13.94	38.32
49.65	16.79	5.78	27.07	0.70	52.58	11.00	36.42
43.12	31.45	4.79	19.47	1.17	56.38	11.26	32.35
48.53	17.35	7.37	26.70	0.05	50.71	13.84	35.45
47.79	18.90	5.97	25.25	2.09	52.75	11.84	35.41
46.45	20.10	6.09	25.89	1.47	51.45	12.12	36.43
49.83	5.04	6.53	37.48	1.11	45.64	10.75	43.61
51.04	14.68	5.36	27.44	1.48	53.42	10.08	36.50
51.81	9.83	4.80	32.38	1.19	51.01	8.49	40.50
51.67	9.64	5.01	33.02	0.66	50.35	8.77	40.88
47.21	17.12	6.69	27.56	1.41	50.09	12.78	37.16
45.82	22.88	7.36	23.94	0.00	51.22	14.77	34.01
47.68	12.54	7.93	30.68	1.16	47.24	14.12	38.63
54.65	11.23	4.64	29.27	0.20	54.55	8.32	37.13
52.53	11.58	5.08	29.54	1.28	52.96	9.20	37.87
AVERAGE							
49.24	**14.93**	**5.98**	**28.90**	**0.95**	**51.06**	**11.15**	**37.79**

Mn adjusted assuming MnS forms.

Table 4.10. GMAW (MULTI) MIDPT inclusion composition data.

ELEMENT ATOMIC PERCENT					OXIDE WEIGHT PERCENT		
Mn	Ti	Al	Si	Zr	MnO	Al_2O_3	SiO_2
39.51	12.45	21.62	25.64	0.78	35.62	35.01	29.37
40.44	6.77	22.01	30.79	0.00	33.95	33.20	32.85
37.15	26.31	15.39	17.55	3.60	42.66	31.74	25.60
37.03	29.16	12.26	16.50	5.05	46.28	27.53	26.20
40.45	22.01	17.06	18.07	2.41	43.01	32.58	24.41
35.15	26.08	15.89	18.08	4.81	40.56	32.94	26.50
39.02	18.64	15.72	24.87	1.75	39.47	28.56	31.96
42.41	21.33	10.82	22.19	3.26	47.10	21.58	31.31
43.40	17.03	14.75	22.59	2.24	44.01	26.87	29.11
44.54	12.07	17.12	24.29	1.96	41.95	28.97	29.07
35.90	30.63	9.31	19.68	4.48	4624	21.55	32.21
37.72	24.13	12.96	21.47	3.73	42.73	26.37	30.90
36.82	22.44	15.26	22.73	2.75	39.54	29.44	31.02
37.96	15.74	19.88	25.64	0.79	35.72	33.62	30.66
37.61	21.36	15.59	21.88	3.56	40.26	29.98	29.76
39.25	19.74	16.42	24.36	0.22	39.37	29.59	31.05
36.58	23.77	13.42	20.89	5.34	41.93	27.65	30.42
38.65	12.23	24.05	24.44	0.63	34.23	29.27	27.50
36.62	21.98	17.72	20.75	2.93	38.62	33.58	27.81
36.49	21.50	16.39	2152	4.10	39.12	31.57	29.31
AVERAGE							
38.63	**20.27**	**16.18**	**22.20**	**2.72**	**40.62**	**30.03**	**29.35**

Mn adjusted assuming MnS forms.

Table 4.11. GMAW (MULTI) C5 inclusion composition data.

ELEMENT ATOMIC PERCENT					OXIDE WEIGHT PERCENT		
Mn	Ti	Al	Si	Zr	MnO	Al_2O_3	SiO_2
29.29	35.54	14.91	15.76	4.50	38.49	35.20	26.32
37.25	35.34	6.37	13.84	7.20	45.20	17.27	26.53
34.14	32.40	11.31	17.17	4.97	44.76	26.64	28.60
46.93	7.79	13.58	31.04	0.66	42.37	22.02	35.61
45.88	18.97	8.79	26.36	0.00	48.21	16.60	35.20
36.12	34.97	11.26	15.73	1.93	47.32	26.50	26.19
34.20	36.91	8.21	15.32	5.36	50.00	21.55	28.45
34.29	32.78	13.66	17.76	1.51	42.13	30.15	27.73
33.47	36.19	9.37	14.35	6.62	48.83	24.56	26.61
40.08	29.69	8.10	19.34	2.79	50.60	18.38	31.02
34.96	35.36	10.53	14.48	4.67	48.37	26.18	25.45
30.14	32.82	15.40	17.73	3.90	37.51	34.45	28.04
36.67	30.54	11.93	17.84	3.02	45.40	26.54	28.06
33.24	31.53	13.56	17.86	3.82	41.39	30.35	28.26
44.62	9.57	14.51	30.48	0.82	40.78	23.82	35.40
36.91	28.28	10.38	20.66	3.77	45.12	22.79	32.09
36.72	30.89	12.46	19.36	0.57	43.87	26.74	29.39
30.83	36.70	10.70	17.64	4.12	42.54	26.52	30.93
33.32	31.24	12.84	17.14	5.47	42.63	29.51	27.86
34.27	32.03	12.20	16.78	4.71	44.21	28.28	27.51
AVERAGE							
36.17	**29.98**	**11.50**	**18.83**	**3.52**	**45.04**	**25.70**	**29.26**

Mn adjusted assuming MnS forms.

Table 4.12. GMAW (MULTI) M4 inclusion composition data.

ELEMENT ATOMIC PERCENT					OXIDE WEIGHT PERCENT		
Mn	Ti	Al	Si	Zr	MnO	Al_2O_3	SiO_2
41.06	53.03	1.92	3.34	0.65	84.23	7.08	8.69
45.29	16.98	5.15	30.67	1.91	48.44	9.89	41.67
42.64	16.54	4.47	35.19	1.16	44.71	8.42	46.88
46.83	13.85	5.81	30.28	3.23	48.92	10.90	40.18
45.77	20.84	5.71	26.13	1.55	51.29	11.51	37.20
48.09	16.27	4.28	38.39	2.97	52.36	8.37	39.27
46.33	17.40	4.34	31.33	0.59	49.32	8.30	42.38
47.94	19.18	4.01	28.28	0.59	52.64	7.92	39.45
48.21	16.57	4.51	28.94	1.78	51.80	8.70	39.50
52.96	5.03	4.93	33.78	3.30	50.57	8.45	40.98
51.47	6.38	5.96	32.92	3.27	49.49	10.30	40.21
48.93	13.62	3.95	33.25	0.24	49.78	7.23	42.99
37.99	32.23	4.24	24.25	1.29	49.71	9.98	40.32
51.35	6.36	2.39	39.42	0.48	48.57	4.06	47.37
45.70	22.57	3.56	26.24	1.93	53.49	7.49	39.02
48.46	12.19	4.91	33.99	0.46	48.23	8.78	42.99
48.09	13.17	3.09	35.43	0.22	48.75	5.63	45.63
48.23	19.72	4.26	26.85	0.94	53.59	8.50	37.91
45.79	21.20	5.08	25.83	2.10	52.18	10.40	37.41
50.69	12.92	3.50	32.18	0.72	51.81	6.42	41.78
AVERAGE							
47.09	**17.80**	**4.30**	**29.33**	**1.47**	**51.99**	**8.42**	**39.59**

Mn adjusted assuming MnS forms.

Table 4.13. GMAW (MULTI) C10/M4 inclusion composition data.

ELEMENT ATOMIC PERCENT					OXIDE WEIGHT PERCENT		
Mn	Ti	Al	Si	Zr	MnO	Al_2O_3	SiO_2
47.37	25.30	3.11	24.22	0.00	56.57	6.68	36.75
45.35	30.86	3.30	18.74	1.75	60.39	7.90	31.71
46.11	19.71	5.15	26.97	2.05	51.44	10.33	38.23
51.29	11.61	5.39	29.88	1.83	51.84	9.79	38.37
48.08	17.78	5.55	26.74	1.84	52.24	10.84	36.92
48.60	13.81	4.87	30.72	2.00	50.42	9.09	40.49
44.16	11.72	5.08	36.41	2.63	44.35	9.17	46.47
46.49	14.47	5.20	33.54	0.30	47.22	9.50	43.29
51.98	15.81	3.27	27.23	1.71	56.21	6.36	37.42
54.19	14.94	3.78	25.49	1.60	58.04	7.27	34.69
55.15	13.46	2.85	27.50	1.04	57.92	5.38	36.70
50.75	13.35	5.17	29.23	1.49	52.22	9.56	38.22
50.01	14.92	4.65	28.79	1.63	52.67	8.80	38.53
48.60	18.78	4.85	25.19	2.58	54.41	9.75	35.84
50.87	17.08	3.93	26.81	1.31	55.30	7.67	37.04
81.83	10.40	0.20	7.41	0.15	89.33	0.39	10.28
56.52	18.26	2.80	21.59	0.83	63.53	5.65	30.83
52.42	4.45	3.45	38.57	1.11	48.70	5.76	45.53
49.69	19.55	3.20	26.13	1.43	56.06	6.49	37.45
54.10	13.77	3.48	27.24	1.41	56.97	6.58	36.45
AVERAGE							
51.68	**16.00**	**3.96**	**26.92**	**1.44**	**55.79**	**7.65**	**36.56**

Mn adjusted assuming MnS forms.

Table 4.14. GMAW (MULTI) C10 inclusion composition data.

ELEMENT ATOMIC PERCENT					OXIDE WEIGHT PERCENT		
Mn	Ti	Al	Si	Zr	MnO	Al_2O_3	SiO_2
40.97	8.41	26.80	22.14	1.68	27.10	46.02	26.88
39.24	9.67	27.65	22.28	1.16	24.08	48.36	27.56
38.85	8.75	29.46	21.83	1.11	24.18	49.75	26.07
34.33	11.09	31.75	20.06	2.77	17.66	56.91	25.43
39.25	8.57	28.62	22.17	1.40	24.91	48.51	26.58
39.12	7.95	30.75	21.24	0.94	24.85	50.48	24.67
39.15	7.70	26.84	24.87	1.44	25.69	44.89	29.42
36.91	6.99	23.61	30.50	1.98	24.56	39.42	36.02
39.67	8.48	25.32	24.91	1.63	25.90	43.70	30.40
37.52	8.44	29.67	22.71	1.66	23.23	49.81	26.97
36.89	7.87	30.54	23.16	1.54	22.93	50.17	26.90
38.09	7.49	30.45	22.55	1.43	24.37	49.63	26.00
37.48	6.40	27.71	25.15	1.27	26.77	44.60	28.63
37.99	11.75	27.46	21.50	1.29	20.98	50.86	28.16
41.72	6.91	24.99	25.26	1.12	28.94	41.44	29.62
38.71	7.48	29.89	22.81	1.11	24.95	48.74	26.31
38.29	8.51	30.37	21.79	1.04	23.68	50.63	25.68
37.91	7.93	30.15	22.75	1.27	23.85	49.65	26.50
37.06	9.81	27.89	23.96	1.28	21.72	48.70	29.58
36.90	7.97	33.94	19.99	1.19	22.41	54.78	22.81
AVERAGE							
38.40	**8.41**	**28.69**	**23.08**	**1.41**	**24.14**	**48.35**	**27.51**

Oxide weight percent assumes pyrophanite ($MnOTiO_2$) forms as Ti rich phase. Mn adjusted assuming MnS forms.

Table 4.15. SAW F289 inclusion composition data.

ELEMENT ATOMIC PERCENT					OXIDE WEIGHT PERCENT		
Mn	Ti	Al	Si	Zr	MnO	Al_2O_3	SiO_2
33.36	16.25	39.01	7.13	4.25	10.20	79.52	10.28
26.40	10.30	49.33	12.40	1.57	9.50	76.84	13.66
25.97	12.41	47.15	12.56	1.90	6.81	78.42	14.77
24.52	10.72	51.91	10.51	2.33	7.33	81.06	11.60
25.34	15.93	45.76	11.33	1.85	1.78	83.59	14.63
20.90	12.07	54.75	9.01	3.28	2.49	87.35	10.16
22.04	8.49	58.58	9.28	1.61	7.37	83.30	9.33
25.14	9.17	53.88	10.87	0.93	9.33	79.35	11.32
24.25	9.40	54.28	9.85	2.23	8.45	81.14	10.41
25.48	13.30	50.75	8.44	2.03	5.14	84.88	9.98
25.80	29.99	38.10	4.86	1.25	-----*	----*	----*
21.58	10.67	55.28	9.96	2.51	4.75	84.49	10.77
26.75	12.15	50.41	8.85	1.83	7.72	82.09	10.19
26.17	9.94	51.07	10.29	2.53	9.70	79.04	11.26
23.96	8.78	54.89	10.94	1.43	8.75	79.98	11.28
23.18	12.76	53.12	7.78	3.15	3.70	87.26	9.04
24.79	12.16	48.73	10.85	3.47	6.06	81.16	12.78
26.44	13.34	47.05	10.69	2.48	6.15	80.85	12.99
24.18	10.29	53.74	9.48	2.31	7.46	82.28	10.26
24.13	5.35	59.67	10.26	0.59	11.81	78.63	9.56
AVERAGE							
25.05	**12.16**	**50.87**	**9.77**	**2.18**	**7.08**	**81.64**	**11.28**

Oxide weight percent assumes pyrophanite ($MnOTiO_2$) forms as Ti rich phase. Mn adjusted assuming MnS forms. *High sulfur content.

Table 4.16. SAW F292 inclusion composition data.

ELEMENT ATOMIC PERCENT					OXIDE WEIGHT PERCENT		
Mn	Ti	Al	Si	Zr	MnO	Al_2O_3	SiO_2
37.11	3.29	20.71	37.93	0.96	27.36	31.64	40.99
39.70	3.98	20.37	34.96	1.00	29.40	31.90	38.71
36.83	6.89	27.64	28.18	0.45	23.67	44.35	31.98
33.25	6.72	27.82	30.09	2.12	20.80	44.87	34.32
39.16	4.89	24.95	29.85	1.16	27.78	39.12	33.10
41.95	5.01	23.28	28.84	0.91	30.49	37.05	32.46
38.24	5.91	24.68	29.43	1.75	26.44	39.91	33.65
36.79	5.40	23.79	32.59	1.42	25.42	37.88	36.70
37.18	5.40	28.61	27.56	1.25	25.18	44.50	30.32
38.88	6.55	22.94	30.13	1.49	26.77	37.97	35.27
35.26	5.54	24.46	31.08	3.66	24.41	39.81	35.78
39.53	6.17	22.94	29.37	1.99	27.83	37.87	34.30
38.96	4.77	24.63	30.55	1.09	27.69	38.52	33.79
33.61	4.79	27.72	33.88	0.00	22.15	41.75	36.09
37.22	6.00	24.61	29.65	2.51	25.63	40.16	34.21
35.95	6.00	36.63	30.39	1.06	23.74	42.20	34.06
36.25	6.91	25.85	29.18	1.81	23.66	42.45	33.89
34.25	6.30	28.33	28.91	2.20	22.06	45.27	32.67
31.81	6.96	26.44	30.08	4.70	19.96	44.36	35.68
37.07	6.10	26.50	28.05	2.27	25.11	42.83	32.06
AVERAGE							
36.95	**5.68**	**25.15**	**30.54**	**1.69**	**25.28**	**40.22**	**34.50**

Oxide weight percent assumes pyrophanite ($MnOTiO_2$) forms as Ti rich phase. Mn adjusted assuming MnS forms.

Table 4.17. SAW F293 inclusion composition data.

ELEMENT ATOMIC PERCENT					OXIDE WEIGHT PERCENT		
Mn	Ti	Al	Si	Zr	MnO	Al_2O_3	SiO_2
49.67	5.99	19.12	25.02	0.20	38.09	32.15	29.76
47.34	4.87	23.67	23.20	0.92	35.74	37.96	26.31
46.11	5.41	21.21	25.78	1.49	34.91	35.01	30.08
45.24	473	20.83	28.23	0.97	34.23	33.58	32.19
45.51	4.93	22.13	26.95	0.48	33.99	35.47	30.54
45.51	5.21	21.11	27.09	1.08	34.25	34.47	31.28
47.10	6.30	18.97	26.34	1.30	35.79	32.40	31.81
46.47	5.81	20.84	25.91	0.97	34.92	34.63	30.45
46.14	4.82	19.53	28.26	1.25	35.41	31.82	32.67
45.85	5.09	20.84	27.49	0.72	34.56	33.86	31.59
45.80	8.40	19.90	25.43	0.47	32.79	35.31	31.90
46.46	5.21	19.53	27.95	0.84	35.37	32.12	32.51
51.60	5.20	17.29	24.86	1.05	41.14	29.19	29.67
49.05	5.17	18.61	26.21	0.96	38.23	30.94	30.83
45.34	5.04	21.64	26.99	0.99	34.05	35.04	30.90
46.65	4.27	19.40	28.60	1.08	36.11	31.27	32.61
38.22	5.40	25.13	30.83	0.48	26.32	39.45	34.23
44.42	5.65	20.98	27.63	1.31	33.05	34.66	32.28
44.70	4.67	19.17	29.63	1.83	34.33	31.37	34.29
2.40	6.30	15.91	24.97	0.42	41.60	27.68	30.72
AVERAGE							
46.48	**5.42**	**20.29**	**26.87**	**0.94**	**35.24**	**33.42**	**31.33**

Oxide weight percent assumes pyrophanite ($MnOTiO_2$) forms as Ti rich phase. Mn adjusted assuming MnS forms.

Table 4.18. SAW F295 inclusion composition data.

ELEMENT ATOMIC PERCENT					OXIDE WEIGHT PERCENT		
Mn	Ti	Al	Si	Zr	MnO	Al_2O_3	SiO_2
36.39	8.23	31.51	21.46	2.41	22.28	52.46	25.26
33.16	9.02	32.17	23.90	1.75	18.20	53.62	28.18
41.02	6.61	22.70	28.27	1.39	28.84	37.84	33.32
32.24	14.18	23.38	20.46	9.74	13.89	53.19	32.92
40.05	6.38	24.79	28.02	0.77	27.55	40.26	32.18
38.16	8.14	28.59	23.26	1.87	24.28	28.06	27.66
43.38	7.64	28.26	19.47	1.25	29.71	47.27	23.02
38.15	7.84	25.46	26.62	1.93	24.91	43.17	31.93
41.40	7.62	29.32	20.62	1.03	27.53	48.40	24.07
42.45	8.13	28.60	19.61	1.21	28.40	48.22	23.38
37.72	7.62	32.86	20.45	1.34	23.61	53.04	23.35
33.75	9.40	37.45	18.43	0.97	17.80	60.98	21.22
38.61	6.63	31.91	21.50	1.35	25.30	50.59	24.11
38.58	6.48	26.84	26.11	1.99	26.18	43.74	30.09
39.20	7.90	31.44	20.11	1.35	25.00	51.64	23.36
38.01	6.96	31.59	22.02	1.42	24.55	50.54	24.91
40.97	7.44	32.48	17.75	1.35	26.92	52.71	20.37
36.94	7.38	35.08	19.16	1.44	22.84	55.66	21.49
40.36	7.58	27.98	20.96	3.11	27.36	47.78	25.15
37.80	7.99	32.90	19.87	1.43	23.43	53.65	22.92
AVERAGE							
38.42	**7.96**	**29.77**	**21.90**	**1.95**	**24.43**	**49.63**	**25.95**

Oxide weight percent assumes pyrophanite ($MnOTiO_2$) forms as Ti rich phase. Mn adjusted assuming MnS forms.

Table 4.19. SAW F296 inclusion composition data.

	Sample	Inclusion Count	Mean Inclusion Size (micron)	Volume Fraction Inclusions (%)
SAW	F289	483	0.320	0.216
	F292	297	0.378	0.185
	F293	408	0.322	0.185
	F295	364	0.323	0.165
	F296	1237	0.423	0.966
GMAW *s*	AR	88 (32)	1.294*	0.231
	M2	548 (197)	0.800	0.551
	MIDPT	723 (260)	0.668	0.507
	C5	592 (213)	0.897	0.718
	M4	749 (270)	0.765	0.689
	C10	626 (225)	0.667	0.437
	M4/C10	567 (204)	0.821	0.600
GMAW *m*	AR	687 (247)	0.310	0.104
	M2	857 (309)	0.440	0.261
	MIDPT	843 (303)	0.367	0.179
	C5	1119 (403)	0.375	0.248
	M4	779 (280)	0.448	0.246
	C10	1017 (366)	0.532	0.452
	M4/C10	1199 (432)	0.503	0.477

s-single pass; *m*-multi pass. Values in () normalize GMAW inclusion count in 500 square microns to SAW inclusion count in 180 square microns per field. *GMAW single pass argon sample inclusion size in error. Actual value is approximately 0.3 microns.

Table 4.20. Inclusion size data. (Kettel 1993, Seraiva 1993)

	AR	M2	MIDPT	C5	M4	C10/M4	C10
0.1	0	0	0	0	0	0	0
0.2	0	0	0	0	0	2	1
0.3	0	0	0	2	4	38	0
0.4	3	8	51	5	18	60	5
0.5	18	58	133	36	62	154	23
0.6	0	145	203	98	172	76	112
0.7	0	143	138	145	136	115	132
0.8	28	0	118	0	162	36	172
0.9	0	104	28	115	58	50	56
1.0	16	596	33	85	74	12	76
1.1	0	22	5	57	28	16	20
1.2	3	8	14	22	19	2	12
1.3	0	2	0	15	9	2	0
1.4	3	0	0	0	2	2	6
1.5	0	0	0	8	5	2	0
1.6	2	0	0	4	0	0	8
1.7	0	2	0	0	0	0	0
1.8	0	0	0	0	0	0	4
1.9	0	0	0	0	0	0	0
2.0	3	0	0	0	0	0	9

Table 4.21. GMAW (single pass) inclusion size distribution data. (Seraiva, 1993)

	AR	M2	MIDPT	C5	M4	C10/M4	C10
0.1	8	4	72	52	2	0	0
0.2	287	83	207	196	84	62	101
0.3	221	179	157	278	134	286	155
0.4	82	200	151	253	183	178	147
0.5	34	195	137	220	196	237	185
0.6	17	125	45	65	100	180	135
0.7	27	40	42	35	53	133	123
0.8	5	21	17	14	15	58	71
0.9	2	7	7	2	8	23	50
1.0	4	3	3	3	0	21	30
1.1	0	0	4	0	2	8	8
1.2	0	0	0	0	2	5	9
1.3	0	0	1	0	0	1	0
1.4	0	0	0	1	0	3	1
1.5	0	0	0	0	0	2	0
1.6	0	0	0	0	0	2	1
1.7	0	0	0	0	0	0	1
1.8	0	0	0	0	0	0	0
1.9	0	0	0	0	0	0	0
2.0	0	0	0	0	0	0	0

Table 4.22. GMAW (multiple pass) inclusion size distribution data.

	F289	F292	F293	F295	F296
0.15	161	84	163	130	265
0.3	146	74	110	115	440
0.4	100	55	62	45	161
0.5	40	35	25	34	126
0.6	18	20	14	18	74
0.7	8	11	14	10	63
0.8	3	5	10	7	23
0.9	3	3	3	1	22
1.0	0	3	2	1	19
1.1	0	4	4	3	9
1.2	2	1	0	0	6
1.3	1	0	1	0	10
1.4	1	1	0	0	0
1.5	0	1	0	0	3

Sample F296 has 16 inclusions larger than 1.5 microns. The largest inclusion is 3.3 micron.

Table 4.23. SAW inclusion size distribution. (Kettel, 1993)

SAMPLES		VOLUME PERCENT ACICULAR FERRITE
SAW	F289	43
	F292	65
	F293	41
	F295	27
	F296	78
GMAW *s*	ARGON	0
	M2	16
	MIDPT	21
	C5	24
	M4	25
	C10/M4	22
	C10	19
GMAW *m*	ARGON	2
	M2	15
	MIDPT	11
	C5	9
	M4	12
	C10/M4	13
	C10	11

s-single pass; *m*-multiple pass

Table 4.24. Acicular ferrite volume fraction. (Brothers, 1994)

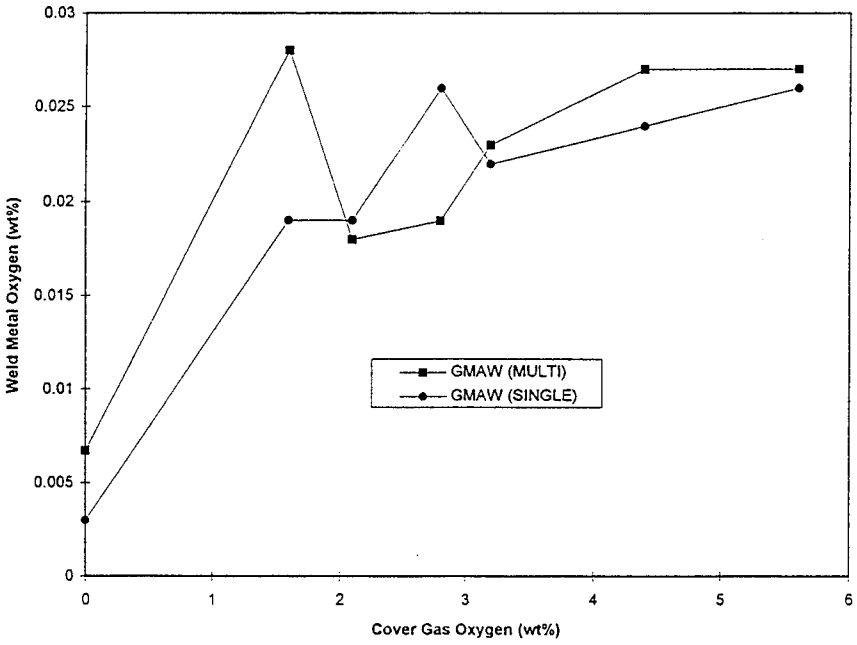

SAMPLE	COVER GAS OXYGEN PERCENT (WT%)
ARGON	0
M2	1.6
MIDPT	2.1
C5	2.8
M4	3.2
C10/M4	4.4
C10	5.6

Figure 4.1. GMAW weld oxygen vs cover gas oxygen.

(a)

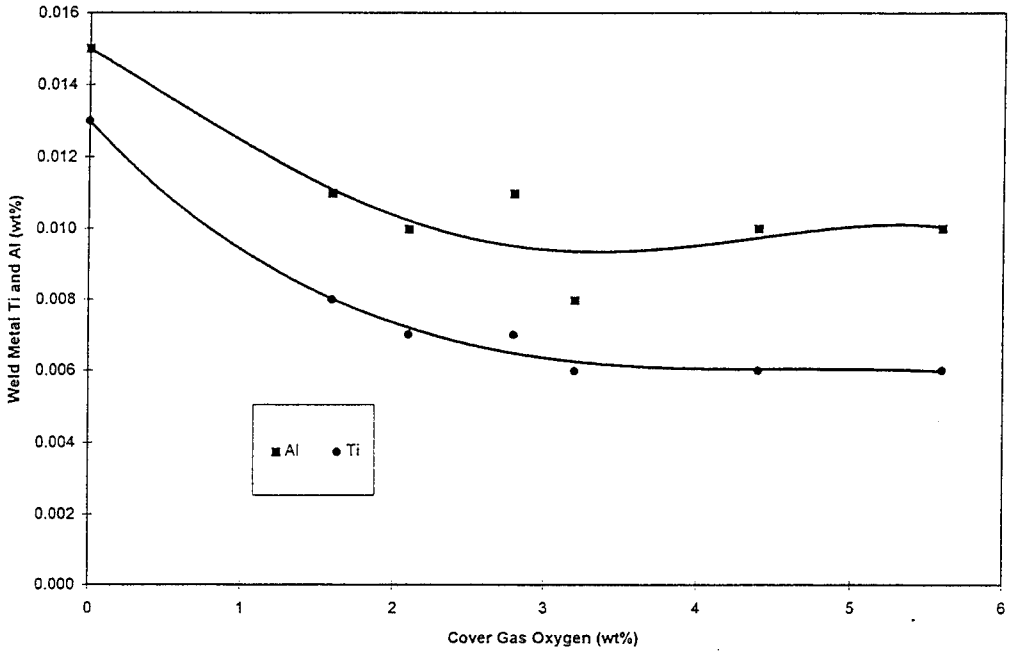

(b)

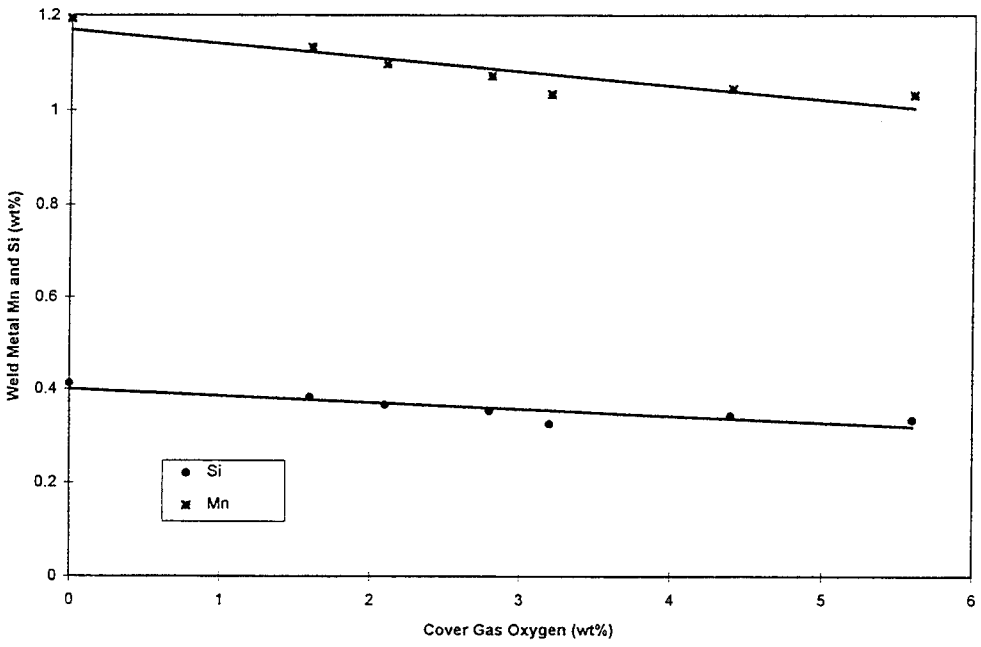

Figure 4.2. GMAW (SINGLE)(a)Weld Ti and Al vs cover gas O.
(b) Weld Mn and Si vs cover gas O.

(a)

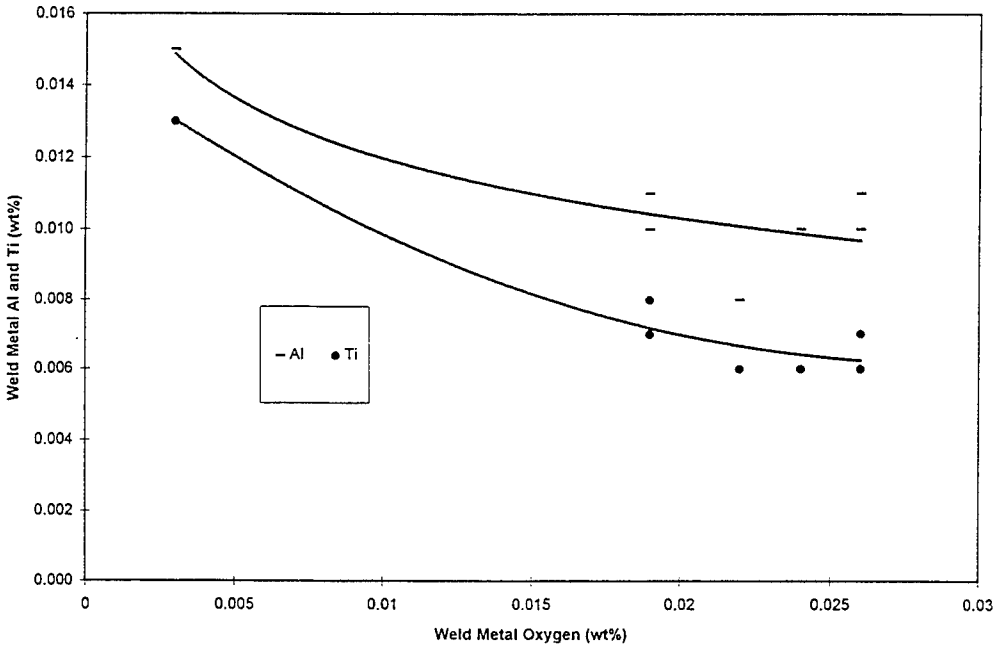

(b)

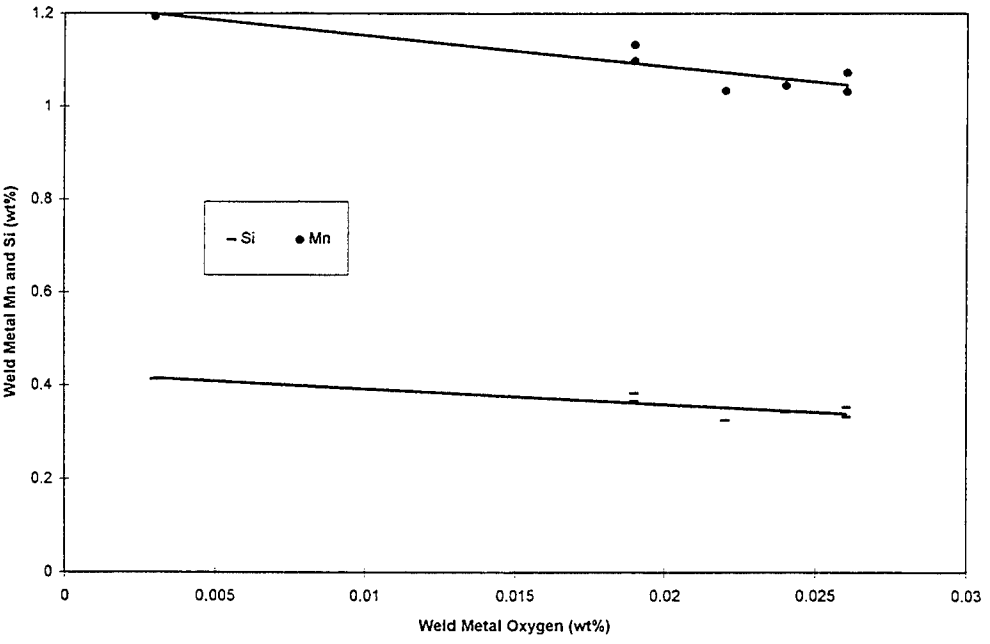

Figure 4.3. GMAW (SINGLE)(a) Weld Al and Ti vs weld O (b) Weld Mn and Si vs weld O.

(a)

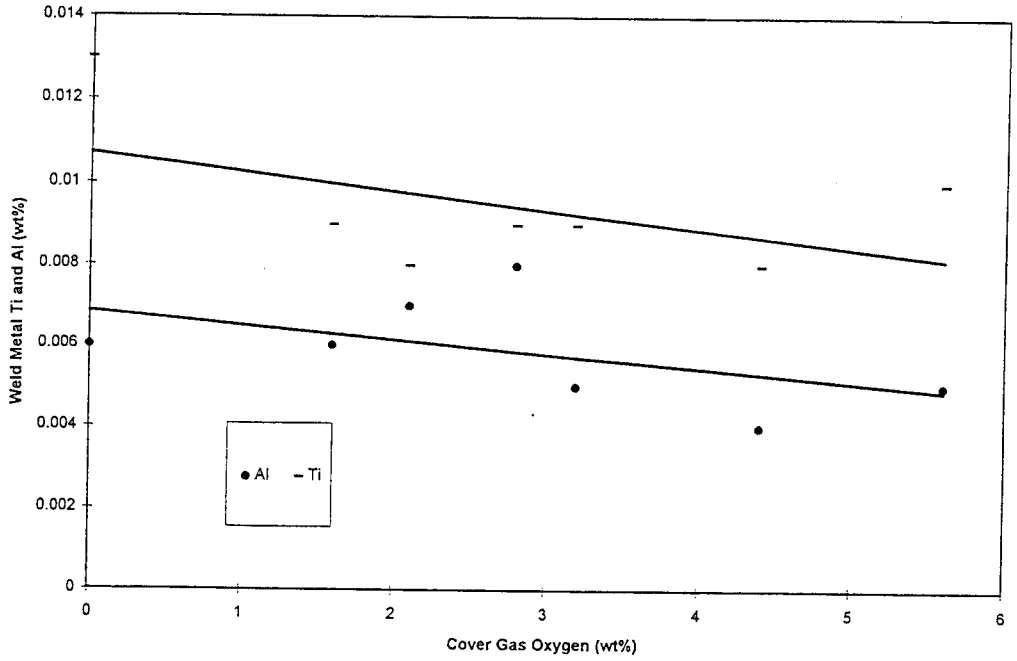

(b)

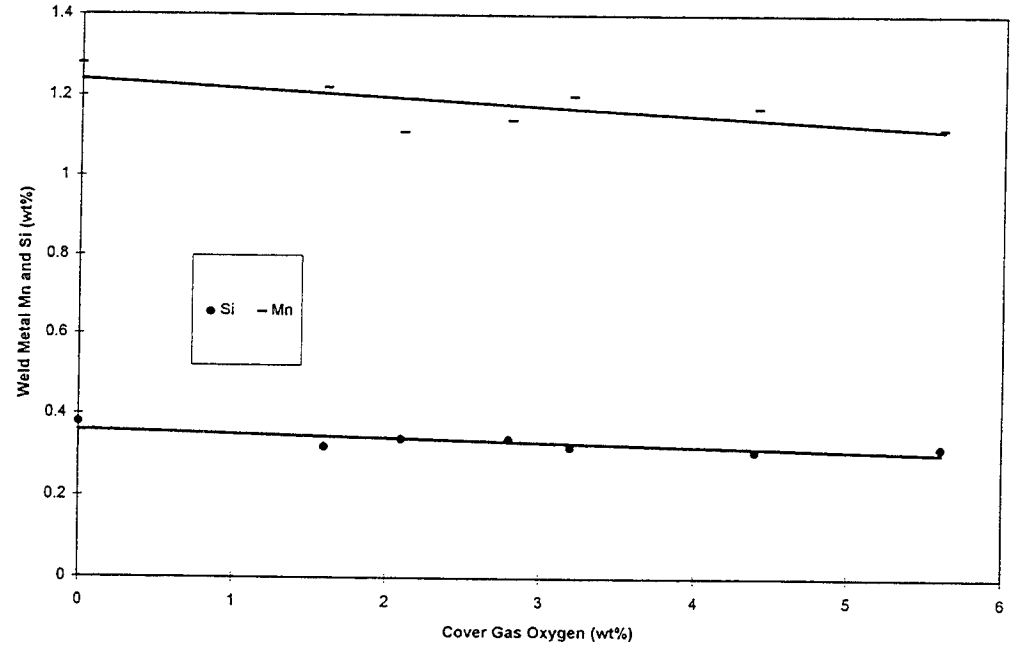

Figure 4.4. GMAW (MULTI) (a) Weld Ti and Al vs cover gas O (b) Weld Mn and Si vs cover gas O.

(a)

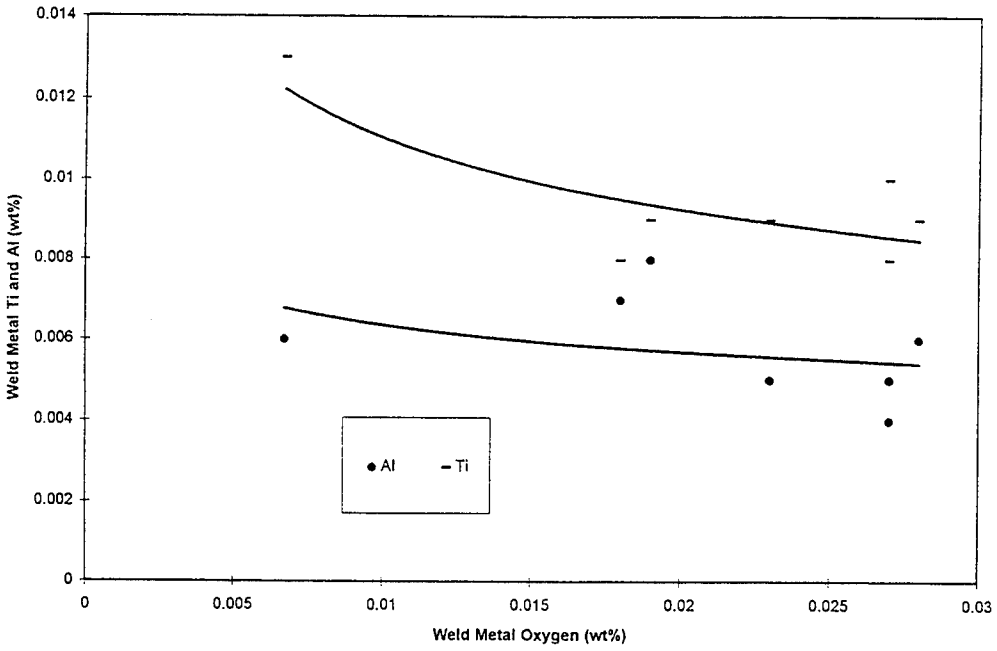

(b)

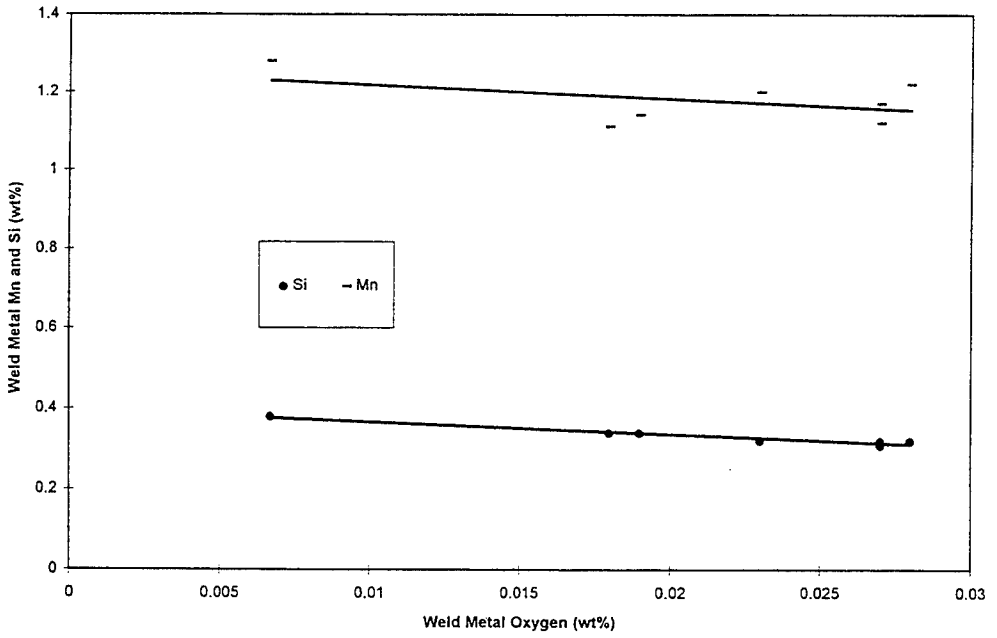

Figure 4.5. GMAW (MULTI) (a) Weld Ti and Al vs weld O, (b) Weld Mn and Si vs weld O.

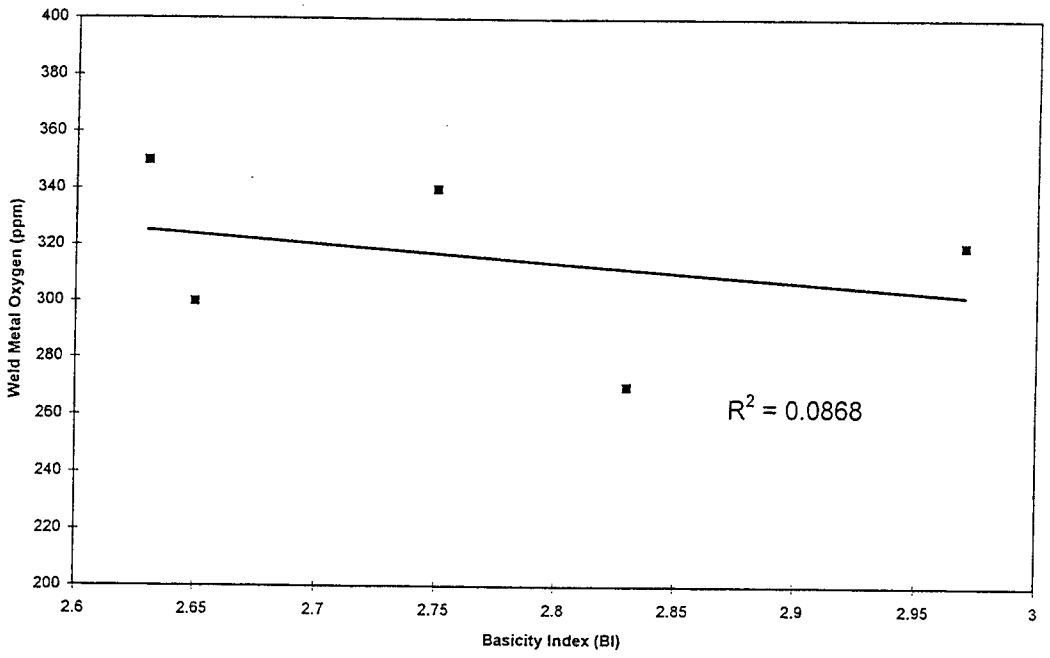

Figure 4.6. SAW weld metal oxygen vs Basicity Index (BI).

(a)

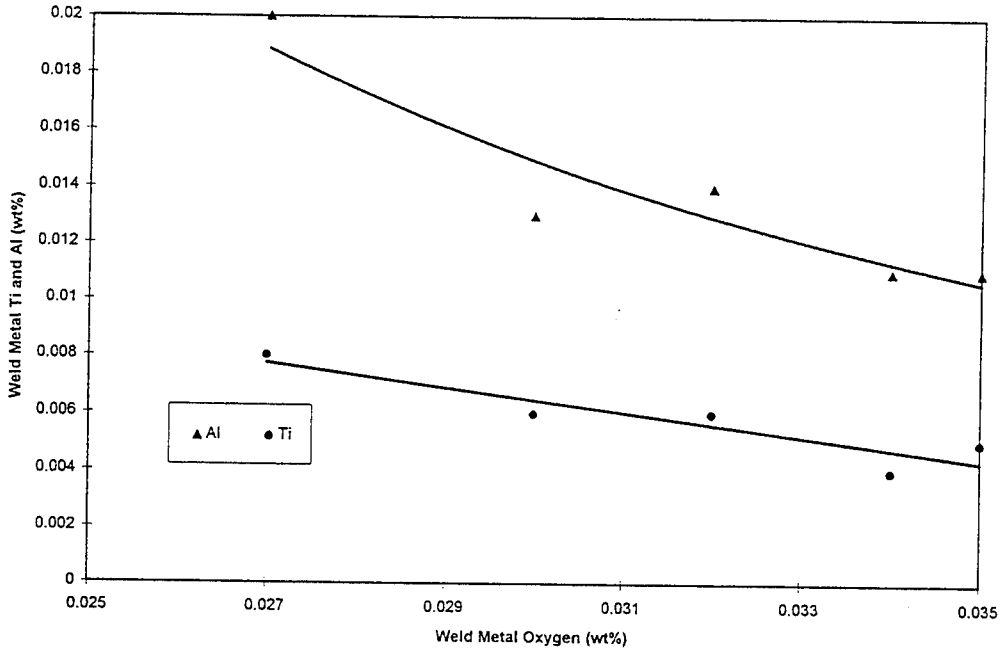

(b)

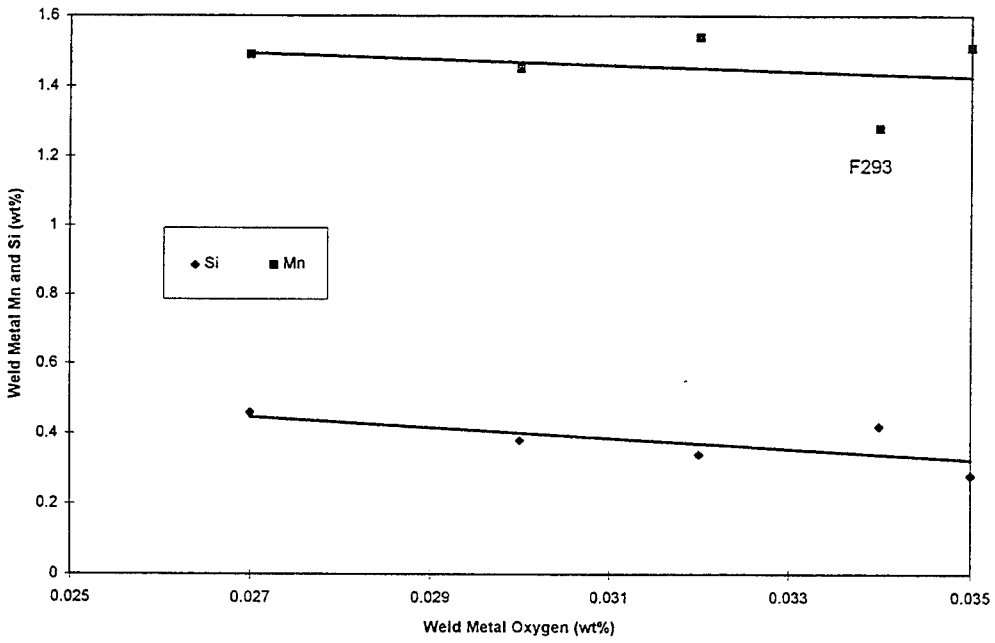

Figure 4.7. SAW (a) Weld Ti and Al vs weld O, (b) Weld Mn and Si vs weld O.

(a)

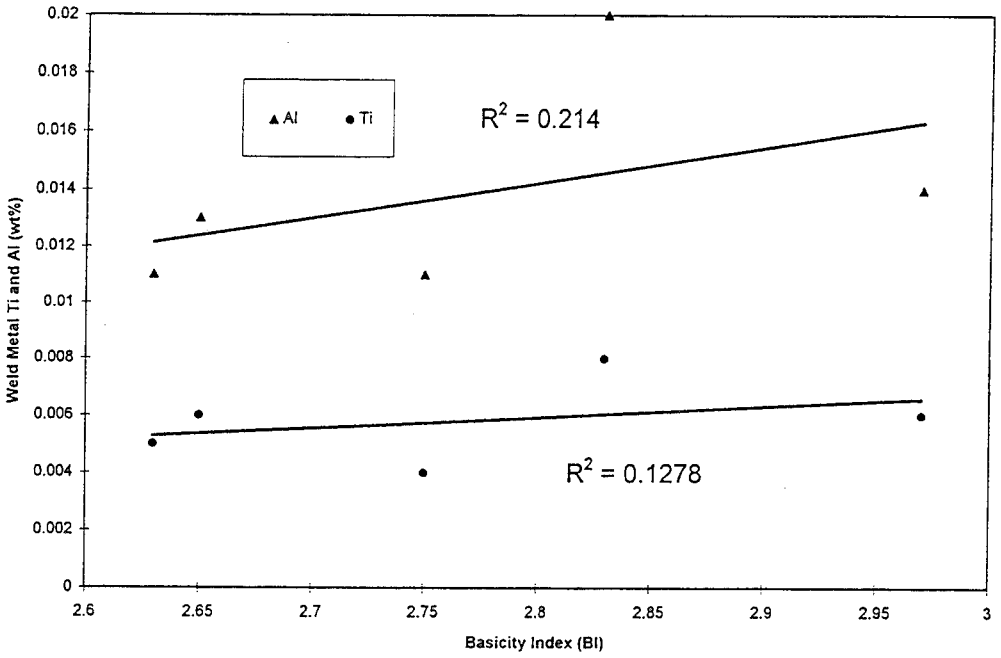

(b)

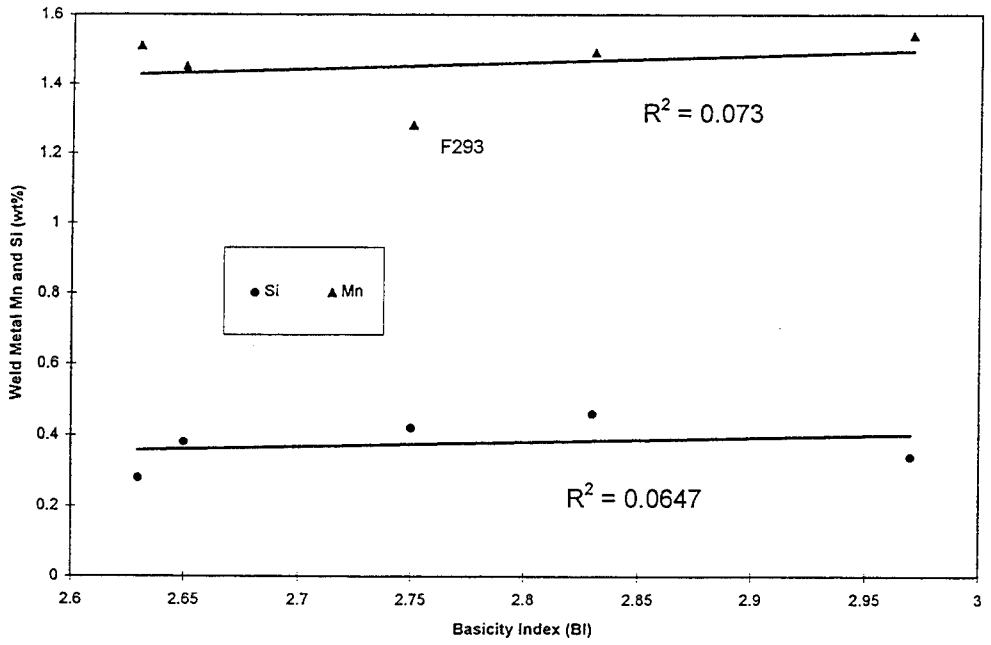

Figure 4.8. SAW (a)Weld Ti and Al vs BI, (b)Weld Mn and Si vs BI.

(a)

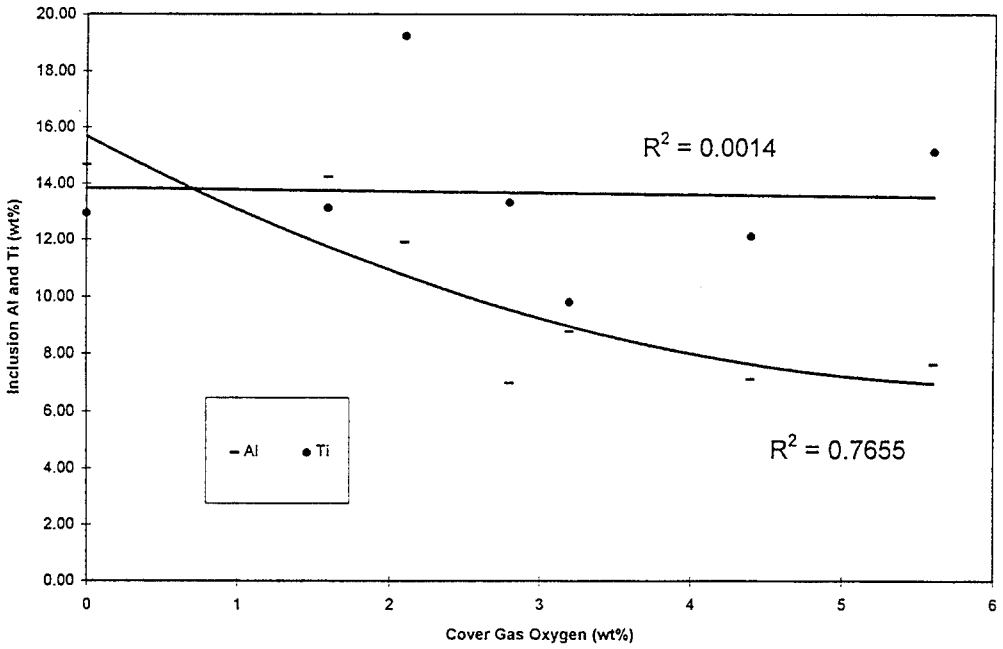

(b)

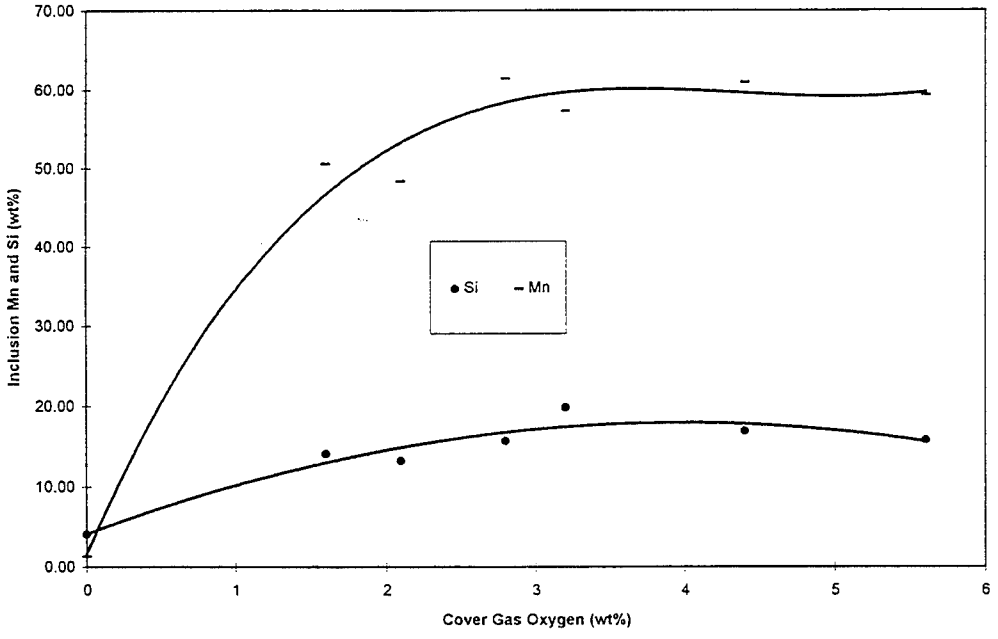

Figure 4.9. GMAW (SINGLE) (a) Inclusion Al and Ti vs cover gas O, (b) Inclusion Mn and Si vs cover gas O.

(a)

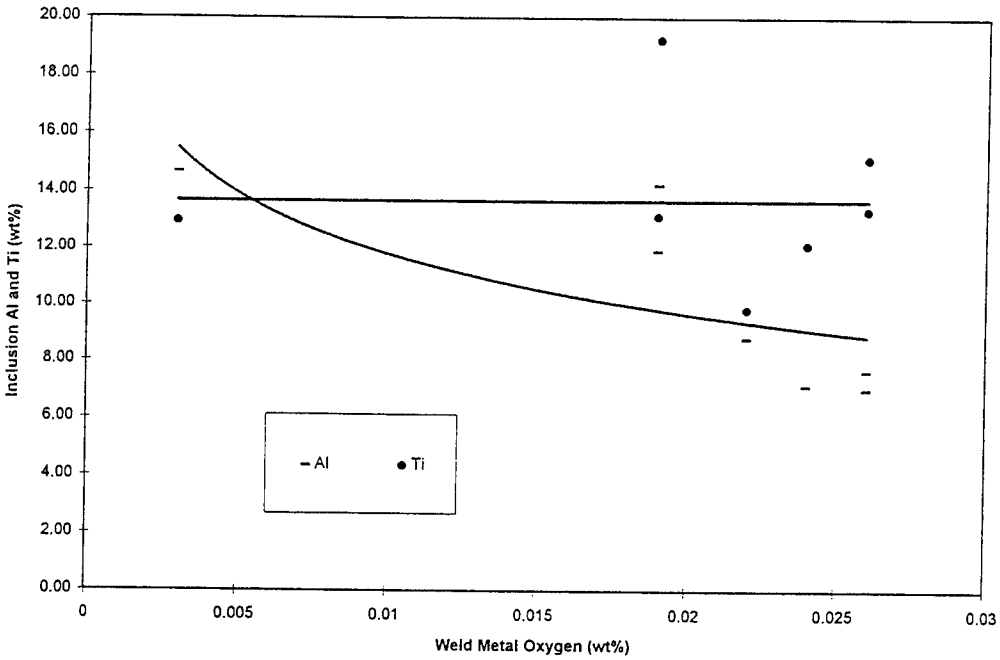

(b)

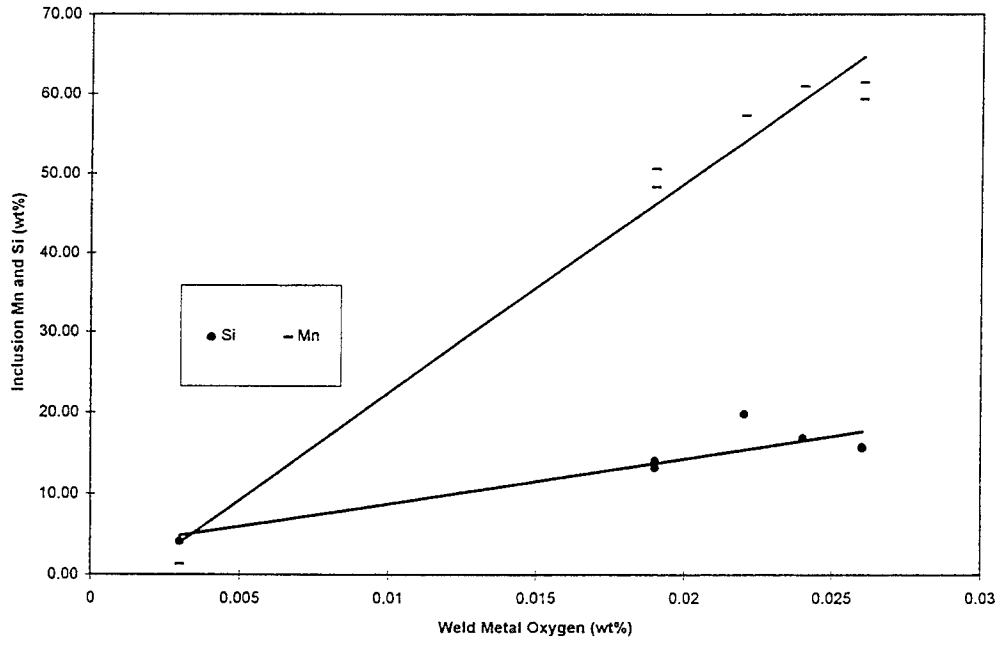

Figure 4.10. GMAW (SINGLE) (a)Inclusion Al and Ti vs weld O, (b)Inclusion Mn and Si vs weld O.

(a)

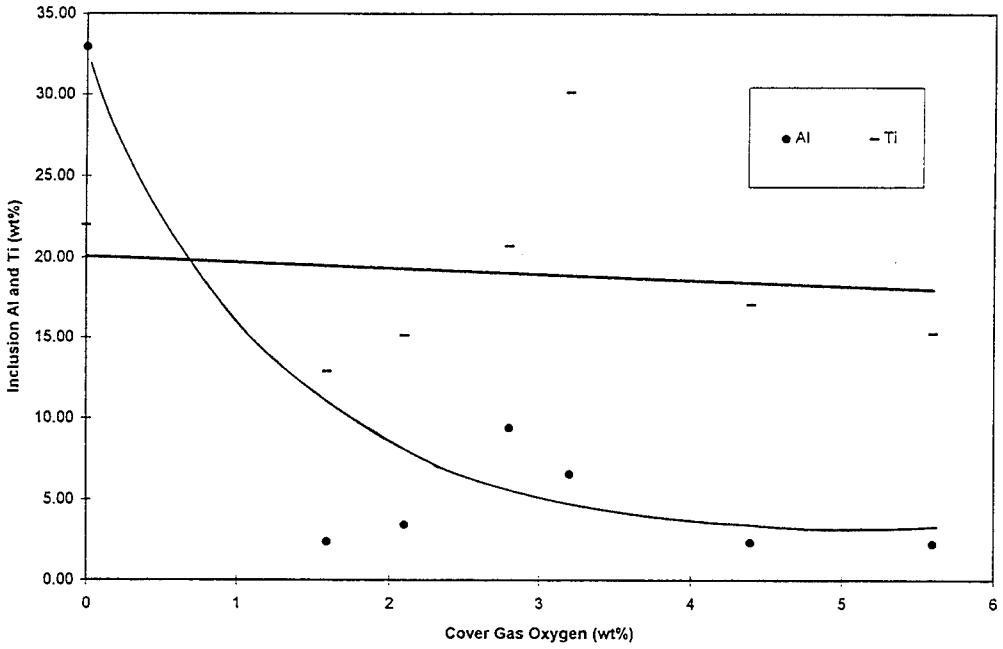

(b)

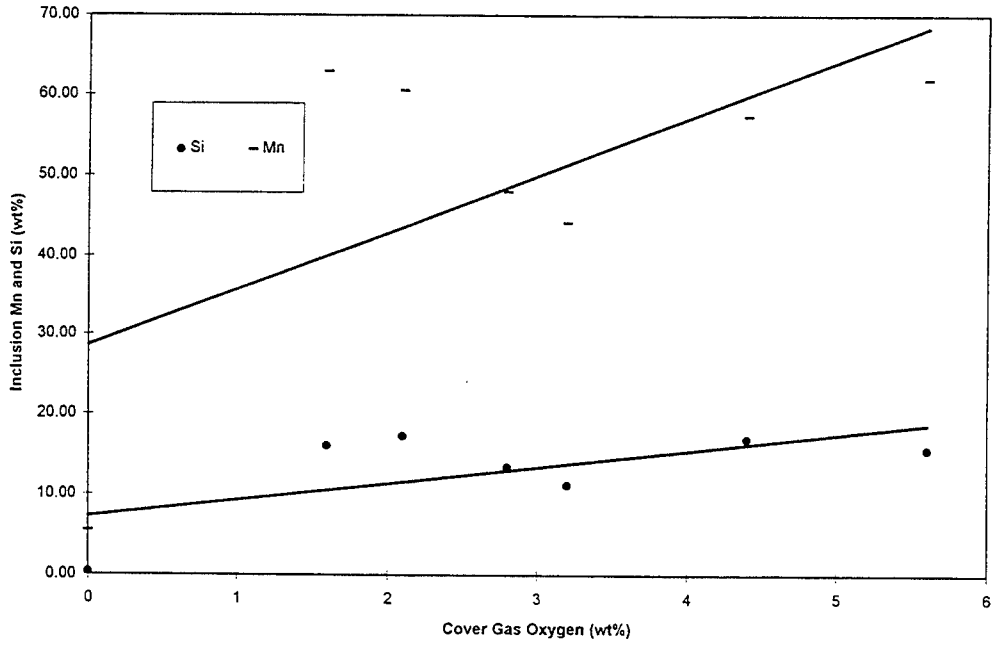

Figure 4.11. GMAW (MULTI) (a) Inclusion Al and Ti vs cover gas O, (b) Inclusion Mn and Si vs cover gas O.

(a)

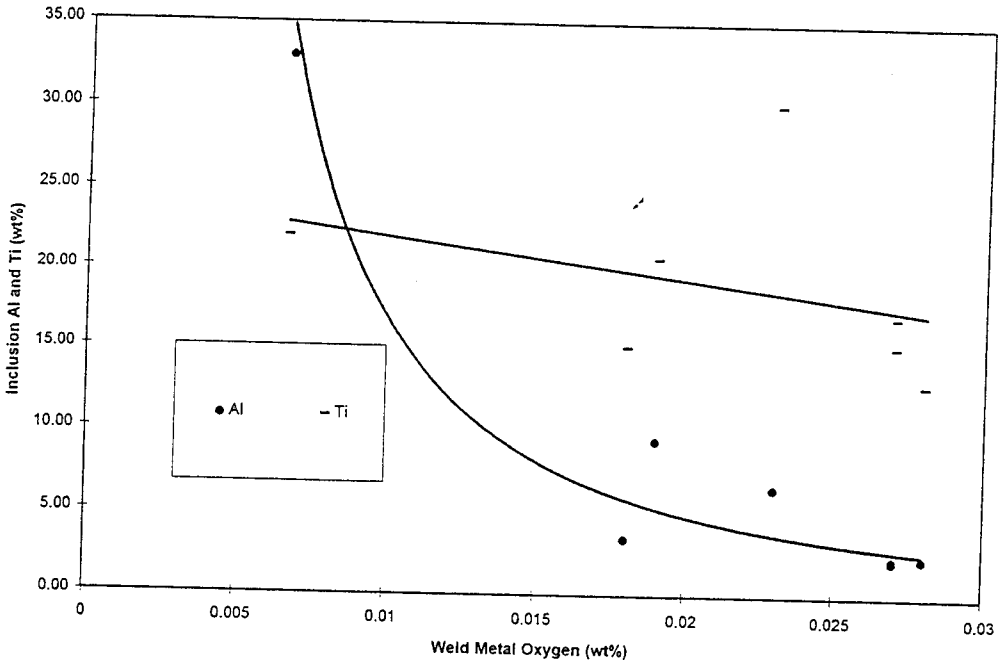

(b)

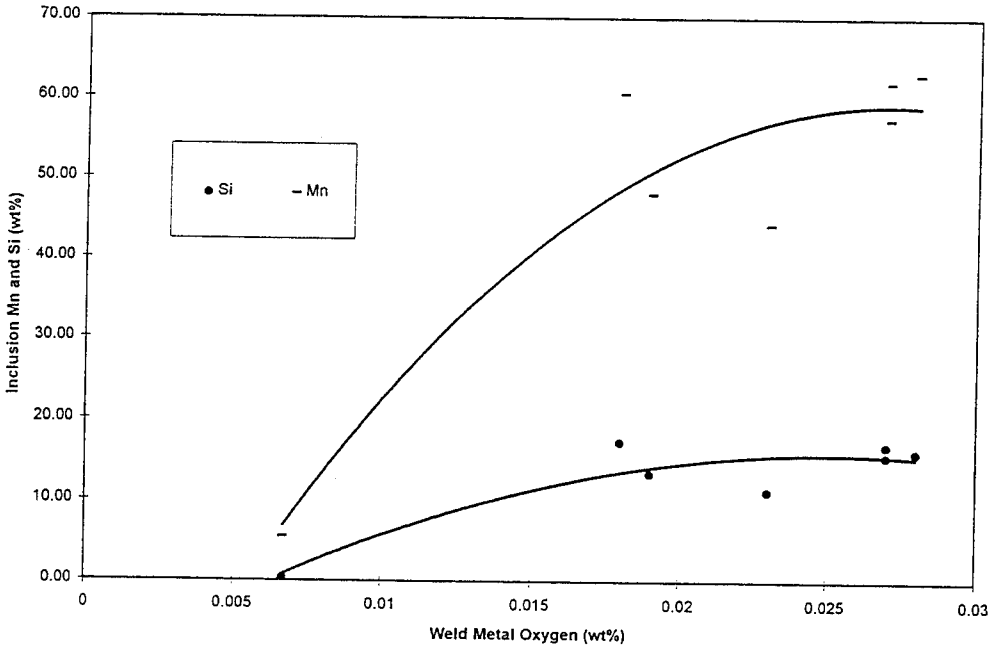

Figure 4.12. GMAW (MULTI) (a)Inclusion Al and Ti vs weld O, (b)Inclusion Mn and Si vs weld O.

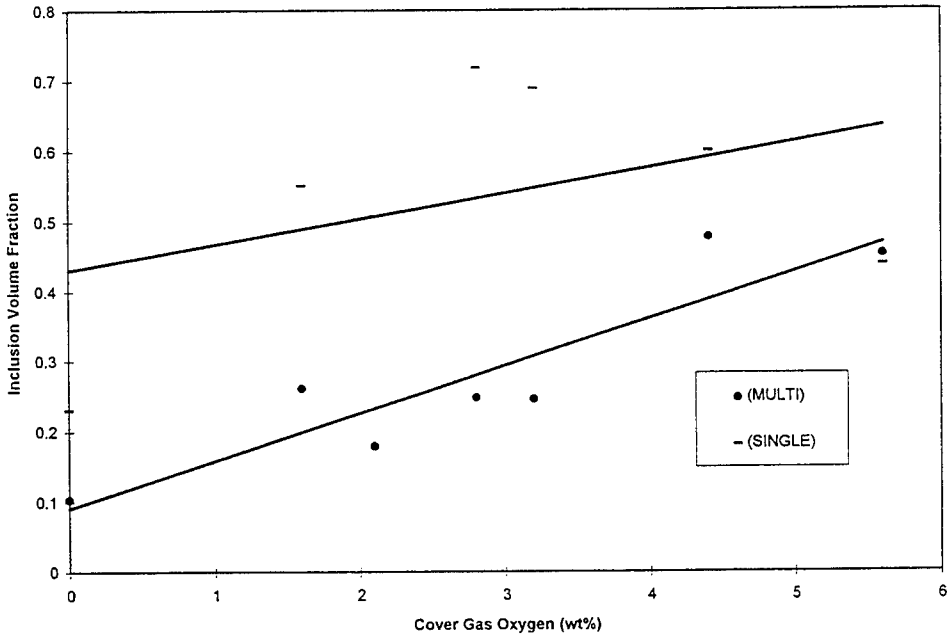

Figure 4.13. GMAW inclusion volume fraction vs cover gas oxygen.

(a)

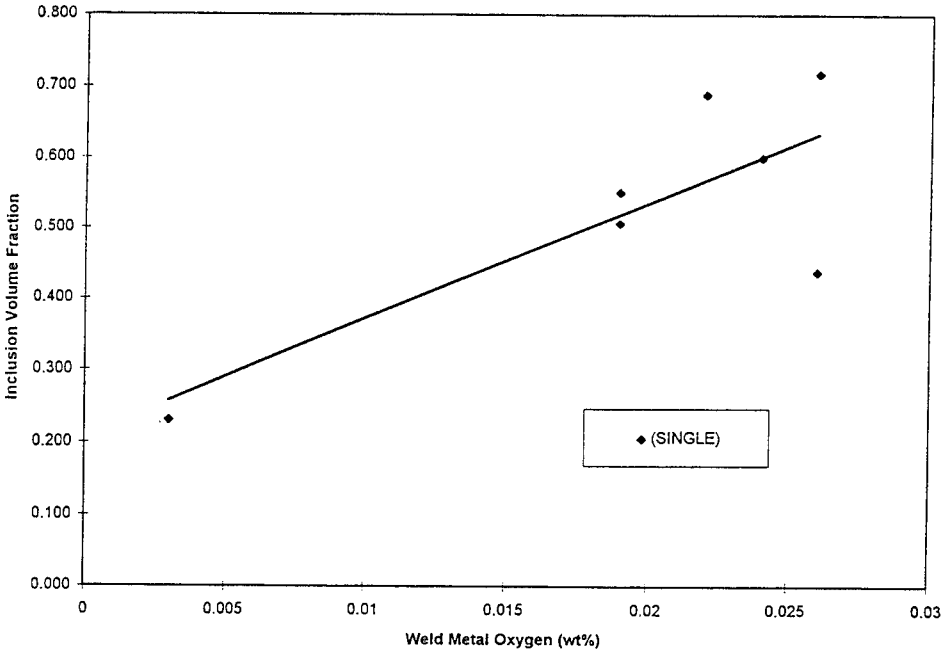

(b)

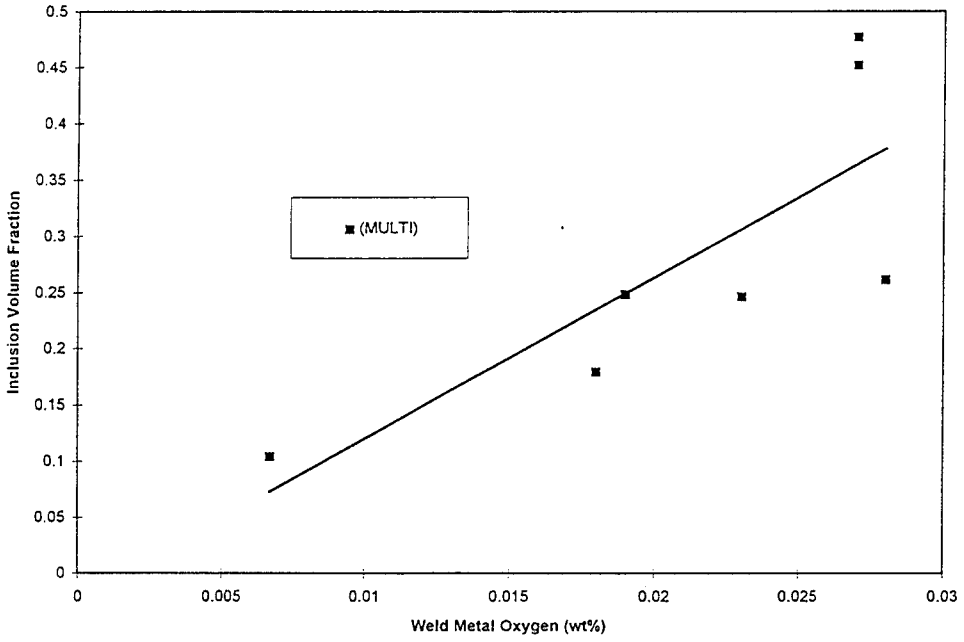

Figure 4.14. (a) GMAW (SINGLE) inclusion VF vs weld O, (b) GMAW (MULTI) inclusion VF vs weld O.

(a)

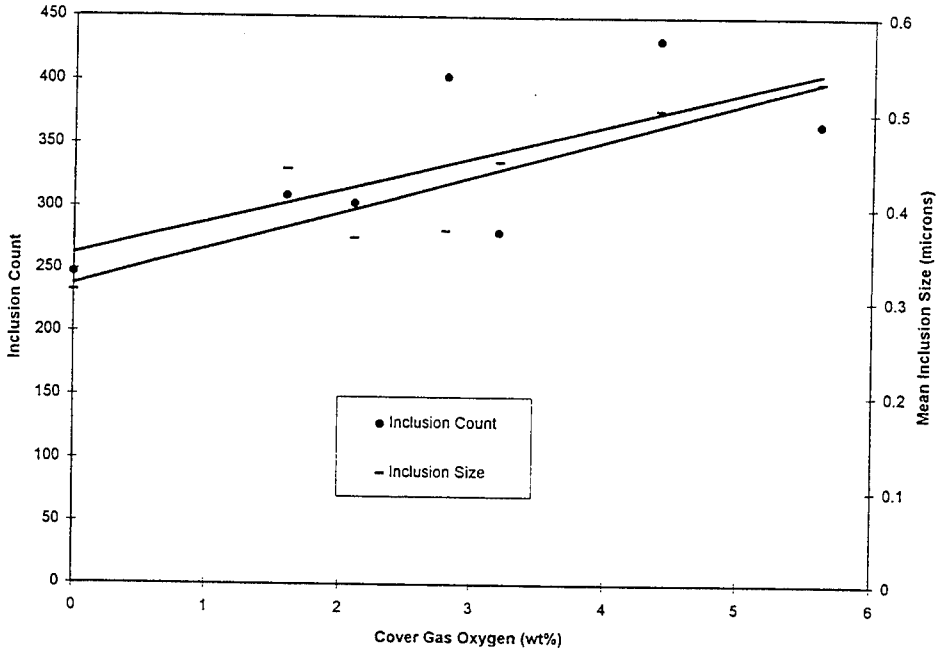

(b)

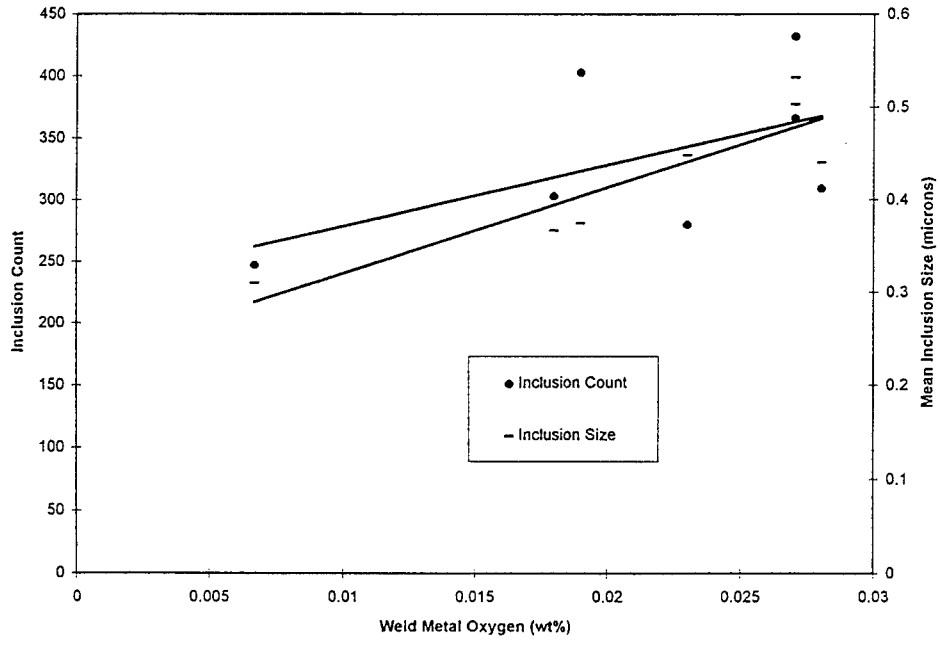

Figure 4.15. GMAW (MULTI) (a) Inclusion count and size vs cover O, (b) Inclusion count and size vs weld O.

(a)

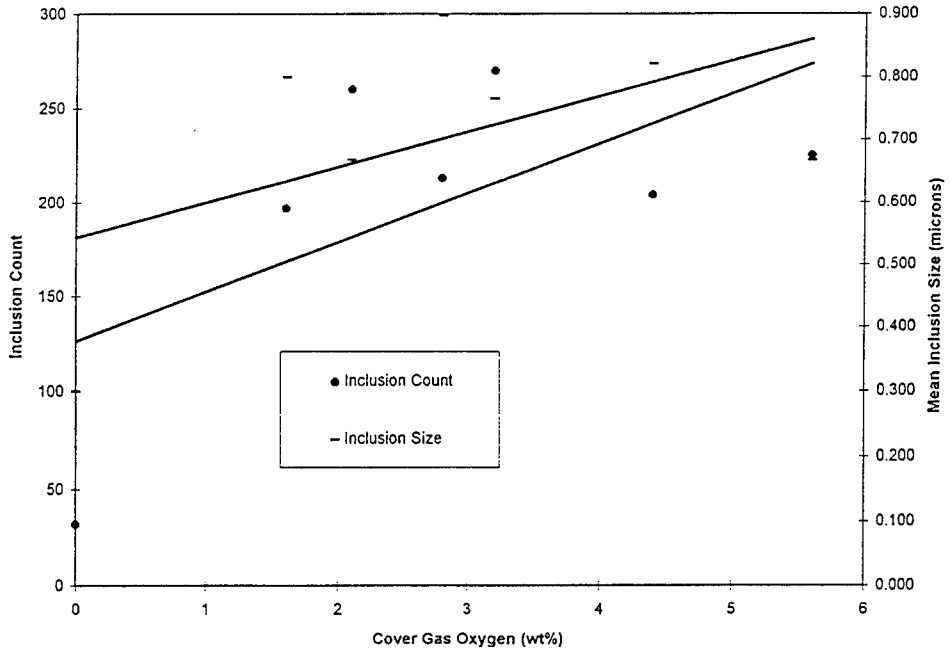

(b)

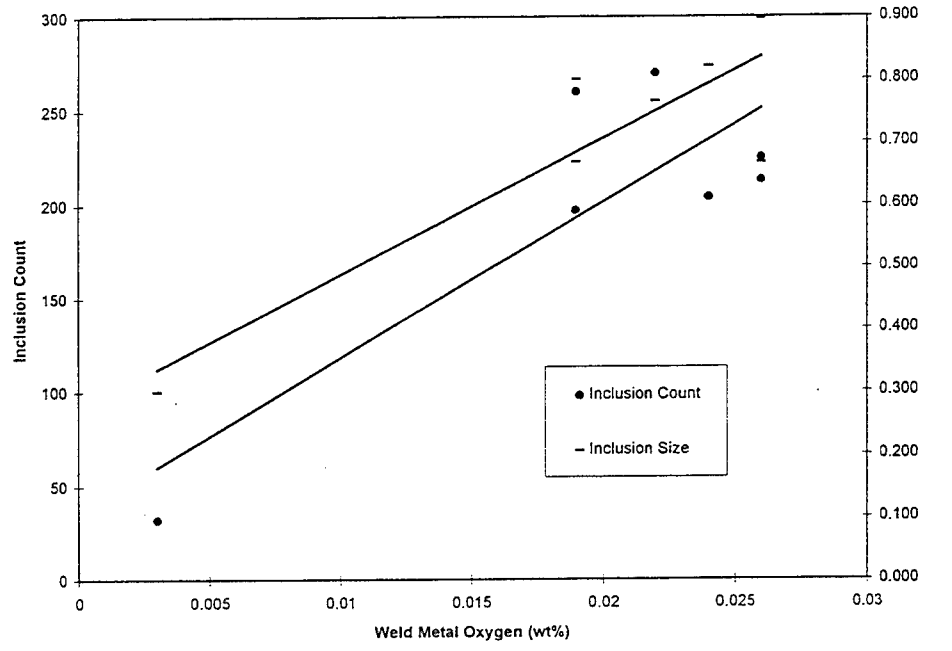

Figure 4.16. GMAW (SINGLE) (a) Inclusion count and size vs cover gas O, (b) Inclusion count and size vs weld O.

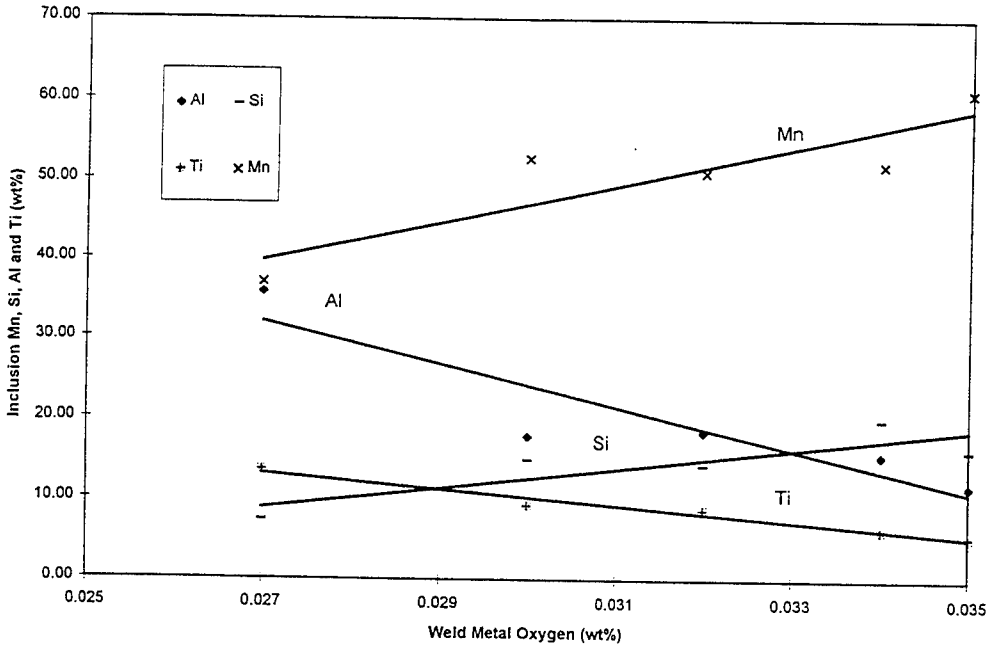

Figure 4.17. SAW inclusion Mn,Si,Al and Ti vs weld O.

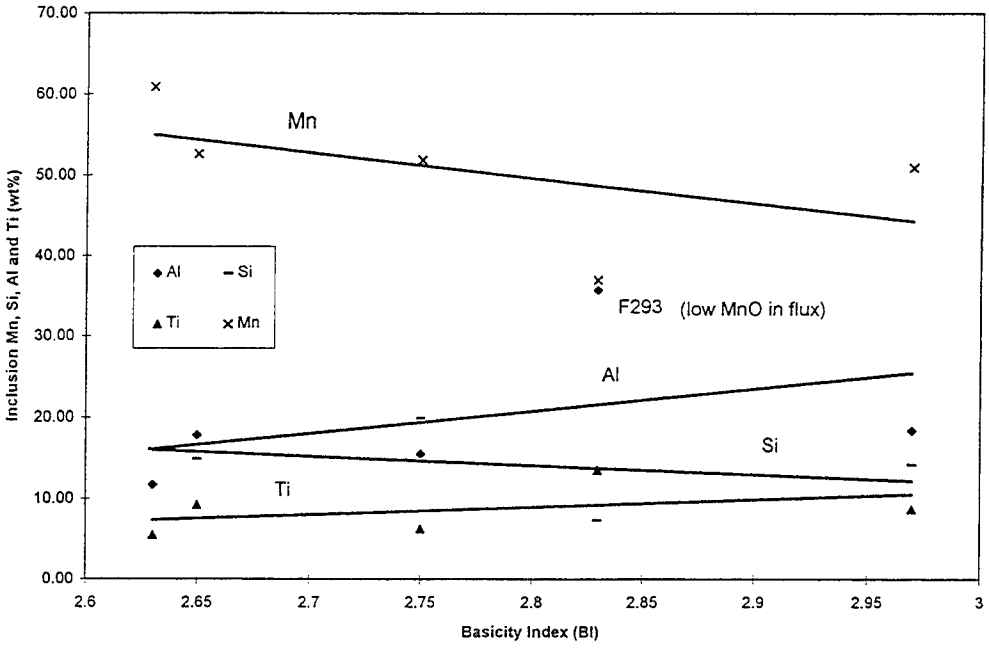

Figure 4.18. SAW inclusion Mn,Si,Al and Ti vs BI.

(a)

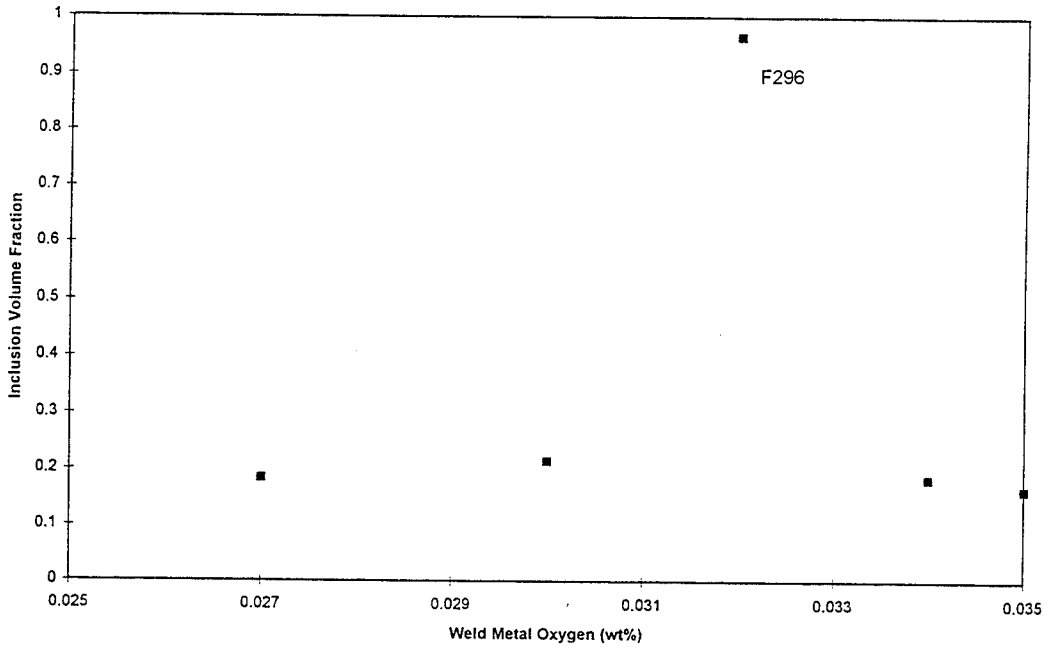

(b)

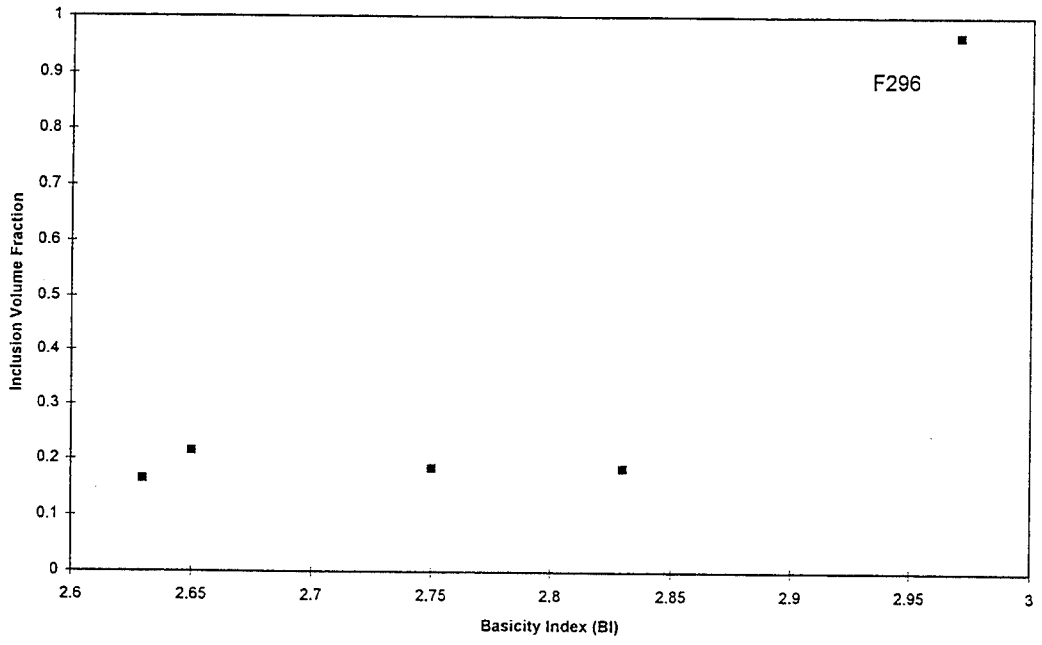

Figure 4.19. SAW (a) Inclusion VF vs weld O, (b) Inclusion VF vs BI.

(a)

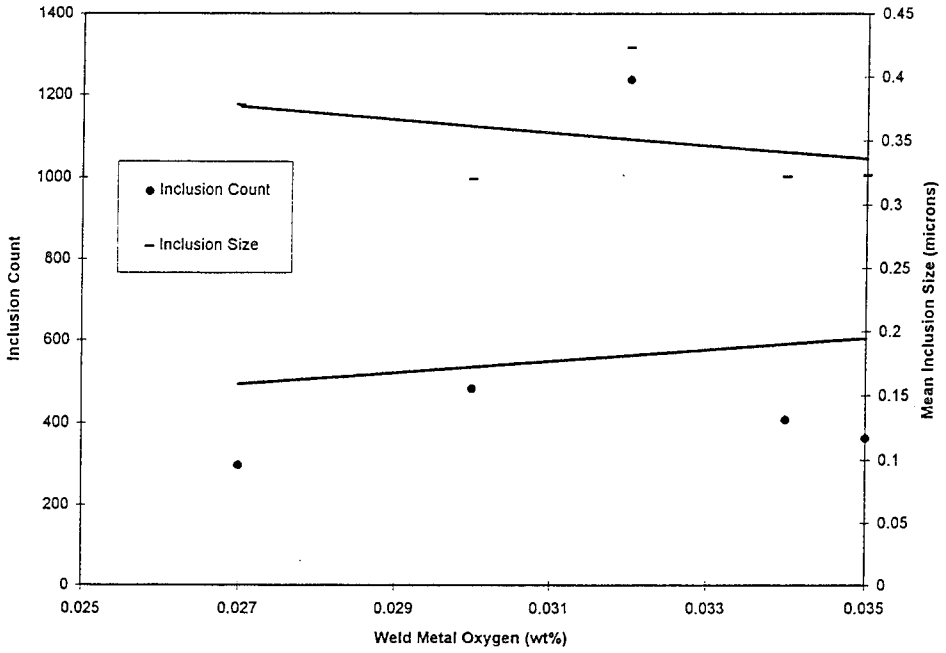

(b)

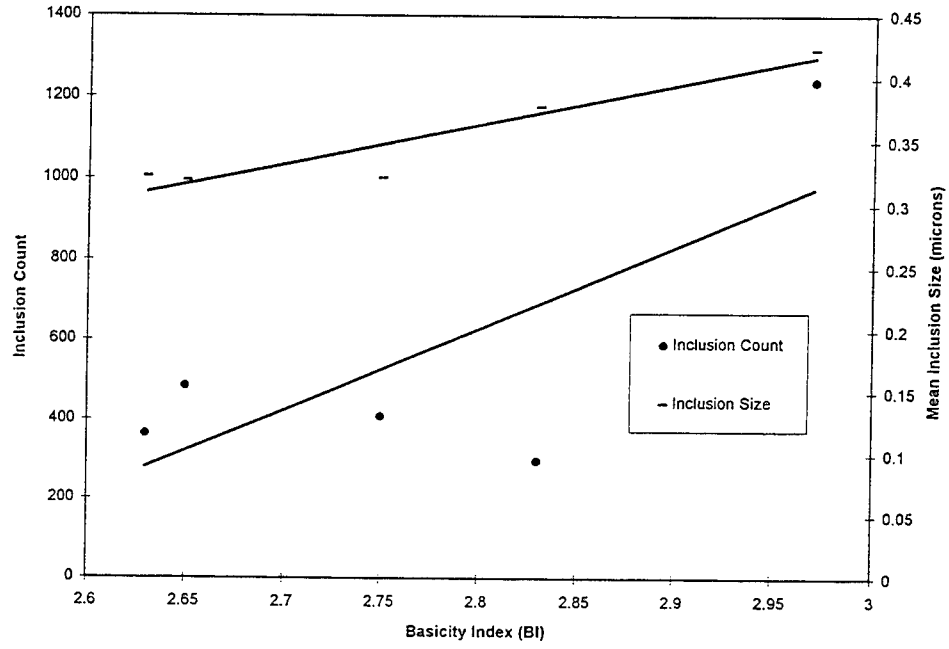

Figure 4.20. SAW (a) Inclusion count and size vs weld O, (b) Inclusion count and size vs BI.

(a)

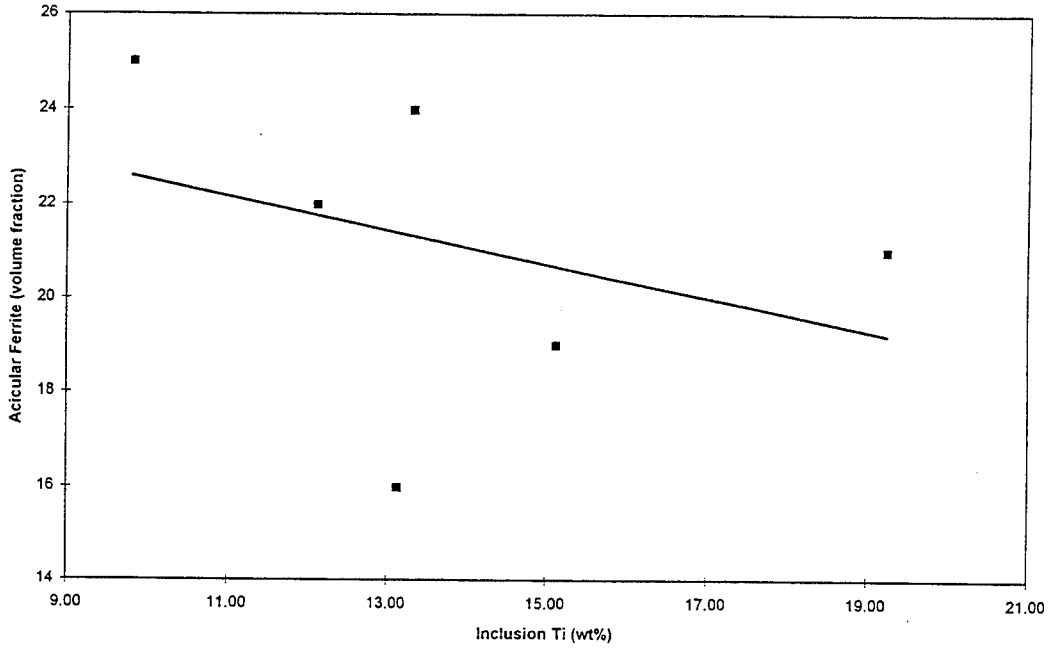

(b)

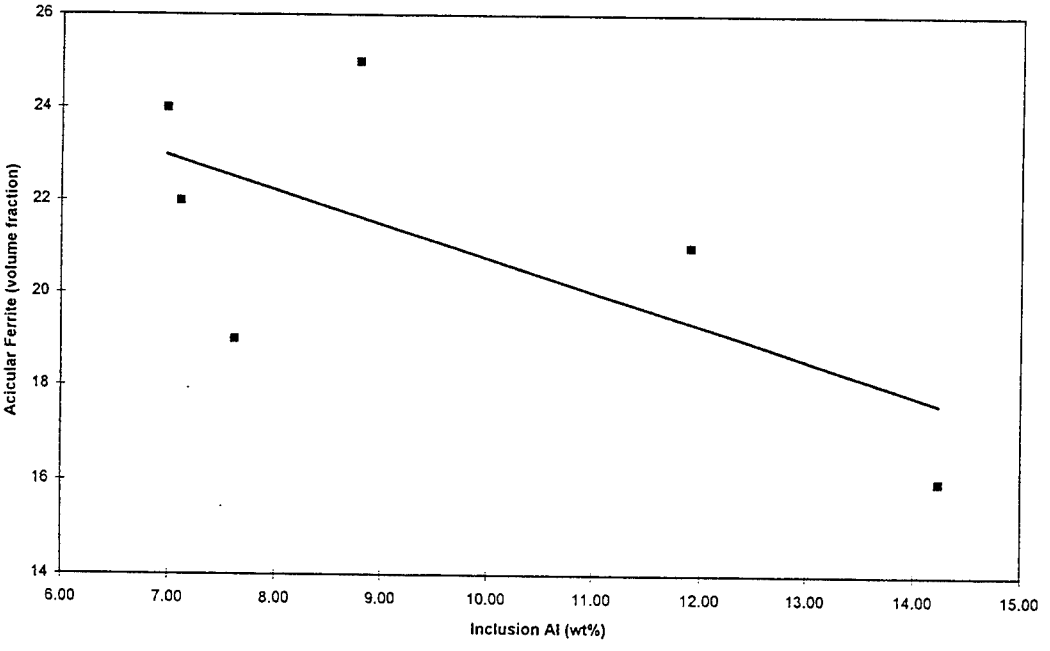

Figure 4.21. GMAW (SINGLE) (a)Acicular ferrite vs inclusion Ti, (b)Acicular ferrite vs inclusion Al.

(a)

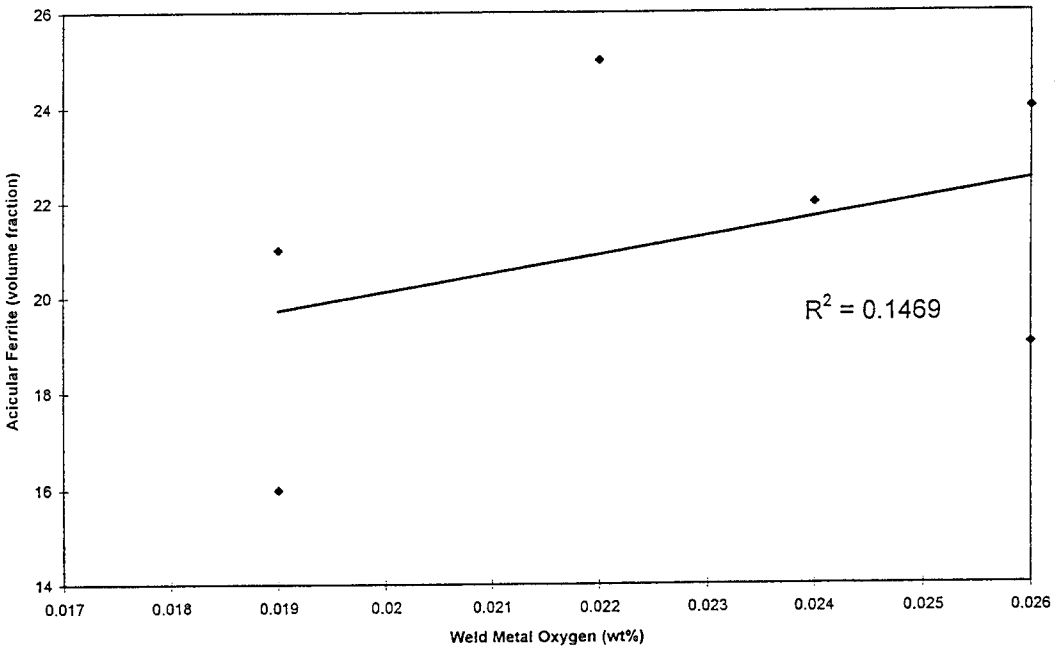

(b)

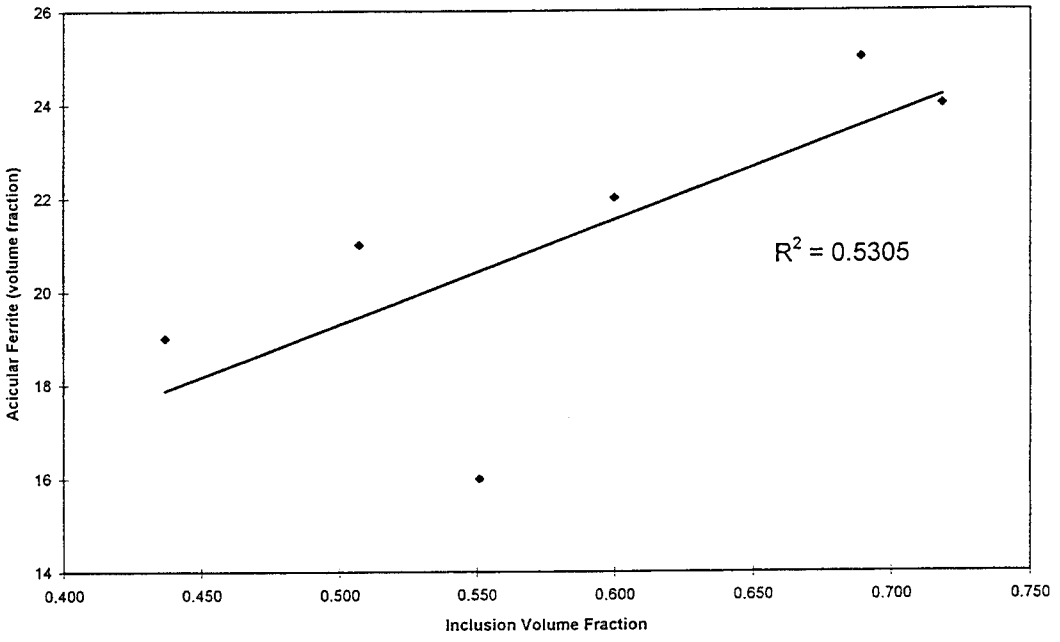

Figure 4.22. GMAW (SINGLE) (a)Acicular ferrite vs weld O, (b)Acicular ferrite vs inclusion VF.

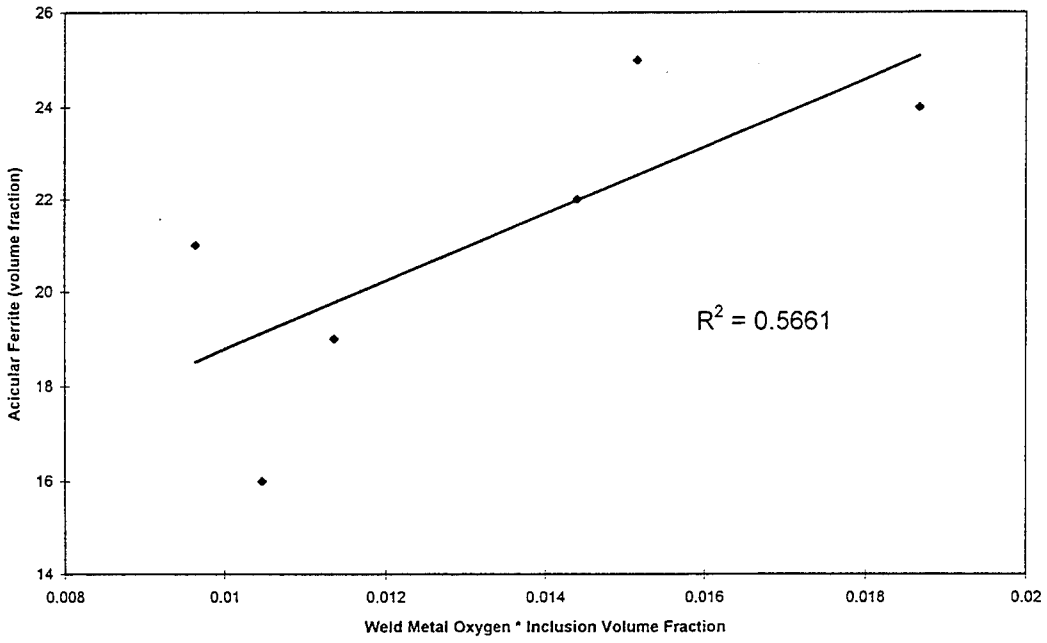

Figure 4.23. GMAW (SINGLE) acicular ferrite vs (weld O * inclusion VF).

(a)

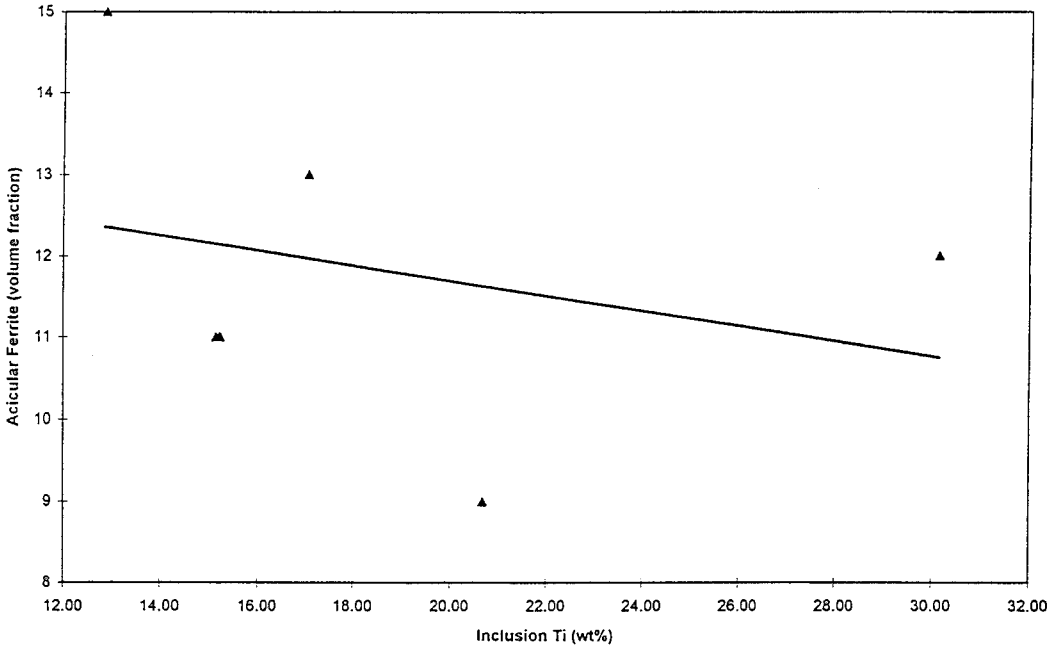

(b)

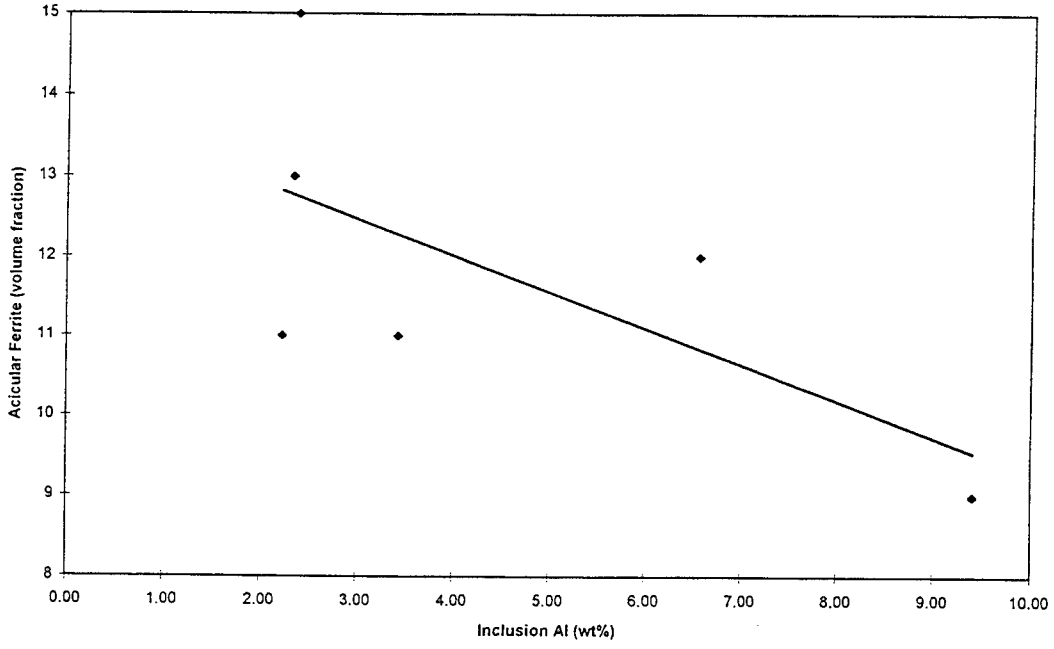

Figure 4.24. GMAW (MULTI) (a)Acicular ferrite vs inclusion Ti, (b)Acicular ferrite vs inclusion Al.

(a)

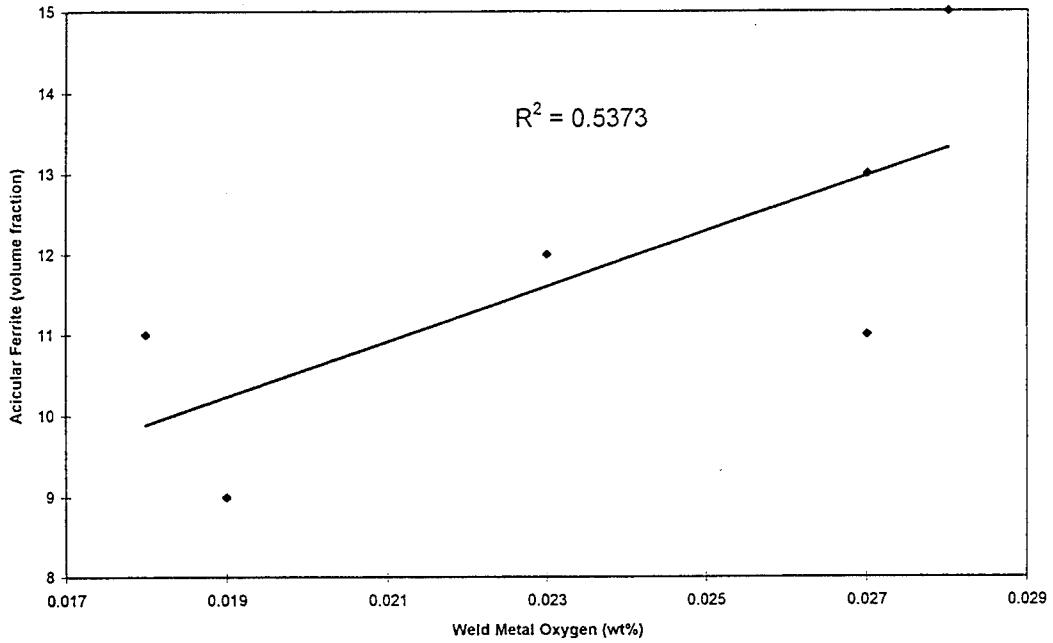

(b)

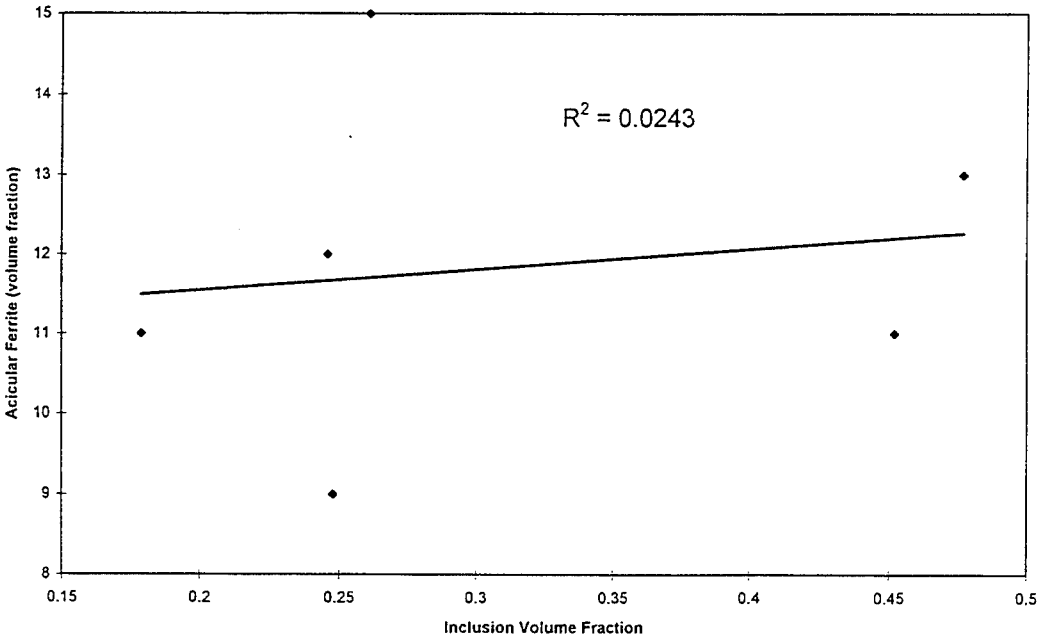

Figure 4.25. GMAW (MULTI) (a)Acicular ferrite vs weld O, (b)Acicular ferrite vs inclusion VF.

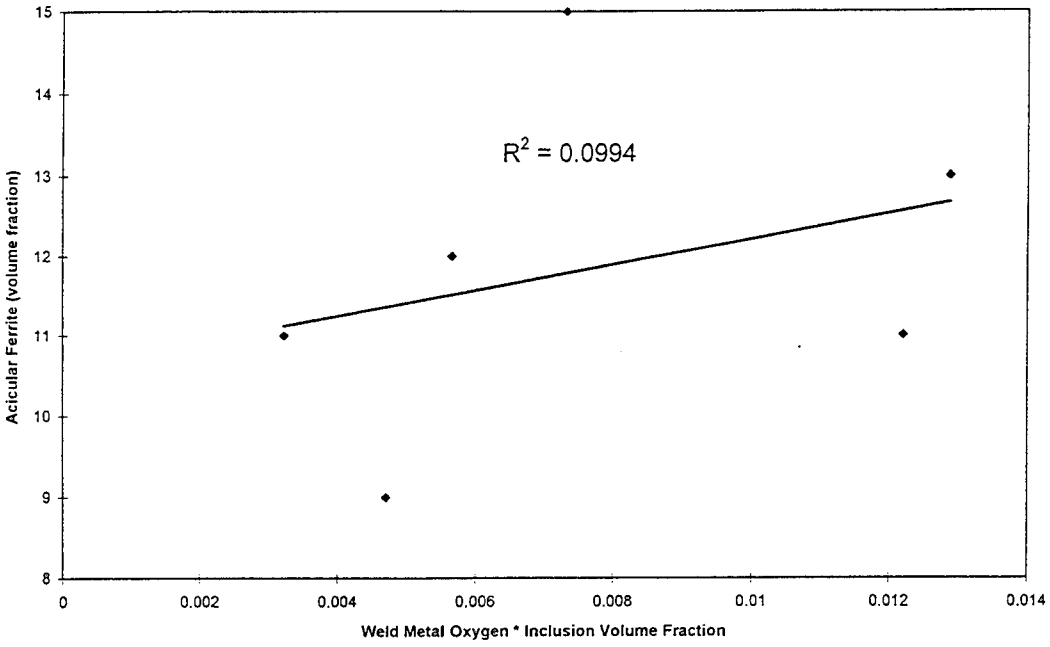

Figure 4.26. GMAW (MULTI)acicular ferrite vs (weld O * inclusion VF).

(a)

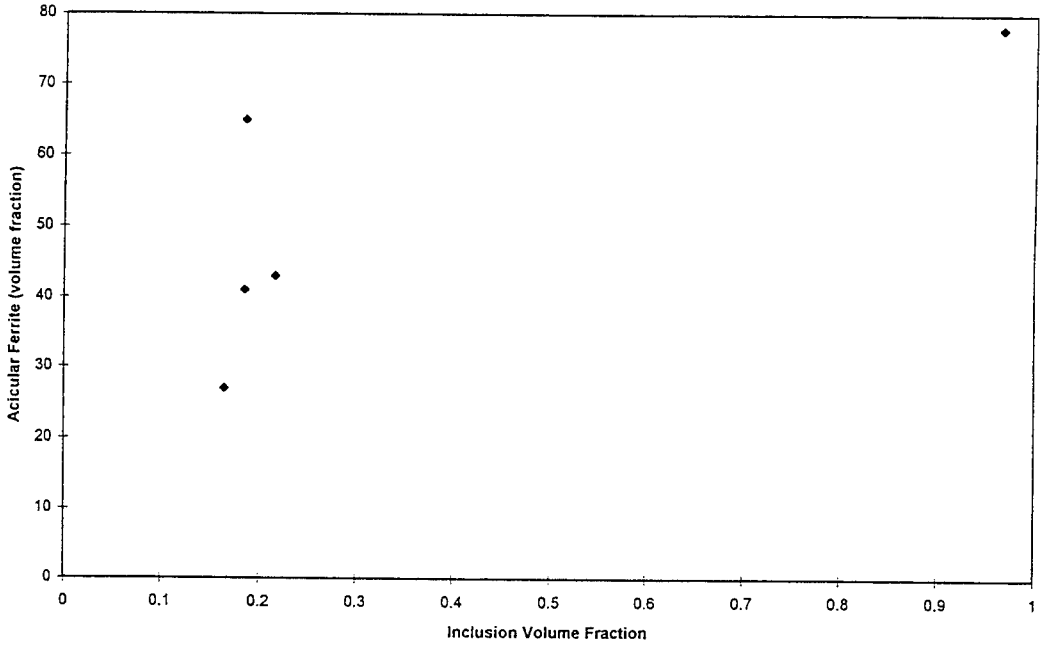

(b)

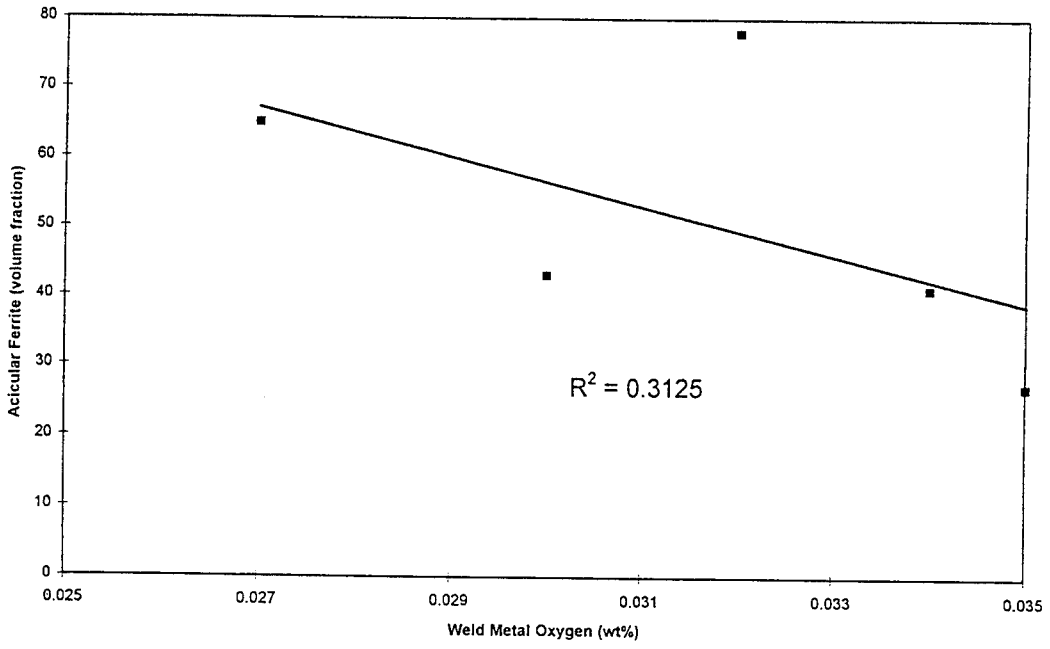

Figure 4.27. SAW (a)Acicular ferrite vs inclusion VF, (b)Acicular ferrite vs weld O.

(a)

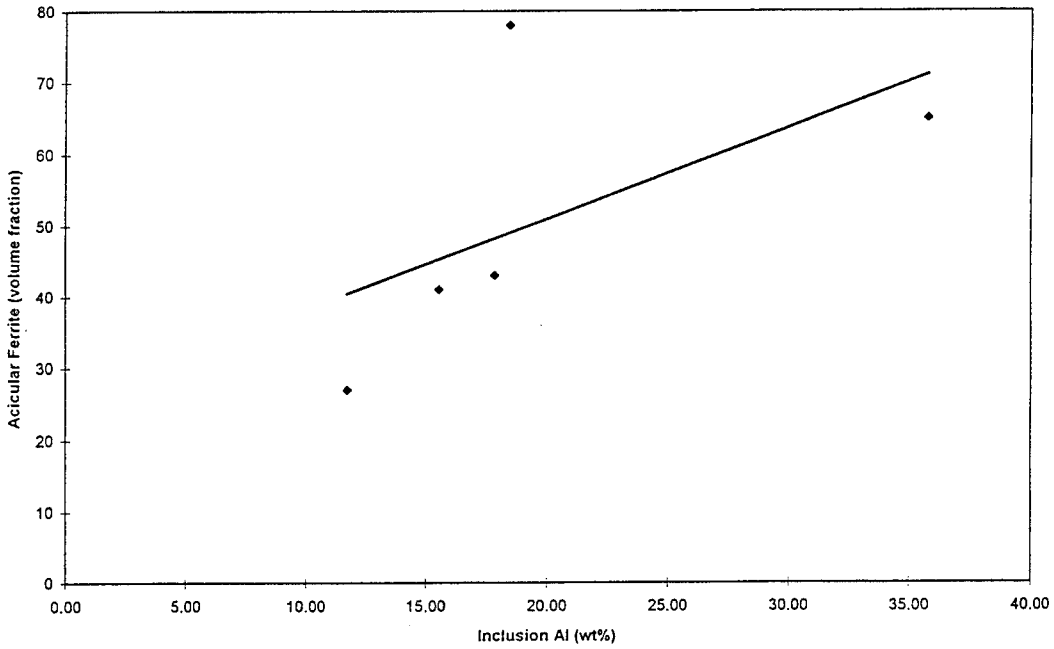

(b)

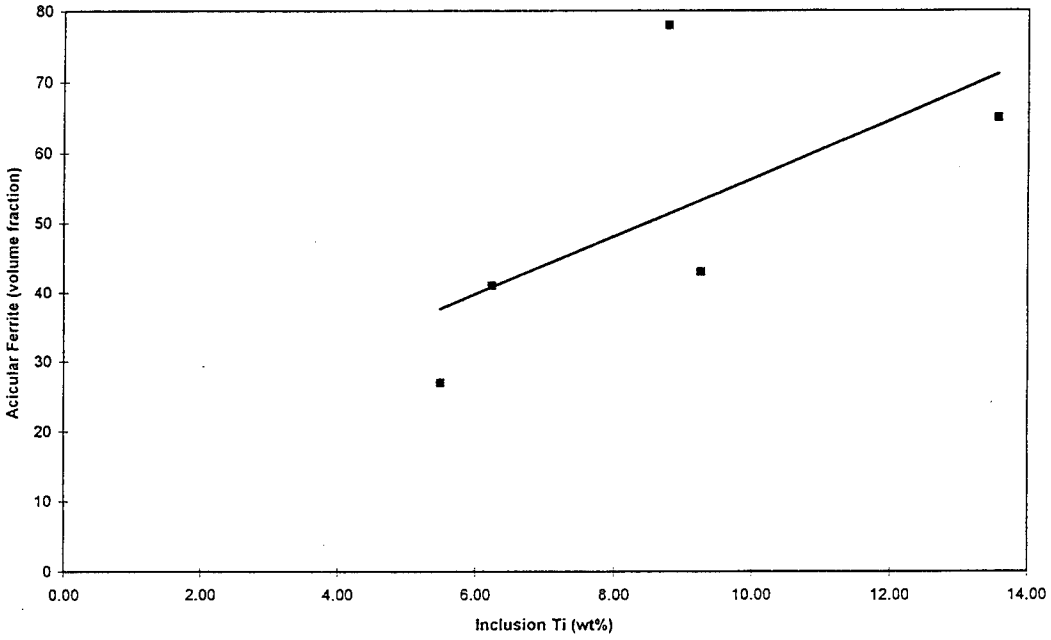

Figure 4.28. SAW (a)Acicular ferrite vs inclusion Al, (b)Acicular ferrite vs inclusion Ti.

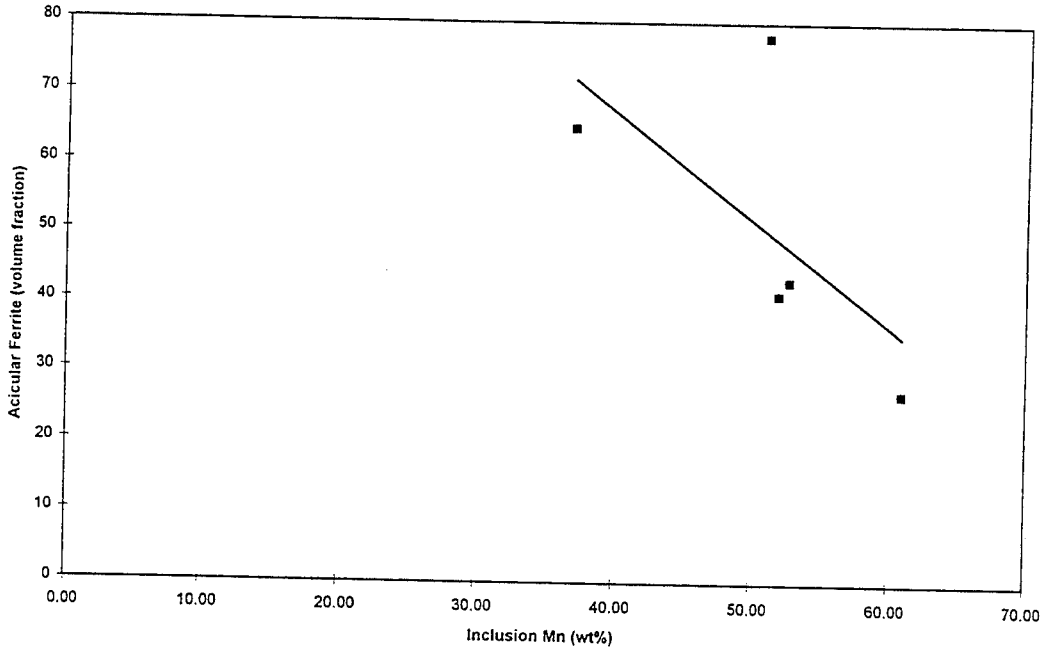

Figure 4.29. SAW acicular ferrite vs inclusion Mn.

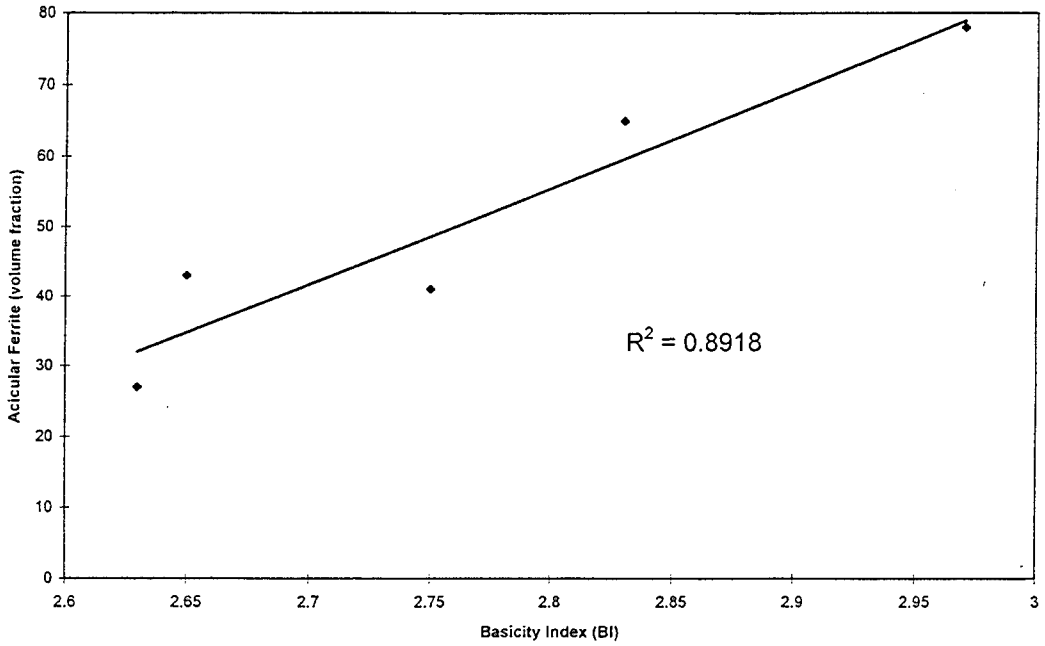

Figure 4.30. SAW acicular ferrite vs Basicity Index (BI).

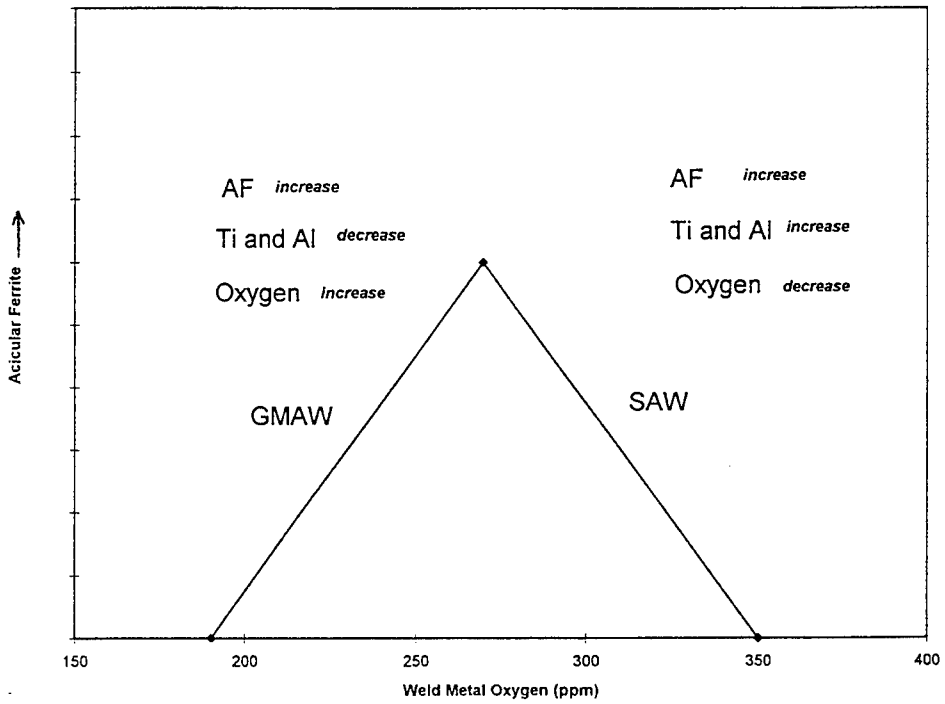

Figure 4.31. Schematic diagram of acicular ferrite versus weld metal oxygen.

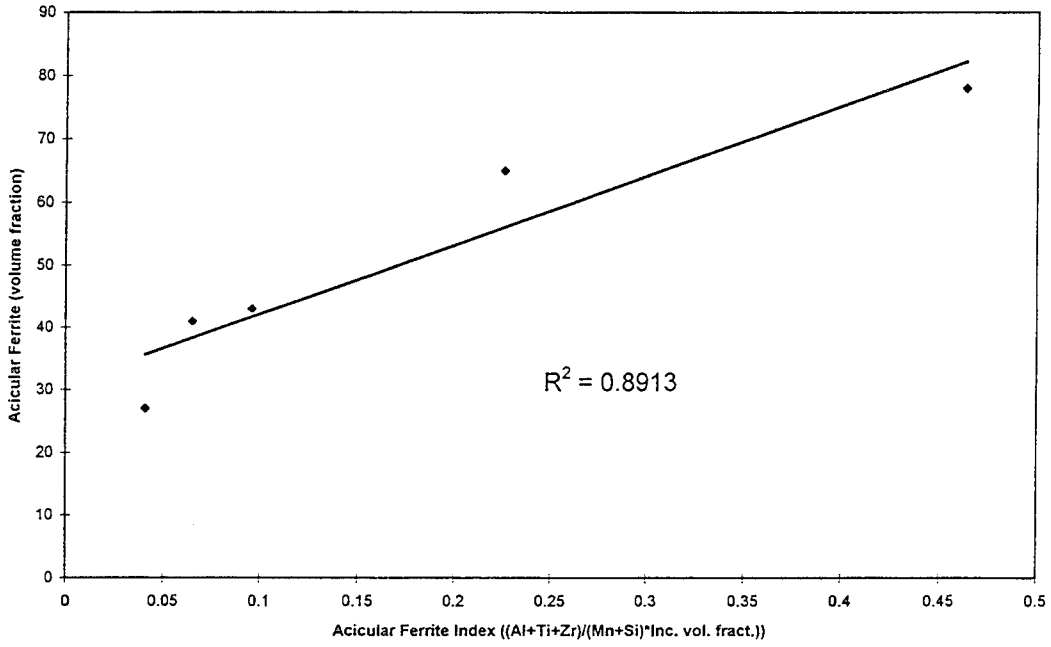

Figure 4.32. SAW acicular ferrite vs Acicular Ferrite Index (AFI).

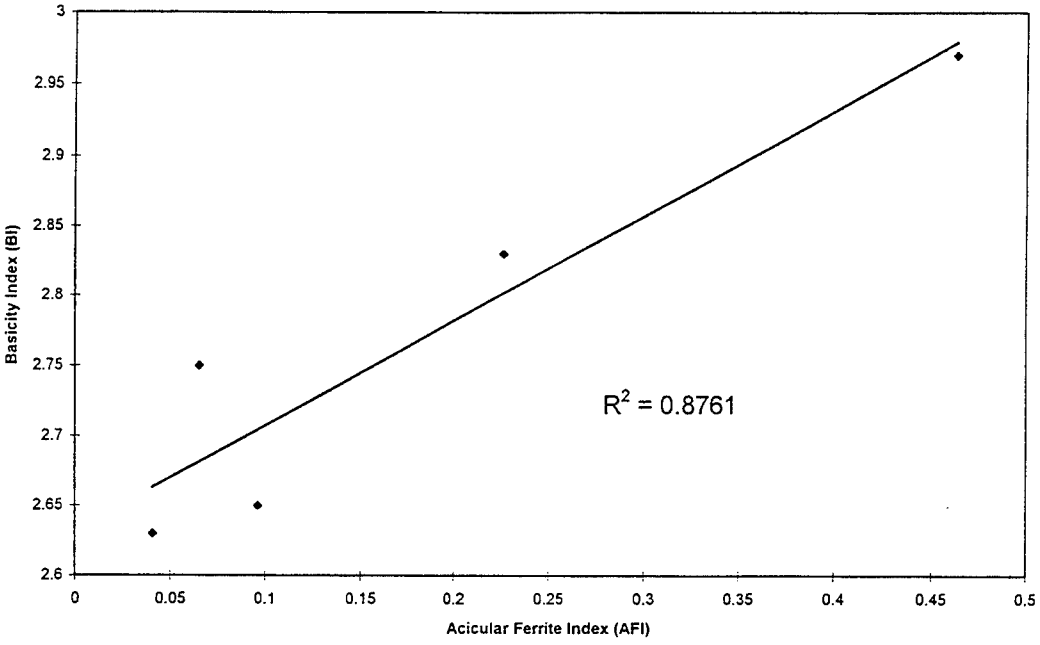

Figure 4.33. SAW Basicity Index (BI) vs Acicular Ferrite Index (AFI).

(a)

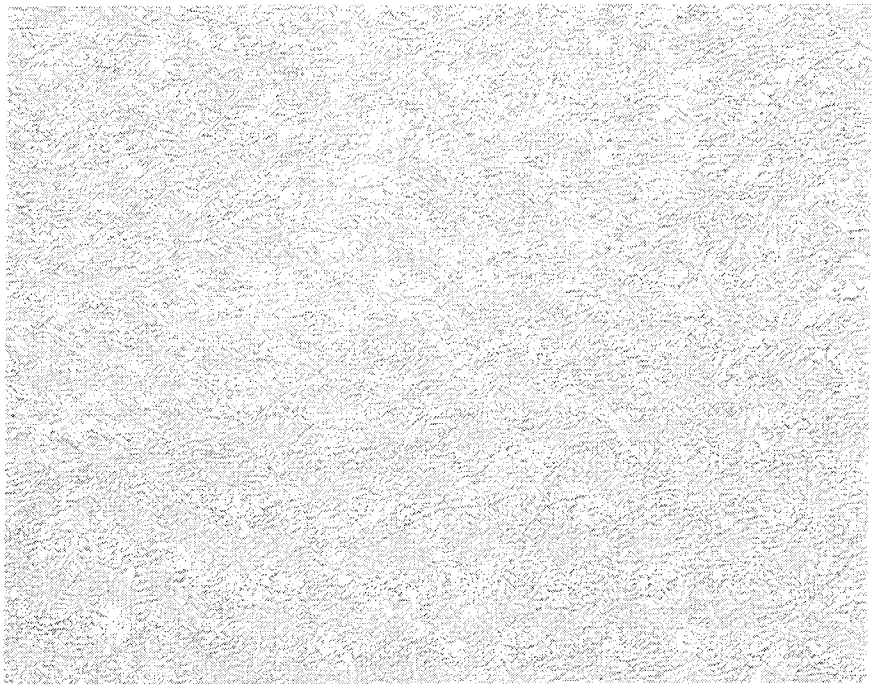

(b)

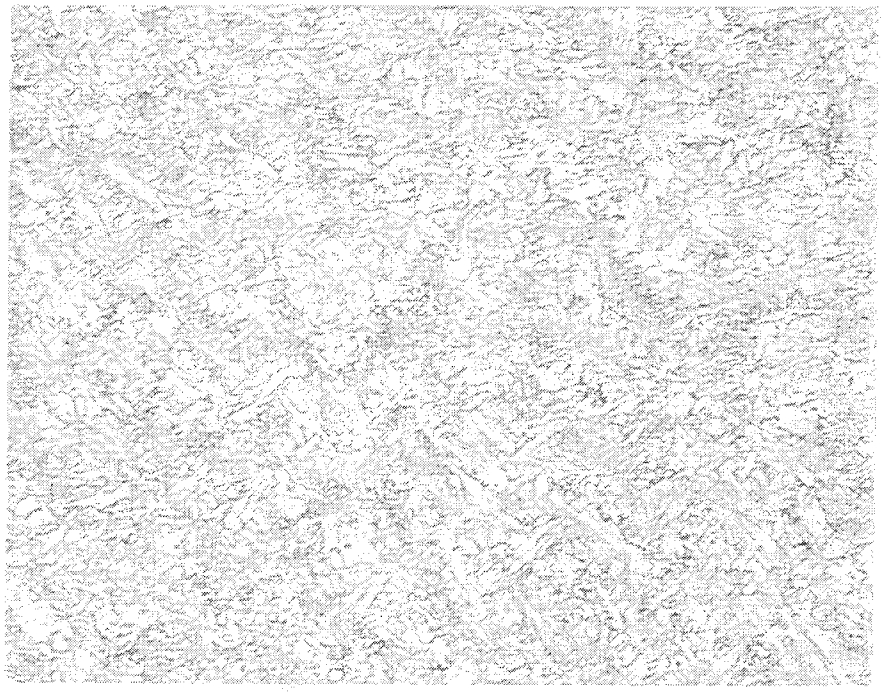

Figure 4.34. Micrographs of (a) SAW F295 (X500), (b) SAW F295 (X1000).

(a)

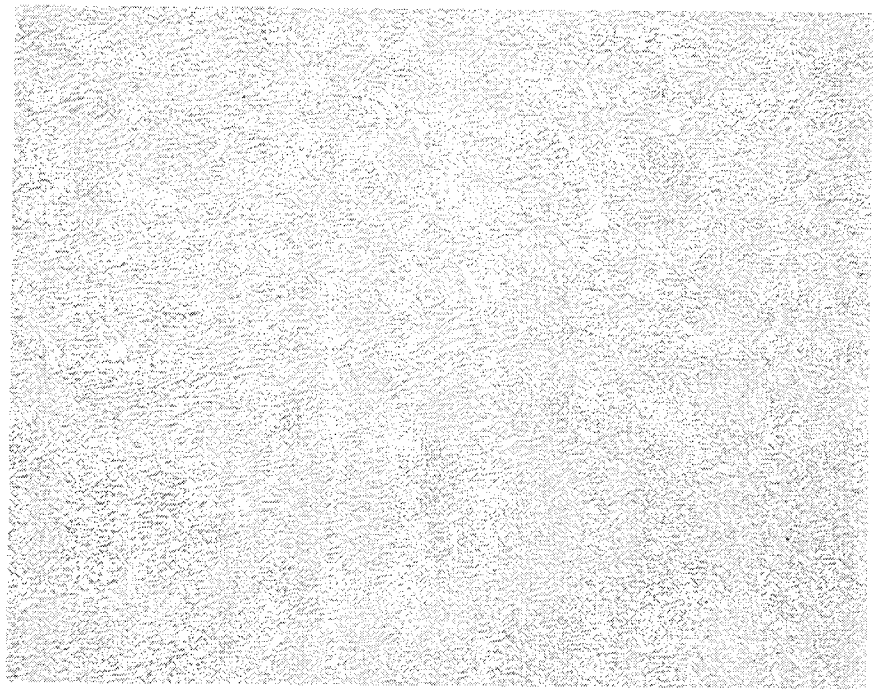

(b)

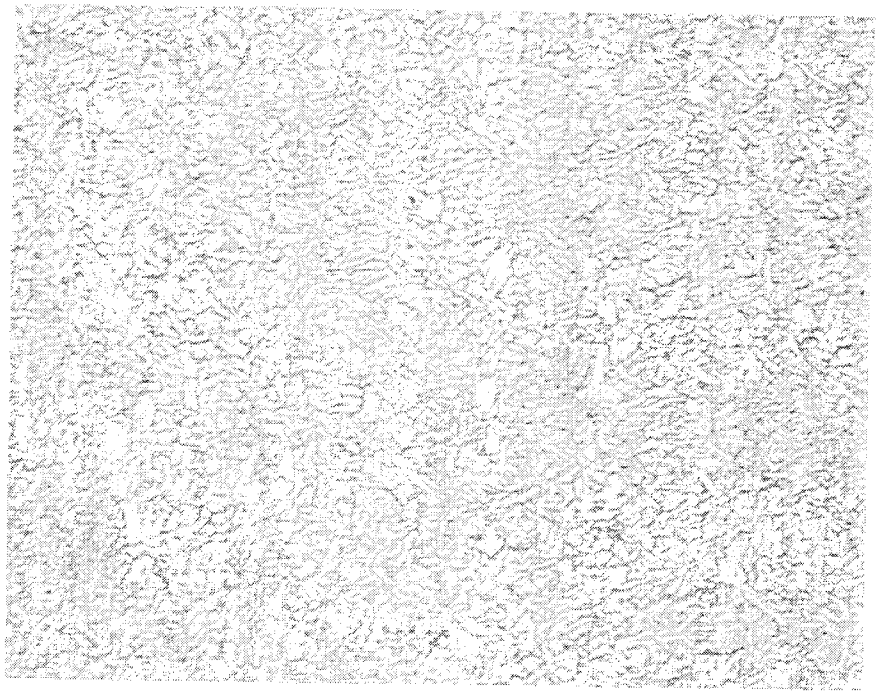

Figure 4.35. Micrographs of (a) SAW F296 (X500), (b) SAW F296 (X1000).

(a)

(b)

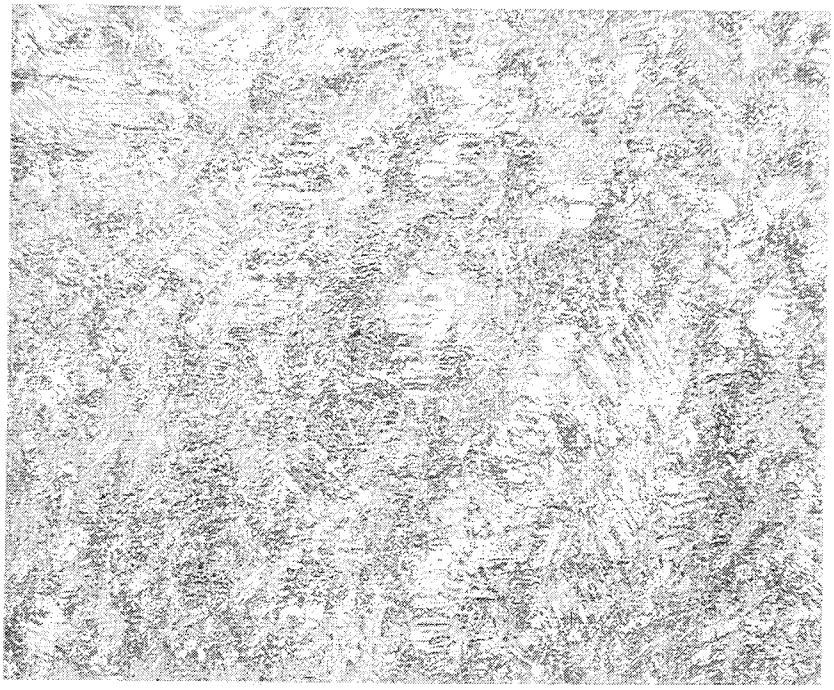

Figure 4.36. Micrographs of GMAW (SINGLE) (a) ARGON (X500), (b) ARGON (X32).

(a)

(b)

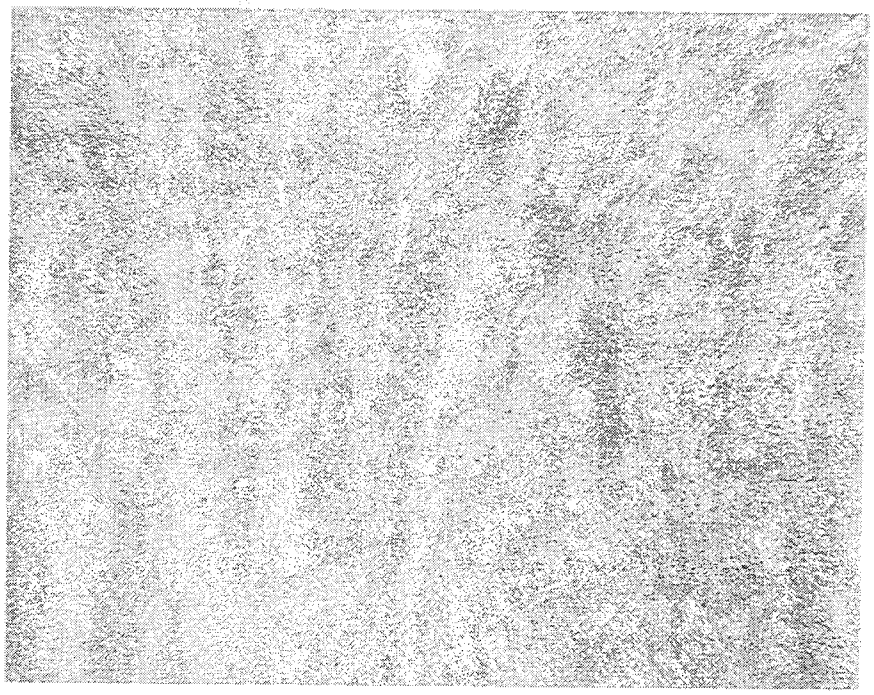

Figure 4.37. Micrographs of GMAW (SINGLE) (a) M4 (X500), (b) M4 (X32).

(a)

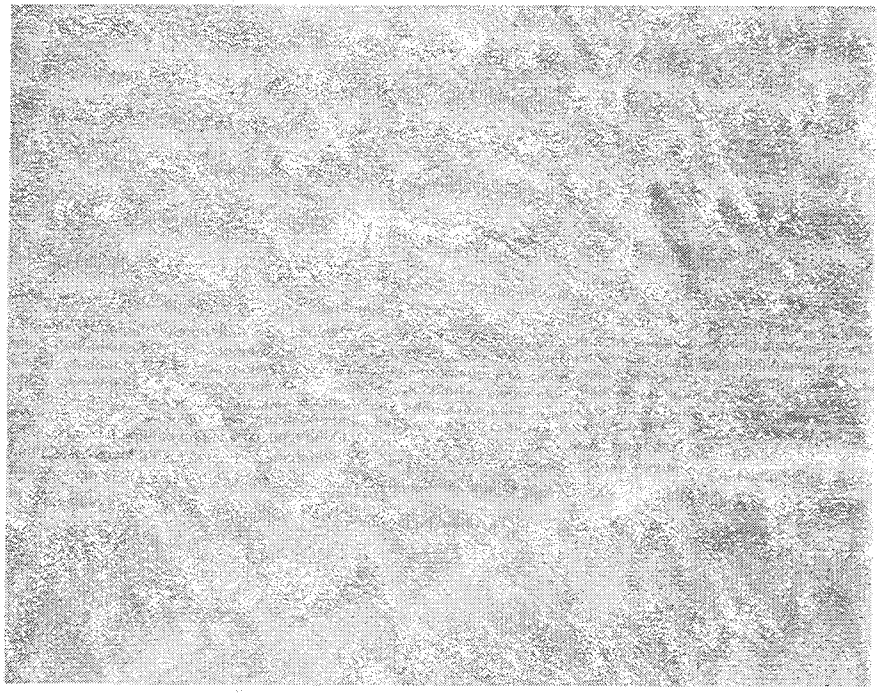

(b)

Figure 4.38. Micrographs of GMAW (MULTI) (a) C10/M4 (X32), (b) C10/M4 (X2000), showing acicular ferrite growing from an inclusion.

(a)

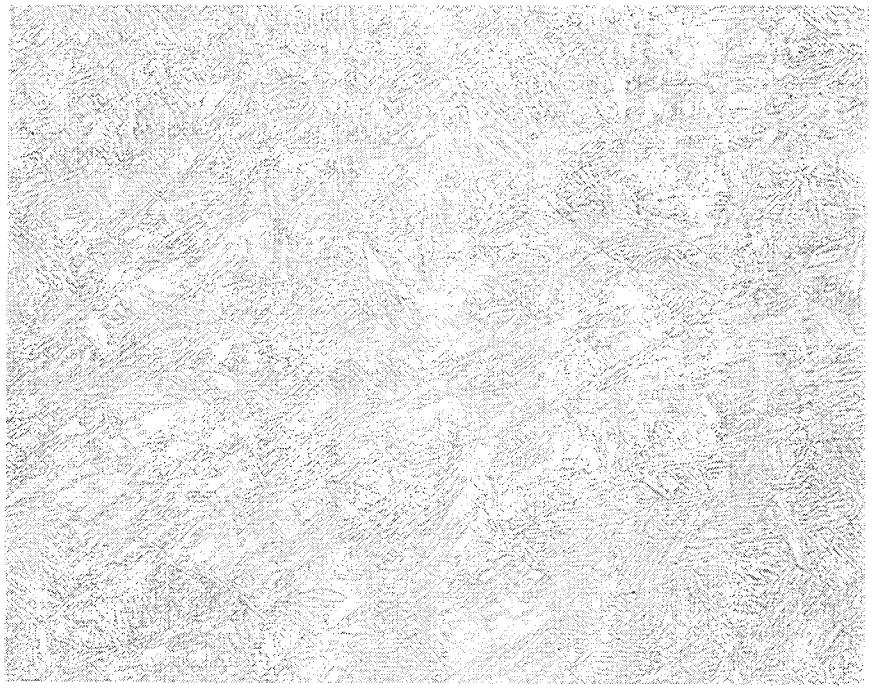

(b)

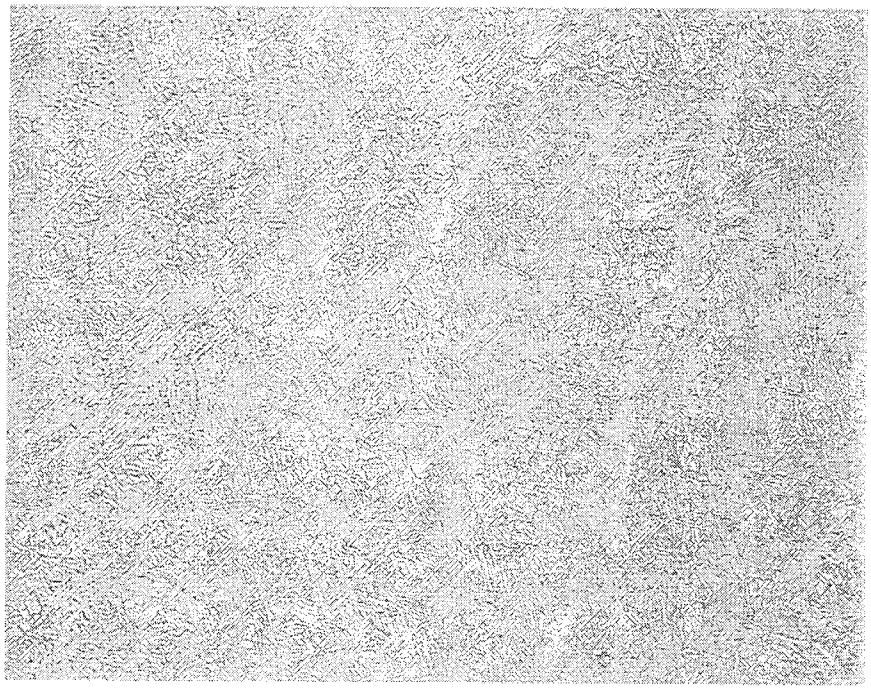

Figure 4.39. Micrographs of GMAW(MULTI) (a) C5 (X480), (b) C10 (X320).

V. CONCLUSIONS

A. SUMMARY

Inclusion composition and size information can be correlated with weld metal chemistry and properties. In GMAW samples, cover gas oxygen correlated strongly with weld metal oxygen and also with weld metal and inclusion elements. The assumptions used in calculating cover gas oxygen activity proved to be fairly on target and this method is a useful first step in trying to predict weld metal behavior with varying amounts of cover gas oxygen or carbon dioxide.

While no real connection could be made between Basicity Index and SAW weld metal oxygen, inclusion analysis proved a rough measure of the oxygen content. The behavior of the inclusion chemistry with varying oxygen levels was consistent in the SAW as well as the GMAW samples. This consistency bodes well for consideration of using inclusion information to aid in the prediction of important weld metal properties.

Of particular interest is trying to correlate inclusions with acicular ferrite. This study, while not exploring the origins of acicular ferrite, demonstrated strongly that inclusion composition can be related to acicular ferrite. Titanium, in particular, appeared to be associated with greater amounts of this desirable microstructure when weld metal oxygen levels were above the optimal level of approximately 270 ppm. When weld metal oxygen levels were below this optimal value, the reverse proved to be true for Ti. Gregg and Bhadeshia, in their study of titanium-rich minerals' ability to nucleate bainite (which they consider acicular ferrite to be a form of), found that TiO_2, Ti_2O_3 and TiO are all effective in enhancing the formation of bainite (Gregg and Bhadeshia, 1994).

An index, called the Acicular Ferrite Index (AFI), was developed to correlate the chemical aspect of acicular ferrite

nucleation and the role of inclusion distribution in forming the interlocking basketweave morphology in SAW. When applied to the SAW samples, good correlation was found. The seemingly unrelated Basicity Index, which showed an unexplained relationship with acicular ferrite, also correlated with this index. The inclusion element ratio in the index serves as a measure of the relative apportioning of the oxides, without requiring specific knowledge of the exact nature of the oxides.

B. RECOMMENDATIONS

The Acicular Ferrite Index should be tested with other SAW inclusion data in order to see if it is a viable measure of acicular ferrite formation. Since inclusions can be taken from a selected area with care, a detailed mapping of a given sample could be undertaken. Inclusion of areas with uniform and non-uniform inclusion distribution, as well as varying amounts of acicular ferrite, could then test the two-stage acicular ferrite formation hypothesis and determine if the AFI is valid or perhaps could be further refined.

LIST OF REFERENCES

Abson D.J. and Pargeter R.J., Factors Influencing As-Deposited Strength, Microstructure and Toughness of Manual Metal Arc Welds Suitable for C-Mn Steel Fabrications, pp 142-143, International Metals Review, v.31, No. 4, 1986.

Bhadeshia H.K.D.H., *Control of Weld Metal Microstructure and Properties*. The Metallurgy, Welding and Qualification of Microalloyed (HSLA) Steel Weldments, pp 41-43, 49, American Welding Society, Houston, 1990.

Brothers D.G., The Origin of Acicular Ferrite in Gas Metal Arc and Submerged Arc Welds, Masters Thesis, Naval Postgraduate School, Monterey, Ca., 1994.

Czyryca E.J., Link R.E., Wong R.J., Aylor D.M., Montemarano T.W. and Gudas J.P., Development and Certification of HSLA-100 Steel Products, pp 64-65, Naval Engineers Journal, v.102, No. 3, May 1990.

David S.A. and DebRoy T., Current Issues and Problems in Welding Science, p 499, Science, v.257, July 1992.

Dowling J.M., Corbett J.M. and Kerr H.W., Inclusion Phases and the Nucleation of Acicular Ferrite in Submerged Arc Welds in High Strength Low Alloy Steels, p 1617, Metallurgical Transactions A, v.17A, September 1986.

Edmonds D.V. and Cochrane R.C., Structure-Property Relationships in Bainitic Steels, p 1533, Metallurgical Transactions A, v.21A, June 1990.

Edwards G.R. and Liu S., Recent Developments in HSLA Steel Welding, pp 226, 241, 254, Proceedings from the First United States-Japan Symposium on Advances in Welding Metallurgy, American Welding Society, June 1990.

Ellis D., The Effects of Titanium Inclusions on HY-80 GMA Weld Deposits, p 260, Masters Thesis, Naval Postgraduate School, Monterey, Ca., 1990.

Evans G.M., The Effect of Titanium in SMA C-Mn Steel Multipass Deposits, p 447, Welding Research Supplement, December 1992.

Fox A.G. and Brothers D.G., The Role of Titanium in the Non-Metallic Inclusions Which Nucleate Acicular Ferrite in the Submerged Arc Weld (SAW) Fusion Zones of Navy HY-100 Steel, accepted for publication by Scripta Metallurgica Et Materiala, 1994.

Francis R.E., Jones J.E. and Olson D.L., Effect of Shielding Gas Oxygen Activity on Weld Metal Microstructure of GMA Welded Microalloyed HSLA Steel, pp 408-414, Welding Research Supplement, November 1990.

Gibson H., Influence of Shielding Gas Composition on Alloy Recovery During Gas Metal Arc Welding, Masters Thesis, Massachusetts Institute of Technology, Cambridge, Ma., 1993.

Graville B.A., Proceeding Welding of HSLA (Microalloyed) Structural Steels (ROMS), p 9, Metals Park, 1978.

Gregg J.M. and Bhadeshia H.K.D.H., Titanium-Rich Mineral Phases and the Nucleation of Bainite, p 10, to appear in Metallurgical Transaction, 1994.

Grong O. and Matlock D.K., Microstructural Development in Mild and Low-alloy Steel Weld Metals, pp 30-43, International Metals Reviews, v.31, 1986.

Grong O., Siewert T.A., Martins G.P. and Olson D.L., A Model for the Silicon-Manganese Deoxidation of Steel Weld Metals, pp 1803-1806, Metallurgical Transactions A, v.17A, October 1986.

Jang J.W., Shah S. and Indacochea J.E., Influences of SAW Fluxes on Low-Carbon Steel Weld Microstructure, p 392, Journal of Materials for Energy Systems, March 1987.

Kettell K.W., Correlation of Flux Composition and Inclusion Characteristics with Submerged Arc Weld Metal Properties in HY-100 Steel, Masters Thesis, Naval postgraduate School, Monterey, Ca., 1993.

Kiessling R., Non-metallic Inclusions in Steel (Part V), Forward, pp 103-104, 112, The Institute of Metals, London, 1989.

Kiessling R. and Lange N., Non-metallic Inclusions in Steel (Parts I-IV), Part I pp 8,62, Part II p 3, The Metals Society, London, 1978.

Kou S., Welding Metallurgy, pp 15-18, 78-81, 191, John Wiley and Sons, 1987.

Liu S., Metallography of HSLA Steel Weldments, pp 3-6, Key Engineering Materials, vv.69,70, 1992.

Metals Handbook, pp 114, 155, 403, 9th edition, American Society for Metals, v.1 and 6, 1983.

Porter L.F. and Repas P.E., The Evolution of HSLA Steels, Journal of Metals, April 1982.

Seraiva F.A., The Study of Single-Pass GMA Welds with Different Cover Gas Compositions on HSLA-100 Steel, Masters Thesis, Naval Postgraduate School, Monterey, Ca., 1993.

Strangwood M. and Bhadeshia H.K.D.H., The Mechanism of Acicular Ferrite Formation in Steel Weld Deposits, pp 212-213, International Conference on Trends in Welding Research, ASM International, 1989.

Sugden A.A.B. and Bhadeshia H.K.D.H., The Nonuniform Distribution of Inclusions in Low-Alloy Steel Weld Deposits, pp 669-670, Metallurgical Transactions A, v.19A, March 1988.

Widgery D.J., Deoxidation Practice for Mild Steel Weld Metal, p 57, Welding Research Supplement, March 1976.

INITIAL DISTRIBUTION LIST

		No. Copies
1.	Defense Technical Information Center Cameron Station Alexandria, Virginia 22304-6145	2
2.	Library, Code 52 Naval Postgraduate School Monterey, California 93943-5101	2
3.	Naval Engineering Curricular Office, Code 34 Naval Postgraduate School Monterey, California 93940-5000	1
4.	Department Chairman, Code ME Department of Mechanical Engineering Naval Postgraduate School Monterey, California 93940-5000	1
5.	Dr. Alan G. Fox, Code ME/FX Department of Mechanical Engineering Naval Postgraduate School Monterey, California 93940-5000	2
6.	Mr. Gene Franke Naval Surface Warfare Center Carderock Division, Annapolis Detachment Code 615, 3A Leggett Circle Annapolis, Maryland 21402-5067	1
7.	Mr. R. Wong Naval Surface Warfare Center Carderock Division, Annapolis Detachment Code 615, 3A Leggett Circle Annapolis, Maryland 21402-5067	1
8.	Dr. Michael G. Vassilaros Naval Surface Warfare Center Carderock Division, Annapolis Detachment Code 615, 3A Leggett Circle Annapolis, Maryland 21402-5067	1
9.	Mark W. Eakes 6046 Pine Valley San Antonio, Texas 78242	2